Mechanical Regulation of Primary Cilia in Tendon

by

Daniel Thomas Rowson

Submitted in partial fulfilment of the requirements

of the Degree of Doctor of Philosophy

School of Engineering and Materials Science

Queen Mary University of London

January 2018

Statement of Originality

I, Daniel Thomas Rowson, confirm that the research included within this thesis is my own work or that where it has been carried out in collaboration with, or supported by others, that this is duly acknowledged below and my contribution indicated. Previously published material is also acknowledged below.

I attest that I have exercised reasonable care to ensure that the work is original, and does not to the best of my knowledge break any UK law, infringe any third party's copyright or other Intellectual Property Right, or contain any confidential material.

I accept that the College has the right to use plagiarism detection software to check the electronic version of the thesis.

I confirm that this thesis has not been previously submitted for the award of a degree by this or any other university.

Signature:

Date:

Details of Collaboration and Publications:

Work in Chapter 3 has been published as "Zonal Variation in Primary Cilia Elongation Correlates With Localized Biomechanical Degradation in Stress Deprived Tendon" in the "Journal of Orthopaedic Research".

Work in Chapter 4 is being submitted for publication in the journal "Scientific Reports"

Abstract

During normal activity, tendons are subjected to dynamic tensile strains of approximately 1-10%, whilst mechanical overload can lead to damage and degradation and the development of tendinopathy. The tenocytes within tendon respond to this mechanical environment although the mechanisms are poorly understood. Primary cilia consist of a slender axoneme composed of acetylated α-tubulin and are known to regulate a variety of signalling pathways including mechanosignalling. In various cell types, mechanical loading also influences primary cilia length. However relatively little is known about tendon primary cilia structure and function.

This thesis set out to examine the structure and organisation of primary cilia in tendon cells and the effect of mechanical loading, both in situ and in isolated cells cultured in monolayer. Studies analysed cilia expression using confocal immunofluorescence microscopy in tendon fascicles from rat tail and isolated human tenocytes.

Results demonstrated that the prevalence and orientation of primary cilia was different in the fascicular matrix (FM) and interfascicular matrix (IFM) regions of the tendon. Stress deprivation caused differential cilia elongation between the FM and IFM, associated with disruption of the surrounding extracellular matrix and alterations in tissue biomechanics.

In isolated tenocytes, primary cilia were significantly longer with a greater prevalence than in situ. Cyclic tensile loading applied using the Flexcell system resulted in cilia disassembly within 8 hours with a dramatic reduction in prevalence and length. This effect was completely reversible on removal of strain. A similar response was observed in situ within both FM and IFM regions of the tendon. This mechanically-induced cilia

disassembly was shown to be mediated, at least in part, by the release of TGFβ and activation of HDAC6 which causes tubulin deacetylation.

These results in this thesis suggest a novel feedback mechanism through which physiological and pathological mechanical loading may regulate primary cilia signalling.

Acknowledgements

Firstly, I would like to thank my supervisors, Professor Martin Knight and Professor Hazel Screen, for their support, guidance and perseverance in keeping me focussed. Thanks to the EPSRC for funding this research. Further, thanks to Dr Chavaunne Thorpe, Dr Steven Thorpe, Dr Dharmesh Patel and Dr Angus Wann, for answering all of my questions and teaching me most of the lab skills and techniques that I know. I would also like to thank everyone at QM who made these 4 years really enjoyable, in particular Marta and Olly, it would not have been the same without them.

Thank you to James, Emma, Michaela and Nimrod for being there for me, especially in the last year, I don't think I would have got through it without them all. Finally, I would like to thank my parents, Anna Coen and Andrew Rowson, for constantly pulling me up on my grammar but most importantly for their constant support, encouragement and belief that I could do this, and always being there to talk when I needed to.

Table of Contents

1 LITERATURE REVIEW 18

1.1 INTRODUCTION TO TENDON 19

1.2 TENDON COMPOSITION 20

1.2.1 Collagen 20

1.2.2 Proteoglycans 22

1.2.3 Elastin 23

1.3 TENDON STRUCTURE AND MECHANICS 24

1.3.1 Fibrils 24

1.3.2 Fibres 26

1.3.3 Fascicles 28

1.3.4 Interfascicular Matrix 31

1.3.5 Tendon Sheath 33

1.3.6 Modelling Tendon Mechanics 33

1.3.7 Cells in the Tendon 35

1.3.8 Proteoglycans 37

1.3.9 Whole Tendon 38

1.3.10 In Vivo Strain 39

1.4 TENDINOPATHY 40

1.4.1 Tears, Tendinitis, Tendinosis and Tendinopathy 40

1.4.2 Risk Factors 41

1.4.3 Cause, Mechanism and Pathology 42

1.4.4 Stress Deprivation 43

1.5 TENOCYTE MECHANOBIOLOGY 44

1.5.1 Testing the Metabolic Effects of Loading 44

1.5.2 Gene Families Investigated in Tendon Mechanobiology Research 46

1.5.3 Summary of Load Induced Changes in Gene Expression 47

1.5.4 Transforming Growth Factor beta 50

1.5.5 Morphology 51

1.5.6 Stress Deprivation 52

1.5.7 Tendon Mechanosensation 53

1.6 PRIMARY CILIA STRUCTURE 53

1.6.1 History of Cilia Research and the Discovery of Ciliopathies 53

1.6.2 Tubulin and Microtubules 55
1.6.3 Ciliogenesis and Structure 56
1.6.4 Cell Cycle and Disassembly 57
1.6.5 Intraflagellar Transport (IFT) 58
1.7 ROLE OF THE PRIMARY CILIA IN SIGNALLING 60
1.7.1 Overview of Cilia Signalling 60
1.7.2 Role of Primary Cilia Mechanotransduction 62
1.7.3 Role of Primary Cilia in TGFβ Signalling 63
1.8 EFFECT OF MECHANICAL LOADING ON PRIMARY CILIA STRUCTURE 65
1.8.1 Loading indirectly causes disassembly in some cell types 65
1.8.2 Theory of Tubulin Polymerisation and Acetylation as Regulators for Load Induced Cilia Disassembly 66
1.8.3 The Role of Actin in Regulating Cilia Length 66
1.8.4 Effect of Cilia Length on Signalling 67
1.8.5 Tenocyte Primary Cilia and their Response to Loading 67
1.9 HYPOTHESES, AIMS AND OBJECTIVES 70
1.9.1 Hypotheses 70
1.9.2 Objectives 70
2 PROTOCOLS & DEVELOPMENT 72
2.1 CELL AND TISSUE CULTURE METHODS 72
2.1.1 Media 72
2.1.2 Primary Bovine Tenocyte Isolation 73
2.1.3 Rat Tail Dissection 74
2.2 BIOMECHANICAL TESTING OF TENDON 75
2.2.1 Mechanical Testing 75
2.2.2 Mechanical Testing of IFM 78
2.3 EQUIPMENT AND VALIDATION FOR MECHANICAL STIMULATION OF TENDON EXPLANTS 78
2.3.1 Loading Conditions 79
2.3.2 Explant Viability During Loading Experiments. 80
2.3.3 Cyclic Loading of Cells using the Flex Cell System 81
2.4 INTRODUCTION TO IMMUNOFLUORESCENT IMAGING TECHNIQUES 82
2.4.1 Confocal Imaging 83
2.4.2 Fixation 84

2.4.3 Immunofluorescent Antibodies for Visualising Primary Cilia 85
2.4.4 Other Useful Antibodies 86
2.4.5 Cilia Staining Protocol for Isolated Cells 87
2.5 DEVELOPMENT OF PRIMARY CILIA VISUALISATION IN TISSUE 88
2.5.1 Bovine Tissue Section Staining 89
2.5.2 Bovine Cryosection Staining 91
2.5.3 Rat tail Staining 92
2.5.4 Rat Tail Staining with Methanol 93
2.6 IMAGE ANALYSIS 96
2.6.1 Imaging and Measuring the Cilium (in Tissue) 96
2.6.2 Nuclear Shape Analysis 98
2.7 SUMMARY 99
3 ZONAL VARIATION IN PRIMARY CILIA ELONGATION CORRELATES WITH LOCALISED BIOMECHANICAL DEGRADATION IN STRESS DEPRIVED TENDON 101
3.1 INTRODUCTION 101
3.2 METHODS 103
3.2.1 Stress Deprivation and Static Strain 103
3.2.2 Time Course 104
3.2.3 Mechanics 104
3.2.4 Treatment with IL-1 105
3.2.5 Data Analysis 105
3.3 RESULTS 106
3.3.1 Cilia Length and Orientation 106
3.3.2 Fascicle and IFM Mechanics 109
3.3.3 Effects of Il-1 113
3.4 DISCUSSION 114
4 MECHANICAL LOADING INDUCES PRIMARY CILIA DISASSEMBLY IN TENDON CELLS VIA TGFB AND HDAC6. 120
4.1 INTRODUCTION 120
4.2 MATERIALS AND METHODS 122
4.2.1 Tendon and Tenocyte Culture 122
4.2.2 Mechanical Loading of Isolated Tenocytes and Tendon Fascicles 123

4.2.3 Immunofluorescence Labelling *125*
4.2.4 Confocal Microscopy and Analysis of Primary Cilia Expression *125*
4.3 RESULTS 127
4.3.1 Isolation of Tenocytes from Tendon Results in Primary Cilia Elongation and Loss of Orientation *127*
4.3.2 Cyclic Mechanical Loading Causes Rapid but Reversible Primary Cilia Disassembly in Isolated Tenocytes *129*
4.3.3 Cell Morphology Does Not Correlate with Cilia Length or Orientation in Cyclically Loaded or Unloaded Cells *132*
4.3.4 Cyclic Mechanical Loading Causes Cilia Disassembly in the Fascicular Matrix Region of the Tendon *137*
4.3.5 Mechanically Induced Cilia Disassembly in Tenocytes is Mediated by TGFβ and HDAC6, Independent of Actin Changes *138*
4.4 DISCUSSION 142
5 ROLE OF PRIMARY CILIA AND MECHANICALLY-INDUCED CILIA DISASSEMBLY IN TENOCYTES 147
5.1 ROLE OF MECHANICALLY-INDUCED CILIA DISASSEMBLY ON MECHANOSIGNALLING 147
5.1.1 Introduction *147*
5.1.2 Methods *148*
5.1.3 Results *151*
5.1.4 Discussion *153*
5.2 ROLE OF IFT88 ON TENDON CILIA EXPRESSION AND MECHANOSIGNALLING 154
5.2.1 Introduction *154*
5.2.2 Methods - IFT88 siRNA Transfection and analysis of cilia expression *155*
5.2.3 Results *157*
5.2.4 Discussion *159*
6 EFFECTS OF CYCLIC LOADING ON TENDON FASCICLE COLLAGEN STRUCTURE 161
6.1 INTRODUCTION 161
6.1.1 Fast Fourier Transforms *162*
6.1.2 Fractal Dimension *163*
6.2 METHODS 165
6.2.1 Sample Preparation *165*

6.2.2 Fast Fourier Transforms *165*
6.2.3 Box Fitting Method (Fractal Dimension) *169*
6.2.4 Testing Fourier Transform and Dimensionality Methods *171*
6.3 RESULTS 171
6.4 DISCUSSION 174
7 DISCUSSION 177
7.1 LOADING REGIMES AND MODEL SYSTEMS 177
7.1.1 Rat Tail Model *177*
7.1.2 Isolated human cell model *178*
7.1.3 Loading Regimes in Isolated cells *180*
7.2 HETEROGENEITY OF CILIA EXPRESSION IN TENOCYTES 182
7.2.1 Cilia Length *182*
7.2.2 Cilia Orientation *183*
7.3 MECHANICALLY INDUCED CILIA LENGTH CHANGES 184
7.3.1 Mechanism of Cilia Disassembly by Mechanical Load *184*
7.3.2 Modulation of TGFβ signalling *186*
7.4 OTHER PATHWAYS WHICH MAY BE REGULATED BY CILIA DISASSEMBLY 188
7.4.1 Downstream effects of length changes *188*
7.4.2 Tendinopathy *189*
7.5 FURTHER WORK 190
7.6 CONCLUSION 192
REFERENCES 194

List of Figures

Figure 1: Schematic showing the hierarchical structure of tendon 24

Figure 2: Fibrillar knots/crimps/kinks 25

Figure 3: Fibril and molecular sliding 27

Figure 4: Crimp waveform in tendon fascicles 28

Figure 5: Representative stress strain curve 30

Figure 6: Tubulin microtubule 55

Figure 7: Cilia Structure 57

Figure 8: Cilia and the cell cycle 58

Figure 9: Schematic of retrograde and anterograde IFT 60

Figure 10: TGFβ signalling pathway 64

Figure 11: Schematic showing calculation of hysteresis 77

Figure 12: Schematic showing the calculation of stress relaxation over cycles 77

Figure 13: Schematic showing the IFM testing set up 78

Figure 14: Custom static strain chamber 79

Figure 15: Custom cyclic strain chamber pictures and cross section schematic 80

Figure 16: Relative cellular activity after 24, 48 and 168 hours for 4% static strain and stress deprived rat tail tendon fascicles 81

Figure 17: Figure showing cut-through schematic of the FlexCell system, collagen coated flex cell plates and 'arctangle' posts. 82

Figure 18: Schematic showing the operation of a confocal microscope compared with a standard flourescence microscope. 84

Figure 19: Bovine tenocytes with cilia *88*

Figure 20: Figure showing cilia in stained with ARL13b in green and DAPI stained nuclei in blue. *95*

Figure 21: Schematic showing the plane in which confocal images of rat tail tendon fascicle were taken. *97*

Figure 22: Diagrammatic visualisation of Equation 1 ..... *98*

Figure 23: Example ellipses of tenocyte nuclei *99*

Figure 24: Under stress deprivation cilia length increases more in the inter-fascicular matrix than in the fascicular matrix. Under static strain the cilia length is partially conserved *108*

Figure 25: IFM cell nuclei are significantly rounder than those in the FM *109*

Figure 26: Stress deprivation time course shows that initially cilia length increases similarly in FM and IFM cells up to 24h but after 1 week IFM cell cilia are significantly longer than FM cell cilia *110*

Figure 27: Under stress deprivation there is significant increase in viscoelastic behaviour *111*

Figure 28: Stress deprivation does not cause significant loss of quasi static mechanical properties in fascicles *112*

Figure 29: The inter-fascicular matrix shows a significant reduction in failure strength after stress deprivation *113*

Figure 30: Treatment with Il-1 does not significantly change the length of fascicle or IFM tendon cell cilia *113*

Figure 31: Isolated tenocytes express elongated cilia without any predominate orientation *128*

Figure 32: Cyclic tensile strain (24 hours 3%, 1Hz) does not cause cilia or nucleus reorientation in isolated human tenocytes *130*

Figure 33: Cyclic tensile strain of isolated human tenocytes leads to progressive disassembly of primary cilia over time *131*

Figure 34:Cyclic strain leads to increased nuclear roundness.....133

Figure 35: There is no correlation between cilia length and nuclear aspect ratio or area regardless of strain duration.....134

Figure 36: There is no correlation between cilia orientation and nuclear aspect ratio or orientation, regardless of strain duration.....135

Figure 37: There is no correlation between nuclear orientation and nuclear aspect ratio, regardless of strain duration.....136

Figure 38: Cyclic tensile strain leads to cilia disassembly in situ within tendon tissue.....138

Figure 39: Cilia disassembly induced by cyclic strain is not caused by changes in actin tension.....140

Figure 40: Cilia disassembly induced by cyclic strain is caused by activation of TGFβ receptors and HDAC6.....141

Figure 41: Schematic diagram showing proposed pathway through which cyclic mechanical loading regulates primary cilia expression to control tendon matrix turnover.....146

Figure 42: Gene expression $\Delta\Delta$Ct with respect to untreated unloaded controls, for (a) ADAMTS5, (b) MMP1, (c) Col1A1 for tenocytes treated with Tubacin or the TGFβ receptor inhibitor over a 24h period with and without cyclic strain.....152

Figure 43: Representative images of human tenocytes treated with SiGlow to quantify transfection efficiency.....157

Figure 44: Primary cilia length does not change with IFT88 transfection.....158

Figure 45: Western blot showing IFT88 levels 48 and 72 hours after transfection for control, SiRNA transfection and scramble.....159

Figure 46: Representative examples of FFTs of sine waves.....162

Figure 47: In this illustration the coast of Great Britain is assessed for dimension using the box-counting method.....164

Figure 48: Figure showing (a) confocal images of fascicle collagen and IFM collagen labelled with DTAF and (b) respective Fast Fourier Transforms. *167*

Figure 49:Representative images showing DTAF images of collagen above tiled thresholded FFT sub images *168*

Figure 50: A DTAF image of the FM (left) and the IFM (right) above circular frequency distribution plots of directionality *169*

Figure 51: Shows an example of using the box fitting method to calculate fractal dimension..... *170*

Figure 52: Example showing both the FFT directionality plugin (dispersion) method and the box fitting (fractal dimension) method applied to a strained and unstrained fascicle image stack..... *172*

Figure 53: Mean dispersion (top) and fractal dimension (bottom) values for unstrained and cyclically loaded tendon fascicles in both the IFM and the FM *174*

List of Equations

Equation 1: Reconstructing Cilia Length from an Image Stack.....*98*

List of Tables

Table 1: Comparison of fascicle mechanical properties across different species *31*

Table 2 : Metabolic response of tenocytes to loading, showing families and signalling pathways affected. *47*

Table 3: Summary of cyclic loading gene response investigations in tendon. *50*

Table 4: Comparison of proteins in IFT complexes A and B *59*

Table 5: Summary of cilia length measurements in tendon tissue *68*

Table 6: Composition of the 5 different culture mediums used during experimental work. *73*

Table 7: Table of fixation and imaging methods used for tendon cilia imaging in previous papers. *89*

Table 8: Fixative lengths and antibody concentrations. *90*

Table 9: Shows fixation durations, antibody concentration, and permeabiliser concentrations and durations for the RTT staining test. *91*

Table 10: Shows fixation durations, antibody concentration, permeabiliser concentration and duration for the RTT staining test. *92*

Table 11: Shows fixation durations, antibody concentration, permeabiliser concentration and permeabiliser durations for the RTT staining test with methanol. *94*

Table 12: Experiments performed during this study. *106*

Table 13: Showing the conditions used to examine the role of mechanically induced cilia disassembly on tenocyte mechanosignalling. *148*

Table 14: Showing details of the primers used for each gene tested in this experiment. *151*

1 Literature Review

Tendons attach muscle to bone, allowing the transmission of force and thus movement[1]. The structure and function of tendons has been studied extensively. However, their complex hierarchical structure and viscoelastic mechanical properties, whilst well suited to meet their functional needs, lead to challenges in fully understanding tendon mechanics.

Tendons experience complex strains in vivo, and tendon cells, known as tenocytes, are responsible for repairing and rebuilding tendon in response to strain induced damage. However, there can be imbalances in damage and repair, and thus tendon injury and disease are common. While the aetiology, nomenclature and treatment of tendon diseases have all been widely debated, chronic degenerative tendon disease, now widely defined as tendinopathy, is common and difficult to treat, with poor prognosis[2–4].

The primary cilium is a cellular organelle which protrudes from the cell body and exists, singularly, on most mammalian cells. Initially thought to be vestigial, over the last 25 years it has been found to be vitally important for a number of physiological processes. Furthermore, diseases of the cilia, termed ciliopathies, have been found to be responsible for a number of serious diseases, most notably Autosomal Dominant Polycystic Kidney Disease (ADPKD)[5]. The primary cilia has also been shown to be involved in mechanotransduction[6–8], and is therefore of particular interest in mechanoresponsive tissues such as tendon.

It has been established that tendon cells express primary cilia and that they respond to changes in mechanical stimulation[9]. However, there is a dearth of information concerning the implications for tendon mechanobiology. This thesis focuses on these

areas, covering tendon and their cilia, specifically focussing on research needs in cilia tenocyte mechanobiology.

1.1 Introduction to Tendon

The function of tendons, to transfer muscle force to bone, has been known since antiquity, and was described by Herophilius in the 3rd century BCE[10]. By the 1920s, with the aid of microscopes and embedded sectioning, it was understood that tendon was made up of collagen fibrils which themselves formed sequentially larger structures, now called fibres and fascicles[11]. The hierarchical structure of tendon was further expanded by Elliot in the 1960s and the seminal studies into tendon composition were done by Kastelic in the late 1970s[12,13]. Despite this, there is still some debate over tendon hierarchy and organisation.

All tendons attach muscle to bone. However, there are 2 major divisions of function; tendons whose primary role is to position the limbs, such as the tendons in the hand which position the fingers, and tendons whose primary role is in the storage and release of energy, like a spring, to enable more efficient locomotion[14]. A notable example of the energy storing tendon is the Achilles tendon. During one legged hopping, the Achilles absorbs energy when landing which is released during the lift off phase, contributing 16% of the mechanical work in the hop[14]. To meet different positioning and energy storing needs, tendons have different specialised mechanical properties which are themselves a function of altered structure[15–17]. Positional tendons need to be strong, more inextensible and be able to maintain high levels of static loading. Energy storing tendons need to be more extensible, resistant to multiple cycles of large transient loads and be energy efficient, with lower hysteresis[14].

Stress strain curves for tendon were first published in the 1960s[18,19]. The curves showed an initial phase during which there is minimal increase in stress, known as the toe region. Following this there is a progressive uptake of stress through the heel region, followed by a linear region in which stress increases linearly with strain[18]. Eventually the tendon reaches a point at which it cannot sustain further stress and will either fail or creep to failure depending on the strain rate. The exact boundaries of these phases vary between tendon type and species but run approximately from 0-3% strain for the toe region and 3-5% strain for the heel region[18]. Failure occurs between 8-25% strain depending on tendon type and strain rate[18,20,21]. This variation in failure strain based on strain rate makes it apparent that tendon is a viscoelastic material.

1.2 Tendon Composition

Tendon, like most soft tissues, is a highly hydrated material composed of around 60-70% water. Of the dry weight around 70-90% is made up of collagen with the remainder made up of elastin, proteoglycans, other proteins and cells, all in varying amounts depending on tendon type[15]. There are also, like in most tissues, numerous inorganic compounds that are required in small amounts for normal cellular function[22]. These include various salts and ions of copper, magnesium, manganese, cadmium, zinc, nickel, lithium, lead, cobalt, silicon, fluorine and phosphorous[23].

1.2.1 Collagen

The human body contains 40-50% protein by dry weight. Collagen is the most abundant protein in mammals and represents around 30% of all protein in the body[24]. Collagen in found in most parts of the body, including cartilage, bone, blood vessels and the cornea. However, it is most abundant in tendon, ligaments and skin, forming around 70-90% of the dry weight of tendon.

Collagen is a family of individual proteins which share certain characteristics. All collagen molecules are made up of a right handed triple helix of long polypeptide chains, known as α-chains[25]. The α-chains themselves are left handed and each collagen molecule can be made up of either, three of the same α-chain (e.g. collagen II & III), two different chains (e.g. collagens I & IV), or three different chains (e.g. collagens V & XI). There are 42 different α-chains which assemble into the 28 different collagen molecules discovered. The most abundant of these is collagen type I which is made of 2 α1(I)-chains and 1 α2(I)-chain. Collagen type I makes up around 90% of all collagen in the body but between 95-98% of all collagen in tendon, with the majority of the remaining few percent made up of collagen type III[22]. Both type I and type III collagen spontaneously bond into fibrils, long thin polymers which provide materials with tensile strength and are the building blocks for many connective tissues in the body. However, some collagen molecules (e.g. XII & XIV) form globules interspersed with their helical regions. These collagens are not well understood but are found in many tissue types in small amounts including tendon.

The diameter of type I collagen molecules has been estimated to be 1.5nm and the length approximately 280nm. Using atomic force microscopy (AFM), Bozec and Horton showed that collagen type I molecules have an average length of 287nm[26], before going on to derive approximate force extension curves for a single type I collagen monomer. They reported non-linear behaviour, with minimal increase in force initially, followed by a rapid uptake of force, essentially a transition from a low modulus to a high modulus state. However, the experiments were ended by the detachment of the molecule from either the AFM probe or the substrate to which it was attached rather than the failure of the collagen molecule[26]. Other methods of approximating the modulus of

tropocollagen have involved Brillouin light scattering and x-ray diffraction, which at small strains have given results in the 3-9GPa range, similar to those found by AFM[27,28].

With the advent of computer models it is also possible to simulate the mechanics of a tropocollagen molecule. Buehler et al suggest an elastic region Young's modulus from 6.99 to 18.82 GPa depending on loading rate[29], whereas Lorenzo and Cafferena calculated the Young's modulus in the low strain region of the curve to be 4.8GPa[30]. At very high strains of around 40% (likely beyond the failure strain of collagen) the Young's modulus from Buehler et al's model was 46.7GPa[30].

1.2.2 Proteoglycans

Proteoglycans are molecules made up of a protein core with one or more attached glycosaminoglycan (GAG) chains. GAGs are long chain polysaccharide molecules. There are many different kinds of proteoglycan, and they fulfil different functions. The properties of a proteoglycan are dependent on both the protein core, the type and number of the GAG chains, and how those chains are structured. Within tendon there are two main types of proteoglycan. Most common are small leucine rich proteoglycans (SLRPs). SLRPs are characterised by short protein cores of 30-50kDa and one or two GAG chains, usually either chondroitin, dermatan or keratan sulphate (CS, DS or KS)[31] and they are termed such because they contain leucine rich regions (LRRs).

The most common proteoglycan in tendon is the SLRP decorin. Decorin has a 36kDa core protein and one DS or CS chain, and occasionally a KS chain in addition. In tendon, decorin is almost always found with a single DS chain. Decorin binds to type I collagen fibrils with the GAG chains projecting perpendicular to the direction of the fibrils. Decorin is important as it inhibits collagen fibrillogenesis and thus stops collagen fibrils from becoming too large, with the size of the DS chain determining the mature diameter

of the fibril[32]. Other SLRPs found in tendon include biglycan, fibromodulin and lumican[31].

The second type of proteoglycans in tendon are large or modular proteoglycans. These have a long protein core (200-400kDa) and a large number of GAG chains (10-100+)[31,33]. The most abundant of the large proteoglycans is aggrecan. Aggrecan has a core protein of around 220kDa and usually contains around 100 long CS chains and up to 60 short KS chains. Aggrecan molecules bind to each other via the long GAG hyaluronan and provide compressive stiffness. The number of KS chains controls how much compressive stiffness is provided and it is thought that areas of tendon which experience compression, such as insertion sites, contain higher levels of aggrecan and the aggrecan contains more KS chains[34,35]. Another modular proteoglycan in tendon is versican which fulfils a similar function to aggrecan and also binds via hyaluronan but is far less abundant[31].

The proportions of the different proteoglycans vary between tendon species and type and may be partly responsible for the variation in structure and mechanics between different tendons[15,31].

1.2.3 Elastin

Elastin is a filamentous protein made up of highly cross-linked thin curled tropoelastin monomers that is found in many connective tissues including tendon. Elastin is characterised by an extremely high recoverable strain capacity of over 100%[36]. Elastin makes up between 1 and 2% of the dry weight of the tendon varying by type and species. The exact purpose of elastin within the tendon is unknown, however, it has been suggested that it plays a role in facilitating elastic recoil in energy storing tendons[15].

1.3 Tendon Structure and Mechanics

Tendon has a complex hierarchical structure as shown in Figure 1. At the smallest level tendon is made up of tropocollagen molecules. These molecules spontaneously attach to each other to form microfibrils and then aggregate into fibrils, the basic collagen unit everywhere in the body. The fibrils are then assembled into fibres, fascicles and finally whole tendons. At each level the collagen fibres are bound by crosslinks or other matrix components. The whole tendon is often surrounded by a sheath, known as epitenon[37].

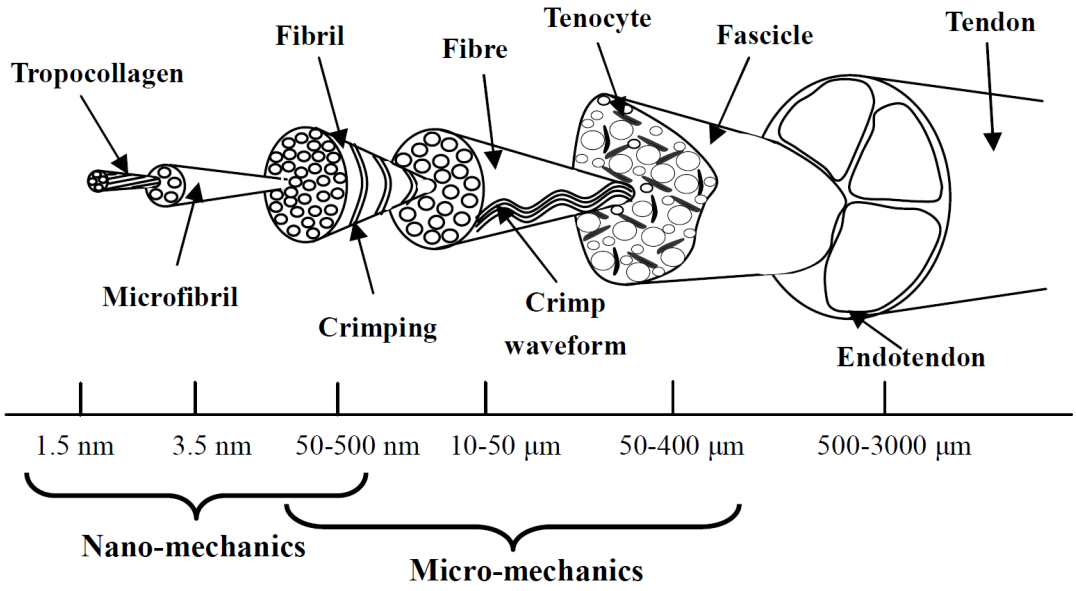

Figure 1: Schematic showing the hierarchical structure of tendon. *From Screen 2012, modified from Kastelic 1978.*

1.3.1 Fibrils

Tropocollagen molecules spontaneously bind to each other, forming collagen fibrils. Collagen fibrils were first described by Bear in 1952 who wrote about their varying sizes[38]. The tropocollagen molecules bind to each other in a regular pattern with each molecule staggered by 67nm with respect to the next. This staggered pattern causes a characteristic banding to appear under x-ray diffraction and the 67nm distance is known as the D-period[29]. Neither the exact mechanism of binding, nor the density of bonds

between the tropocollagen molecules in fibrils is known. Fibrils range in diameter from 50-500nm, with embryonic fibrils being thinner than their mature counterparts due to lateral fusion with ageing[39].

Fibril mechanics have been tested using x-ray diffraction, microelectromechanical systems (MEMS[40]) and computer models[41]. These methods are difficult to compare but give a general idea of fibril stiffness from a toe region stiffness of between 0.3 and 5GPa and a linear portion stiffness of over 10GPa. While fibrils have generally been found to be less stiff than tropocollagen, likely due to the multiple extension mechanisms of collagen stretching as well as collagen sliding, the values are of the same order of magnitude[40].

Fibrils have also been shown to have crimps or knots, small areas where the fibril abruptly changes in direction which are repeated along the length of the fibril. These can be observed using SEM as shown in Figure 2[42].

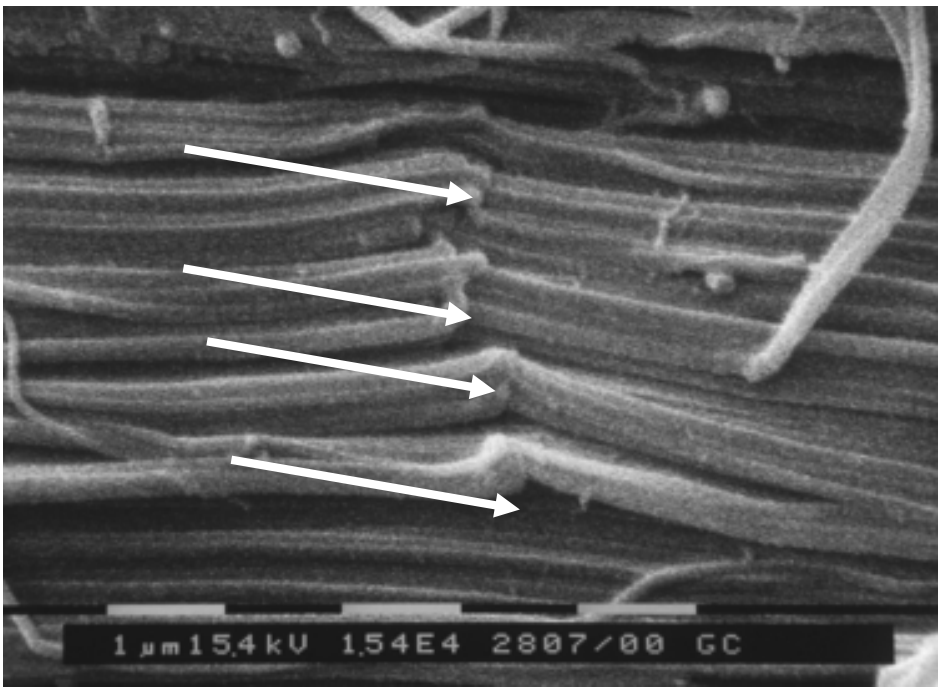

Figure 2: Fibrillar knots/crimps/kinks *from Franchi et al 2010[42]. The white arrows show the crimps.*

1.3.2 Fibres

Fibrils are bound together into fibres by proteoglycans, primarily decorin, which form 'bridges' between the fibrils.

The extent to which these bridges transmit force and the strength of the bond is a contentious area. Studies with chondroitinase B, which breaks down proteoglycans, have demonstrated minimal differences in quasi-static tensile properties between treated and untreated tissue, leading some to hypothesise that the proteoglycans merely act as an interfibrillar lubricant[43]. However, it has been suggested by other studies that the decorin bridges provide mechanical stability and that much of the force is transmitted through the decorin bridges. Indeed, Liu et al used laser tweezers to demonstrate that the binding force of decorin GAG chains is 16.5±5.1 pN suggesting that decorin would be able to transmit force[44].

The diameter of fibrils appears to be regulated by decorin, which inhibits lateral fusion, as well as by a small amount of collagen type V[32]. Knockout models of collagen type V lead to tendons with few correctly formed fibrils and it is suggested that collagen type V crosslinks between fibrillar collagens[45].

A related area of contention is fibril length. If fibrils can be shown to be shorter than whole tendon length, then that would imply that force must be transmitted through decorin bridges. However, if fibrils run the full length of the tendon then it is unlikely that force is transmitted through decorin bridges. It has been difficult to identify fibril ends[46]. Using scanning electron microscopy (SEM) Provenzano et al found no fibril ends in 7275 fibrils in mature tendons over a total length of 2.1mm, although they did find many ends in embryonic tendon[47]. However, this does not agree with models and experimental data which suggest that fibrils are far stronger than fibres[48].

Arguments by adherents to continuous fibrils are that the difference is entirely due to the unkinking of the crimp structure. However, this does not agree with x-ray diffraction data from Sasaki and Odajima which showed that the d-period increased by only 40% as much as the applied fascicle strain, implying that there is relative slippage between entire fibrils[27]. Nor does it fit with the fact that tendons significantly change in cross sectional area and shape from one end to the other. A schematic showing fibril and molecular sliding is shown in Figure 3.

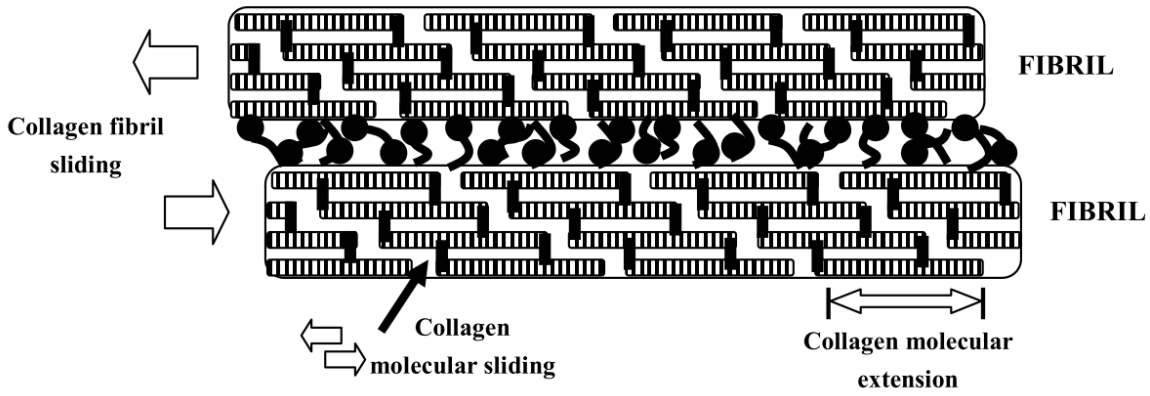

Figure 3: Fibril and molecular sliding, From Screen et al 2009[37]

Using polarising light microscopy Diamant et al showed that fibres have a regular crimp or kink (zig-zag) structure[49]. This crimp waveform appears to be formed by the collective crimping/knotting of all the fibrils in a fibre with the same periodicity. This can be seen in Figure 2 where all the knots line up. Further, these crimps lead to a left-handed helical structure in the fibres. They also showed that the number of crimps in the fibril does not change with age. However, the crimp period becomes longer and the crimp angle decreases in proportion with increasing tendon length. This crimp waveform is thought to give rise to the toe region of tendon mechanics[49].

Mechanical tests of fibres by Miyazaki and Hayashi showed a small strain stiffness of 54.3± 25.1MPa[48]. This shows that fibres are orders of magnitude less stiff than fibrils.

This implies that mechanics are controlled by fibril sliding and is thus controlled by the strength of the proteoglycan, primarily decorin, crossbridges between fibrils as opposed to the strength of fibrils.

1.3.3 Fascicles

Fibres are bound together into fascicles by a sticky proteoglycan and cell rich matrix called inter-fibre matrix. These cells, found between the fibres are crucial for building and repairing tendon and form a major focus for this thesis. Fascicles vary in diameter from 50-500μm depending on tendon age and type[13].

Fascicles appear to have a regular banding pattern which is observable with the naked eye. The banding was shown by Kastelic to be a crimp waveform emerging from that observed in fibres, which is easily observable with light microscopy[13]. Fascicles can also be seen to exhibit a subtle left-handed helical structure which may also derive from the crimp waveform[42].

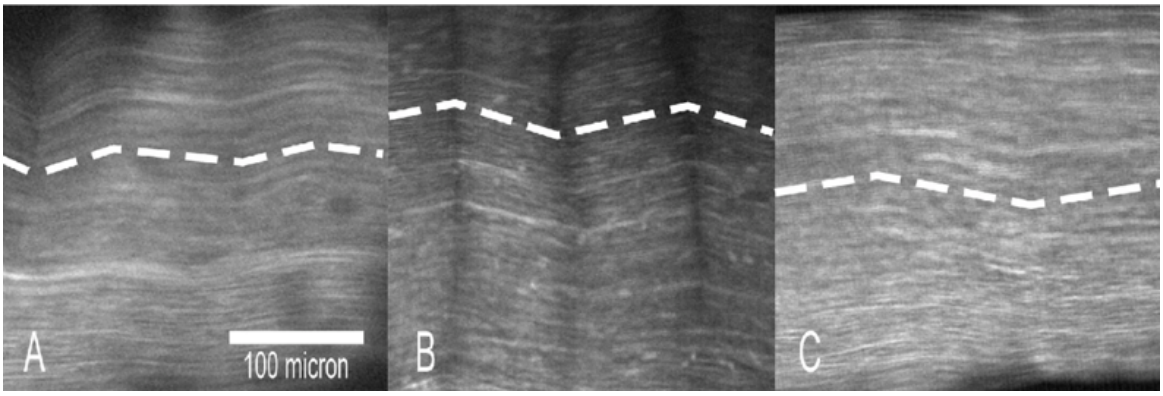

Figure 4: Crimp waveform in tendon fascicles, *from Lavagnino et al 2016*[50].

Much of the work on tendon mechanics has been done at the fascicle level. This is for a few reasons. Firstly, tendon fascicles are relatively easy to dissect. They are also of a size which is easy to work with and straightforward to test mechanically. Further, a large number of fascicles can be obtained from each tendon. One particular fascicle which

has been used extensively is the rat tail tendon fascicle which is particularly simple to dissect and each rat tail gives between 20-40 testable fascicles.

The mechanics of the fascicle can be tested through conventional mechanical testing whereby the object to test is placed between two grips and stretched while force is measured. This allows for the construction of stress strain curves. However, there is a further complication to the mechanics of tendon, in that it is a viscoelastic material, meaning that the rate of strain applied has significant effect on the resulting stress[20].

Some of the earliest work on the mechanics of tendon fascicles was done by Rigby et al in the late 1950s. They found that while the general shape of the curves always contained a toe, heel and linear region, the strains at which these occurred and the stress and strain at failure varied greatly depending upon the strain rate[19]. The existence of the toe region has been suggested to come from the unbending of the crimp waveform. Fascicle crimps have been shown to reduce progressively in both number and angle under strain and to have almost fully disappeared by the beginning of the linear region of the tendon[51]. A representative stress strain curve schematic is shown in Figure 5.

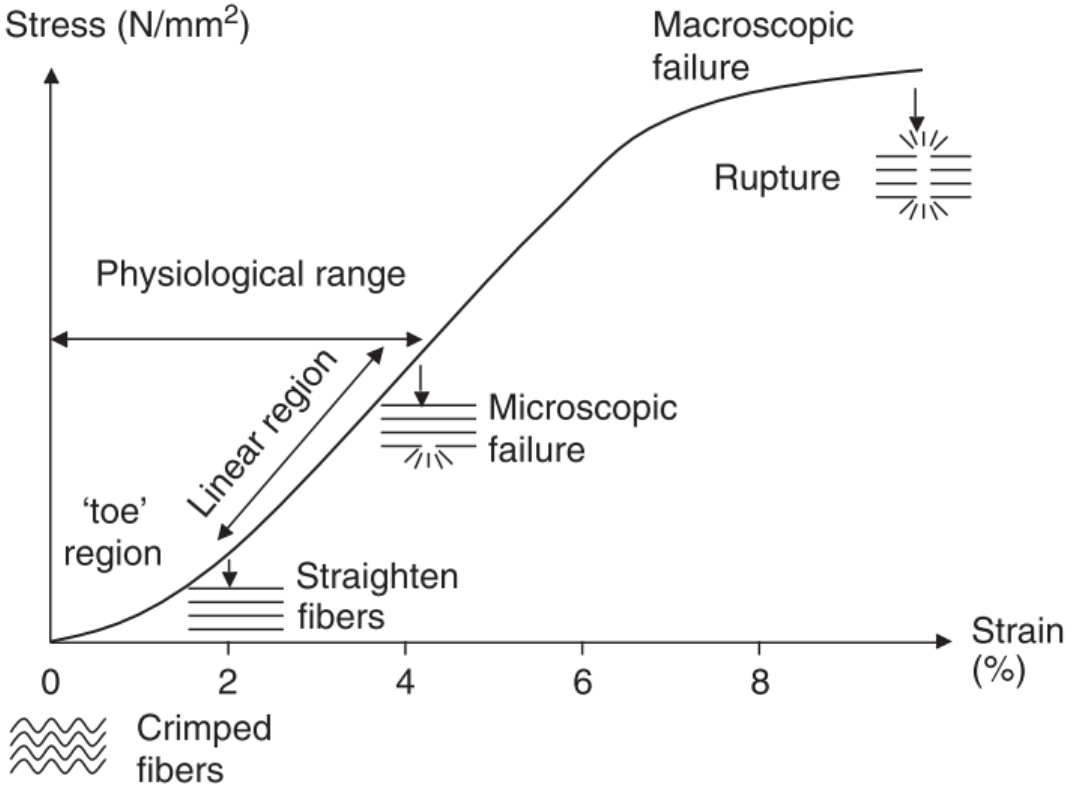

Figure 5: Representative stress strain curve, from Wang 2006[52]

At higher strain rates the modulus and failure force is higher and the failure strain is lower. A further notable viscoelastic property is that of stress relaxation. If the fascicle is strained and then maintained at a constant strain the resultant stress will slowly decrease before stabilising. The amount of relaxation depends on the degree of strain, with smaller strains within the toe region leading to almost complete relaxation and larger strains leading to proportionally less relaxation[53].

Rigby et al also investigated the fatigue properties of rat tail fascicles, showing that small cyclic loads were recoverable whereas at large strains permanent damage was caused by each cycle and the resultant stress at each cycle quickly diminished. Rigby et al attributed the recoverability of fascicles at small cyclic strains to the crimp waveform, suggesting extension became irrecoverable when loading beyond the toe region. However, it was also noted that while small, toe region, strains were recoverable, repeated cyclic strain

for durations of over 60 minutes led to permanent loss of mechanical function in tendon fascicles even at small strains[19].

Interestingly, fascicles from tendons with different functions can have very similar mechanical properties even when the gross tendon has significantly different mechanical properties as seen in the equine SDFT and CDET. A summary of fascicle properties across species is included in Table 1.

It is also important to note that almost all fascicle mechanics tests have been performed after preconditioning, usually the application of one or more small cyclic strains. This is because the first stretch of a tendon fascicle does not appear to be characteristic of that tendon's actual mechanical properties, predominantly due to the water movement and fibre realignment that occurs in the first cycle ex-vivo and to a lesser extent in each subsequent cycle.

Species	Tendon	Linear Modulus	Tensile Strength
Rabbit	Patellar	216 MPa	17.2 MPa[54]
Equine	CDET (positional)	310.24 MPa	40.21 MPa[16]
Equine	SDFT (energy storing)	335.82 MPa	37.43 MPa[16]
Rat	Tail	800 MPa[19]	None Given
Rat	Tail	~600MPa	~12 MPa[55]

Table 1: Comparison of fascicle mechanical properties across different species

1.3.4 Interfascicular Matrix

The interfascicular matrix (IFM), sometimes known as endotenon, is a soft, sticky, highly hydrated matrix which binds the fascicles together. While its composition is not

fully known, it has been shown to have a different proteome from the rest of the tendon and two proteins found in higher concentrations in the IFM than the FM are elastin and lubricin[15]. Indeed, much of the elastin in tendon appears to be localised to the IFM, with the IFM in energy storing tendons containing particularly large amounts[15].

The mechanics of the inter-fascicular matrix (IFM) have not been extensively studied. This is partially because it was historically not recognised to affect tendon mechanics significantly as well as the difficulty in testing it. However, recently it has become apparent that the IFM may play a role in tendon specialisation and further that the cells in the IFM may play important roles in tendon metabolism and mechanotransduction[56]. IFM is significantly less structured than the fascicles it binds and this makes it difficult to test. It is not possible to isolate regions of IFM and test them directly without destroying or damaging the IFM. However, it is possible to test the ability of the IFM to resist the shear forces generated when two attached fascicles are pulled in opposite directions[17]. This has the advantage of somewhat replicating the in vivo mechanics. Further, more general tests include transverse tendon tests which test the IFM as well as the matrix between fibres and fibrils.

Thorpe et al, testing the IFM in shear, found that while the SDFT and CDET had very similar fascicular properties, they had substantial differences in IFM mechanics. In particular, the toe region modulus of the SDFT IFM was significantly lower than that of the CDET. Furthermore, both hysteresis and fatigue resistance were found to be significantly lower. This led to the conclusion that differences in gross mechanical properties between tendons are strongly controlled by differences in inter-fascicular matrix, rather than differences at the fascicle level. The mechanism by which the IFM controls gross tendon properties is likely through the facilitation of fascicle sliding, with the stretchy elastic IFM allowing recoverable fascicle sliding in energy storing tendons,

while the stiffer, less elastic IFM in positional tendons restricts fibre sliding[17]. This also provides further evidence that fascicles, and therefore also the smaller collagen subunits, are discontinuous throughout the tendon.

1.3.5 Tendon Sheath

The tendon sheath, sometimes called the epitenon, is a protective layer surrounding the whole tendon. It is particularly relevant in tendons which have to go around corners such as those in the hand, where it provides a channel in which the tendon can slide. It contains primarily synovial cells and is well vascularised. In other tendons it may not exist or may merely be a layer of very loose IFM and is much less well defined[57].

1.3.6 Modelling Tendon Mechanics

Utilising data from studies of tendon mechanics, numerous mathematical or computational models for tendon and fascicle mechanics have been created. These can be useful for understanding how small changes in micro-structure can affect mechanics at a tissue level. Such models enable data to be scaled across different tendon type and species and to examine the effects of localised damage or collagen disorganisation. Furthermore, these computational models have the potential to reduce the use of experimental animal studies as well as allowing the ability to examine the contribution of individual parameters.

The earliest tendon models were mathematical models, which approximated the mechanical properties of the tendon. The foundation for many of these models was the quasilinear viscoelastic (QLV) model developed by Fung et al in the 1970s[58], This dramatically improved the accuracy compared with simple linear-elastic models which did not fully capture the complex viscoelastic properties of tendon. More recent tri-

phasic models have been further refined by including interstitial fluid flow although their accuracy is dependent on the nature of the loading conditions [59–62].

A second type of modelling operates by modelling collagen fibrils or even fibres and building a fascicle or tendon model out of the individual components. This allows for the incorporation of properties such as crimp into the model. The underlying fibril models are usually based on linear-elastic, bi-linear elastic or QLV models. The fibrils can be built into fascicles by using probability distribution functions (PDFs) to determine the orientation of each fibril[63,64]. These models can be modified by including the interfibrillar matrix which is generally modelled as a substrate in which the fibrils are contained[64–66]. A further enhancement of these models is the modelling of proteoglycans such as decorin binding the fibrils. In some cases the fibres are modelled as discontinuous with force being transferred through crossbridges enabling fibre sliding [64,67], but in other cases fibres are modelled as running the full length of the tendon[64,67].

An alternative to mathematical modelling methods are computational methods. These include finite element modelling, generally done on a whole tendon scale, and often utilising detailed 3D ultrasound scans of tendon. These are often combined with whole joint modelling approaches and allow for an understanding of stress concentrations within specific tendons[64,68].

Computational methods also enable fibril or fibre-based mathematical models to be created without the need for PDFs, utilising modern computational power to calculate all of the forces in each fibril and the complex interactions between them. These methods allow for many changes of structure and composition, such as fibril diameter, to be investigated[64,69,70].

Despite all the advances in mathematical and computation modelling of tendon biomechanics, a significant challenge remains in incorporating the biological effects due to the response of the living cells within the tendon. This will require new multidisciplinary approaches as well as a thorough understanding of the underpinning mechanobiology.

1.3.7 Cells in the Tendon

Tendon cells, known as tenocytes, are the primary cell type found in tendon and like the cells of most other structural tissues, derive from mesenchymal stem cells.

Other cells that are present in small numbers in the tendon include mesenchymal stem cells, synovial cells, nerve cells, endothelial cells, chondrocyte like cells and smooth muscle cells[71]. These cells are mostly present in the vascularized areas of the tendon and the tendon sheath.

While tenocytes have historically been considered to be a single population it has recently been suggested that the cells found inside fascicles are distinct from those found in the inter-fascicular matrix between fascicles. Tenocytes within the fascicle matrix are long spindle shaped cells with elongated nuclei which run along and parallel to the fibres[72]. The IFM by contrast has a much higher concentration of cells than the fascicle matrix, which could suggest increased cellular activity in the IFM compared with the FM. Further, the cells in the IFM are more rounded and do not align in rows like the cells in the fascicle[73]. It is unclear whether these cells constitute a second population or whether the differences are due to differences in the matrix. This could have implications for disease, tissue remodelling and load response.[74].

Tenocytes, both those in the FM and IFM, are responsible for the synthesis of collagen and proteoglycans although the balance of responsibility is not wholly clear. Tenocytes are also responsible for the production of the proteases which facilitate matrix turnover as well as all other matrix components. As such, tenocytes are responsible for the repair of damage to the tissue. Tenocytes have numerous cellular protrusions, allowing them to form a 3D network, both along the direction of the collagen as well as through the collagen. It is this 3D network which allows the cells to deposit collagen in the correct 3D shape during development[39]. At the connection between the cellular protrusions are numerous GAP junctions facilitating cell communication[75,76]. The number of tenocytes in a tendon varies with age and tendon type, with younger tendons and tendons which experience a higher strain in vivo having a higher cell density per mm^2 cross section[77].

It has been difficult to identify the phenotype of tenocytes reliably, as the distinctions between tendons and other MSC derived cells are not easily attributable to any single set of genes. This is further exacerbated by the fact that the tenocyte phenotype is likely heterogeneous. A number of tenocyte markers have been proposed. However, none of these has been found to be totally tenocyte specific. In a study by Taylor et al in normal tensional adult tendon, COL1A1, scleraxis and tenascin-C were found to be the best candidates for tenocyte phenotype markers[78,79]. While individually each marker shared expression profiles with other tissues, the combination of high COL1A and scleraxis and low tenascin-C appears to be tenocyte specific[78].

Tenocytes, as would be expected from a tissue which regularly undergoes considerable cyclic strain have been shown to be mechanosensitive and respond to applied longitudinal and shear strains[80]. This response is likely to be part of the adaptive

mechanism for repairing tendon damage and will be explored in more depth later in the discussion.

1.3.8 Proteoglycans

Proteoglycans have been discussed briefly in how they influence tendon structure, such as decorin controlling collagen crosslinking and fibril diameter[31], however, tendon has numerous proteoglycans many of which have effects on tendon structure and function. For instance, the higher levels of proteoglycans found in the IFM likely relate to its soft and sticky properties, further, differences in the amounts of proteoglycans between the IFM of different tendon types may be the cause of some of the variation in mechanical properties [15,56]. Decorin is the most abundant proteoglycan within tendon, however other proteoglycans are also present and important. Biglycan binds collagen fibres together, fibromodulin binds to collagen I and promotes the formation of large fibrils[31]. Lumican, like decorin inhibits the size of collagen fibrils[31]. Aggrecan and versican, the globular proteoglycans, provide resilience and viscoelastic properties, and are both found with more abundance in the insertion points of the tendon[31]. Aggrecan and versican can form large aggregates with hyaluronic acid. The negative charges of the glycosaminoglycan (GAG) side chains repel each other and attract water such that the macromolecule forms an expanded brush shape. This inherent swelling pressure provides tendon with its compressive properties and explains their relative abundance in areas of tendon which experience compression[81]. Furthermore, when under compression these molecules give up their water which is one of the reasons that tendon has a high poisson ratio >0.5. The complex role of many of these proteoglycans in tendon structure and mechanics are not yet fully understood[31,81].

1.3.9 Whole Tendon

While fascicles are broadly similar in structure between species and tendon type, the aggregation of fascicles and IFM into whole tendon gives rise to numerous different shapes and sizes of whole tendons. Moreover, while fascicles from different species often look very similar whole tendons can vary by many orders of magnitude both between species as well as within one individual.

In some tendons, such as rat tail tendon, fascicles are clearly visible, all of different lengths and serially attach to the spine in order to flex the tail[82]. In many ways rat tail fascicles are functionally indistinguishable from miniature tendons. However, in other tendon types fascicles can be less easily distinguished from each other and the lengths of the fascicles are less clear. Sectioning and imaging studies have suggested that the fascicles fuse, bifurcate and have discontinuities within tendon[83]. This makes intuitive sense since neither the cross sectional area nor the shape of most tendons is constant along the length of the tendon.

Whole tendons have mechanical properties that are broadly similar to the mechanical properties of fascicles in the sense that they show a toe, heel and linear regions and also show the same broad viscoelastic trends[16,84]. However, tendon mechanical properties are also closely tied to their function and as such their mechanics vary between species and function far more than at any of the smaller hierarchical levels, fascicles included. Elastic energy storing tendons, such as the Achilles or SDFT have low hysteresis, lower stiffness and higher strain to failure than similar positional tendons[16]. Further, it is interesting that different but related tendon types often also have similar fascicle mechanics even while the whole tendon mechanics differ. For example, Thorpe et al showed that while the equine SDFT and CDET have similar fascicle stiffness (336 and 310 MPa respectively)

they have very different whole tendon stiffness (614 and 1012 MPa respectively)[16]. These differences in whole tendon mechanics, when fascicle mechanics are quite similar suggests a role for IFM in determining whole tendon mechanical properties[16].

1.3.10 In Vivo Strain

Understanding the mechanical properties of ex-vivo tendons is crucial to understanding tendon function. However, tendons operate within the body, and understanding the range of physiological stresses and strains that tendons are under within the body is vital to understanding how they respond and adapt to those loads.

During in vivo tests of the human Achilles, using electrical muscle stimulation to stretch the tendon and ultrasound to measure strain, whole tendon strains of 0.7-2.5% were observed[84]. However, these purely muscle generated strains are substantially smaller than those observed during the one legged hopping tests by Lichtwark et al, who, using ultrasound, observed an average peak strain of 8.3% across subjects and the peak strain in one subject as high as 11.4%[14]. This difference in maximum strain between muscle generated strain and impact generated strain suggests that the in vivo strain experienced by energy storing tendons is significantly higher than that experience by positional tendons which are stretched entirely by muscle contraction.

Unfortunately, this does not tell us what strains are experienced by the cells in tendons, although it can be assumed that those experienced by the cells in energy storing tendons will be higher than those in positional tendons. It seems likely that the cells in tendons experience longitudinal strain from the stretching of the tendon, as well as potential shear strains from fibre or fascicle sliding. It is also likely that the tensile and shear strain profile experienced by the cells will vary between the FM and the IFM as well as between tendon types. While it seems likely that the cells of the FM experience predominantly

longitudinal strain, along with perhaps some lateral compression due to the thinning of tendon due to water evacuation under strain, the cells of the IFM are likely to experience more complex strain profile due to the shear forces on the IFM due to fibre sliding as well as the lack of predominant orientation of IFM cells. These differences are likely key to understanding the response of tenocytes to applied strains.

1.4 Tendinopathy

1.4.1 Tears, Tendinitis, Tendinosis and Tendinopathy

Tendon injuries and disease are common and notoriously difficult to treat[2,85]. Furthermore, there are a range of different injuries as well as debate over the terminology used to describe those injuries. The simplest to understand and least controversial is the tear or rupture. Tears generally come in two varieties, partial and full thickness. A partial tear is where the tendon has been torn but has not completely snapped. This tear can be transverse or longitudinal, when it is also known as a delamination[86]. Tears are commonly caused by trauma, which is a fairly unambiguous cause. However, some tears are spontaneous and there may be other associated pathologies. Tendon injuries due to trauma are particularly common in the hand and are the second most common type of hand injury forming 29 percent of hand injuries in a study of 50,272 Danish A&E admissions[87]. Of those, most are open traumatic injuries to the flexor or extensor tendons. Other tendon injuries caused by external trauma are sheath injuries usually caused by crushing as well as avulsions[88].

Tendonitis was the original name given to painful degenerative tendon disease, due to the common symptom of increased tendon size, which was assumed to imply inflammation. However, this name fell out of favour due to debate as to whether there is inflammation in chronic tendon disease, and at what stage of the healing process any

inflammation may occur. Initially the term tendonitis was replaced with tendinosis, however this was quickly replaced by the name tendinopathy which merely means disease of tendon and is now the most widely used terminology in tendon disease literature due to its lack of specificity[3]. Tendinopathy is characterised and diagnosed primarily by chronic pain[3]. However, other common symptoms include swelling, stiffness and reduced strength[89,90]. In severe tendinopathy the tendon sometimes forms adhesions to the surrounding surfaces which cause loss of function. While tendinopathy can affect the whole tendon it is usually more localised, either in the mid portion of the tendon or at the insertion point where the tendon attaches to the muscle or bone[85,91]. However, the variation and nuance between different regional tendinopathies is beyond the scope of this review[92].

Histologically, tendinopathic tendons are characterised by disorganised collagen fibres with particularly large diameters as well as increased cellularity[3]. Furthermore, tendinopathic tendons are more likely to suffer tears and ruptures, complicating the diagnosis of non-tendinopathic tears and ruptures[88].

1.4.2 Risk Factors

The cause(s) of tendinopathy are not well understood, but, tendinopathy is now generally considered to be an overuse injury.

A study of tendinopathy among former Olympic athletes by Kujala at al found a lifetime incidence of 23.9% (n=785) compared with 5.9% in a non athlete control (n=416)[93]. The incidence was especially high, 52% and 36%, for long and short distance runners respectively (n= 99 & 94). The injury known as tennis elbow, tendinopathy of the tendons on the lateral epicondyle, is common among tennis players as well as manual workers who make repeated motions with tools such as hammers[94]. However, despite

the exceptionally high incidence in athletes and those who perform repeated strenuous motions, tendinopathy also affects a vast number of people who perform strenuous physical activity only occasionally or not at all[95]. Furthermore, some tendinopathies are associated with a lack of physical activity. One interesting example is rotator cuff (supraspinatus) tendinopathy, which is associated with both overuse and underuse. It is particularly common in baseball players and swimmers who have overused the tendon as well as older sedentary people, where it has been underused[95,4].

Probably the largest risk factor for tendinopathy, regardless of activity history, is age, and it has been found that most tendinopathies occur in people in late middle age[85].

1.4.3 Cause, Mechanism and Pathology

Despite broad agreement that tendinopathy is a load-associated disease, the exact cause, mechanism and pathology of tendinopathy is not well understood and there are many theories. There are three main, and not necessarily mutually exclusive, hypotheses for how tendinopathy occurs, 'overload', 'changing load' and 'stress deprivation'[,4,73,96–98]. During normal function tendon cells break down damaged collagen and synthesise new collagen. The overload hypothesis suggests that there is a point beyond which the tenocytes are unable to repair the continual micro-damage accumulated during use[74,99]. Since cell activity and turnover is higher in younger tendons this may explain the increased incidence of tendinopathy in older people[22,93]. The second hypothesis, proposed by Jill Cook, is that tendinopathy is a pathology in which sudden changes to loading cause an improper cellular response and this causes tendon to progress down the tendinopathy continuum with further changes to loading exacerbating the tendinopathy[4]. For example, an athlete coming back from the off season and going straight back to full intensity has a higher chance of injury. This is well understood as a

cause of a wide range of physical issues in professional and amateur sports and therefore programmes to build up intensity are widely used[93]. A potential mechanism, consistent with both hypotheses described above, has been suggested, in which overload causes micro-damage which leads to areas of micro stress-deprivation within the tendon and it is these areas of stress deprivation which initiate tendinopathy[100].

All of these hypotheses are consistent with a study that has shown evidence of tendinopathy after forced overload of rat supraspinatus tendon in vivo, achieved by high levels of forced exercise[101]. Further, Andarawis-Puri et al showed that in-vivo cyclic loading of rat patellar tendons led to damage, and that with enough cycles the cellular response shut down[102].

It is possible that tendinopathy is caused by a combination of overload and changes to load, with both initiating disease in certain circumstances. However, all hypotheses suggest that, regardless of specific mechanism, tendinopathy is a cell mediated pathology and thus the cellular response to loading is of crucial importance.

1.4.4 Stress Deprivation

Stress deprivation, also known clinically as stress shielding is where the applied load on the tendon is either removed or is lower than would normally be physiologically expected[103]. Stress deprivation has been shown to significantly affect the tensile strength of tendon[104]. Yamamoto et al showed in rabbit patellar tendons that 2 weeks of 70% stress shielding caused no significant reduction in tensile strength, but did cause a reduction in cross sectional area[105]. It was also shown that 100% stress shielding significantly reduced the tensile strength to below 30% of the initial strength. After 12 weeks of the reapplication of normal stress the 100% stress shielded tendons had recovered to 79% of their original strength. The total strain to failure was not

significantly different in any of the conditions[97,105,106]. It was also noted that as the extent of stress deprivation increased, the proportion of tendons failing at the bone insertion site reduced significantly[97].

Changes in the transverse mechanical properties of stress deprived tendons have also been investigated. Yamamoto et al found significant reductions in the failure stress and tangent modulus of stress deprived tendons. Additionally, they found that transverse stress relaxation was 74.3% for stress deprived tendons but only 45.5% for control tendons[107]. It has also been shown that stress deprivation in vivo leads to increased tendon cross sectional area[106]. As with tendinopathy these changes are cell mediated and therefore it is important to understand how cells respond to stress deprivation, as well as loading.

1.5 Tenocyte Mechanobiology

Tendons experience large amounts of loading daily for an entire human life. Under ex vivo cyclic loading at physiological levels, acellular tendon fascicles quickly fatigue and fail[108]. It is therefore clear that the cells in the tendon are working to continually repair and remodel the tendon as otherwise it would not last for a whole human lifetime. Therefore, the cellular response of tendon cells to loading is vitally important to understanding how tendons repair and remodel. Further, as tendon pathology is highly associated with both cell driven effects and mechanics it is important to investigate tenocyte mechanobiology.

1.5.1 Testing the Metabolic Effects of Loading

Numerous studies have investigated the response of cells to loading, predominantly focussed on changes in gene expression.

There are four main methods by which groups usually apply strain to tenocytes. Cells can be seeded on flexible 2D membranes and then cyclic strain is applied by stretching the membrane. 2D systems have the benefit of well controlled and understood loading parameters as well as allowing for the use of downstream techniques such as immunofluorescent imaging which can be difficult in 3D structures. A second related method is seeding cells into a 3D hydrogel and then applying strain to the hydrogel. This has the advantage of retaining the cells in a 3D structure, which is probably more similar to conditions in tendon. However, the cells are not usually arranged in the same regular pattern as in tendon and it can be difficult to determine the exact strains experienced by the tenocytes as compared with a 2D system. A third method is to directly apply strain to tissue explants, with the advantage that the strains the individual cells experience should better approximate in vivo strains and the cellular environment is the same as in vivo. However, tissue can be difficult to acquire, difficult to work with, and there are limits to the downstream processes that can be applied. Finally, some groups have used live in vivo models where the tendon is used in vivo before immediate euthanasia of the animal and extraction of RNA. However, this requires extensive time consuming live animal work[109,110].

An important challenge when investigating tenocyte strain response is the wide potential variation in the amount, frequency and duration of the applied strain in any experiment. As discussed above, it is still not clear what the range of physiological strains experienced by tenocytes is. Further, even where the strains may be approximately physiological it is important to know whether these strains would exist in normal function or whether they would cross the threshold into the proposed tendinopathy-causing 'overload'. Obviously, methods where tissues are directly strained are easier to match physiologically, but can provide their own specific challenges.

1.5.2 Gene Families Investigated in Tendon Mechanobiology Research

Despite the variations in methods and some contradictory results there are six main families of genes which appear to be mechanoresponsive and are likely to be important in tendon. These are described in Table 2.

Gene Family Name	Acronym	Protein Family
Collagen	COL	The family of genes which make collagen proteins.
Matrix Metalloproteinase	MMP	The MMP family of genes encodes for a group of proteinases. MMPs are responsible for the breakdown of many ECM components including collagens, elastins, gelatine and proteoglycans[111]. MMPs are therefore crucially important for the turnover of ECM and are expressed continually in tendon.
A Disintegrin And Metalloproteinase with Thrombospondin Motifs	ADAMTS	The ADAMTS family of genes encodes for a group of proteinases. There are 19 members of the ADAMTS family and their main functions are cleavage of aggrecan, versican, brevican and neurocan.
Tissue Inhibitors of Metalloproteinase	TIMP	The TIMP family of genes encodes proteinase inhibitors which inhibit the activity of the MMP family of proteinases. There are four members of the TIMP family numbered 1-4 all of which can inhibit any member of the MMP family.
Transforming Growth Factor beta	TGFβ	TGFβ is a cytokine, the activation of which is crucial in the regulation of a number of vital cellular processes including proliferation, differentiation, growth and apoptosis.
Interleukin	IL	Interleukins (IL) are a family of cytokines whose function relates to the immune system.

Table 2 : Metabolic response of tenocytes to loading, showing families and signalling pathways affected.

1.5.3 Summary of Load Induced Changes in Gene Expression

A non exhaustive summary of gene response experiments in cyclically loaded tendon tissue and cells is shown in Table 3.

Gene	Species & Tendon	Load Conditions	Method	Result
COL1A1	Human Achilles isolated cells in 3D constructs	24 & 48h, 5%, 1Hz	RTqPCR	⇑ 2x[80]
	Bovine CDET fascicles	1hr, 7%, 1Hz	RTqPCR	⇑~2-5x [112]
	Rabbit Achilles	8hr/day, 6 days, 0.25Hz, 3/6/ 9% strain	RTqPCR	⇓~2x @ 3%[99] ⇑~2x @ 6%[99] -- @ 9%[99]
MMP-1	Human Patellar isolated cells on 2D microgrooved silicone	4h, 4/8%, 0.5Hz	RTqPCR	⇑ 1.2x @ 4%[113] ⇑ 2.45x @ 8%[113]
	Rat Patellar Isolated cells	1dyn/cm^2, 6h	RTqPCR	⇑[114]
	Equine SDFT fascicles	1800 cycles 2-12% 1Hz followed by 24h static 2% strain	Semi-Quantitative immunostaining analysis	--[74]
	Rabbit Achilles	8hr/day, 6 days, 0.25Hz, 3/6/ 9% strain	RTqPCR	⇑~15x @ 3%[99] ⇑~4x @ 6%[99] ⇑~2x @ 9%[99]
MMP-3	Rat Patellar Isolated cells	1dyn/cm^2, 6h	RTqPCR	⇑[114]
	Human Achilles isolated cells in 3D constructs	24 & 48h, 5%, 1Hz	RTqPCR	--@24h ⇓~8x @ 48h[80]

MMP-3	Equine SDFT fascicles	1800 cycles 2-12% 1Hz followed by 24h static 2% strain	Semi-Quantitative immunostaining analysis	⇑[74]
	Rabbit Achilles	8hr/day, 6 days, 0.25Hz, 3/6/ 9% strain	RTqPCR	⇑~8x @ 3%[99] ⇑~4x @ 6%[99] ⇑~3x @ 9%[99]
MMP-13	Equine SDFT fascicles	1800 cycles 2-12% 1Hz followed by 24h static 2% strain	Semi-Quantitative immunostaining analysis	⇑ 2.3x[73]
ADAMTS-5	Rat tail fascicle	1/24h 2% static +3% cyclic 1Hz Fascicles	RTqPCR	⇓ @ 24h[115] - @ 1h
	Human Achilles isolated cells in 3D constructs	24/48h, 5%, 1Hz constructs	RTqPCR	⇑~2x @ 24h[80] -- @ 48h
TIMP-1	Human Achilles isolated cells in 3D constructs	24 & 48h, 5%, 1Hz 3D constructs	RTqPCR	-- @ 24/48h[80]
TIMP-2	Human Achilles isolated cells in 3D constructs	24 & 48h, 5%, 1Hz 3D constructs	RTqPCR	-- @ 24/48h[80]
TIMP-3	Human Achilles isolated cells in 3D constructs	24 & 48h, 5%, 1Hz 3D constructs	RTqPCR	⇑~4x @24/48h[80]
IL-1β	Rat Patellar isolated cells	1dyn/cm^2, 6h	RTqPCR	⇑[114]

IL-6	Equine SDFT fascicles	1800 cycles 2-12% 1Hz followed by 24h static 2% strain	Semi-Quantitative immunostaining analysis	⇑ 4x[73]
	Bovine flexor fascicles	1h, 7% strain, 1Hz	RTqPCR	⇑~10-100x[112]
$TGF\beta_1$	Human Achilles isolated cells in 3D constructs	24 & 48h, 5%, 1Hz	RTqPCR	-- @24/48h
COX-2	Rat Patellar isolated cells	1dyn/cm^2, 6h	RTqPCR	⇑[114]
	Equine SDFT fascicles	1800 cycles 2-12% 1Hz followed by 24h static 2% strain	Semi-Quantitative immunostaining analysis	⇑[73]

Table 3: Summary of cyclic loading gene response investigations in tendon.

As can be seen from Table 3, the studies investigating tendon response to load use a wide range of methods and tissue types, and this makes comparing them difficult, especially where there are contradictory results. This table is also not comprehensive and only includes commonly investigated genes. A number of other genes have been found to be involved in either tendinopathy or the tenocyte response to strain. These genes only have a small amount of data on their responses, usually from a single study. However, these genes may still be relevant and some might have been overlooked by other researchers. However, a detailed examination of these is beyond the scope of this work.

1.5.4 Transforming Growth Factor beta

While TGFβ expression has not been shown to be regulated by cyclic strain in tenocytes as summarised in Table 3, the activation of the $TGF\beta_1$ cytokine does occur due to cyclic

strain. Jones et al showed that cyclic load induced gene expression changes in MMP1, MMP3, Col1A1 and ADAM12 were caused by the load induced activation of TGFβ$_1$ and that the inhibition of TGFβ$_1$ signalling inhibited the mechanoresponse of those genes[80]. Furthermore, TGFβ has been found to have numerous effects in tendon. TGFβ signalling has been shown to be downregulated in diseased tendon[3], and TGFβ is often involved in wound healing[116], and although exactly what role it may play in tendon healing and repair is not fully understood, application of TGFβ to tendon explants was shown to lead to increased production of collagen I and III[116]. TGFβ has also been shown to bind to and regulate proteoglycan synthesis in tendon[31].

1.5.5 Morphology

Tendon cells, within fascicles, are long spindle shaped cells that run parallel to the fibres, whilst within the IFM are more rounded with no predominant orientation. Despite tendon cells having two distinct and interesting morphologies, there is little characterisation of these cells in situ or after isolation, and little information about isolated cells beyond the fact that isolated tenocytes tend to have a rounder shape more akin to that of IFM tenocytes than FM tenocytes[73,79].

In vivo studies indicate that increased cellularity and cell roundness is characteristic of tendinopathy and can be used as a diagnostic factor for tendinopathy[3]. Further, studies have shown increased nuclei roundness after forced in vivo overload of rat achilles[96].

A comparison between the CDET and SDFT tendons of active and inactive horses found no difference in cellularity or morphology of either fascicle or IFM cells[77]. However, a study using SDFT explants found that applying high levels of cyclic loading, designed to mimic chronic overload, led to increased cell roundness[73].

1.5.6 Stress Deprivation

The cellular response to stress deprivation has also been widely studied. Stress deprivation can occur for numerous reasons in tissue including trauma and tumours, and stress deprivation has been shown to cause mechanical degradation of the tendon (loss of strength and stiffness)[105,117], and the expression of genes that are associated with tendinopathy. This latter observation has led some to suggest that tendinopathy is caused by microtears in tendon leading to localised stress deprivation[100]. Most studies of stress deprivation either use in-vivo models where a limb is splinted to deprive or 'shield' the tendon from strain[97,105]. Alternatively to live studies, tissue explants can be cultured in an unconstrained stress deprived state[9].

In vivo experiments have repeatedly shown significant reduction in mechanical integrity compared with non stress deprived tendons. Majima et al investigated both partial and complete stress deprivation of rabbit patellar tendons in vivo. They found that completely stress deprived tendons had significantly lower tensile strength and tangent modulus after 1 week, with both parameters continuing to decrease over the 12 weeks[97]. Partial stress deprived tendons had significantly lower tangent modulus after 1 week, however, the modulus did not reduce further. Partially stress deprived tendons also had significantly lower tensile strength after 2 weeks which did not decrease further[97].

A study by Uchida et al showed, using immunofluorescent staining, that after 2 and 6 weeks of complete stress deprivation of rabbit patellar tendons, IL-1β, TGFβ and TNFα were up-regulated. They also showed that stress deprivation in vivo leads to increased cellularity[118]. Northern blot analysis of stress deprived ex-vivo rat tail fascicles showed an up-regulation of MMP-1 which was significantly inhibited by the application of static strain[119]. IL-1β antagonists have been used as a treatment for tendinopathy and

have been shown in vivo to slightly reduce the mechanical degradation effects of stress deprivation. However, it is important to note that there was still substantial and significant mechanical degradation in the IL-1β antagonist treated samples[120].

A study by Thornton et al found stress deprivation led to increased expression of MMP-3, MMP-13 and TIMP-2 while hydrostatic compression did not significantly change MMP-3 or TIMP-2 expression and only elevated MMP-13 in one of the tissues investigated.

1.5.7 Tendon Mechanosensation

There are many mechanisms by which cells can 'detect' strains, including longitudinal, compressive, hydrostatic and shear. These include cytoskeletal structure changes, focal adhesions and integrin mediated TGFβ activation[121].

One particular cellular organelle that may play a role in tendon mechanotransduction, the conversion of mechanical signals to chemical ones, is the primary cilia.

1.6 Primary Cilia Structure

1.6.1 History of Cilia Research and the Discovery of Ciliopathies

Cilia are a class of eukaryotic organelle with a slender microtubule structure approximately 0.25μm in diameter and usually 1-10 μm in length. Cilia typically project from the cell surface and come in both motile and non-motile forms. Primary cilia, the focus of this thesis, are solitary and non-motile, with a single cilium found on almost every cell in the human body.

Motile cilia were first described by Anthony van Leeuwenhoek around 1674-75 as "incredibly thin feet, or little legs, which were moved very nimbly". He was using one

of the earliest microscopes and it is thought he was seeing ciliated protozoa[122]. The first person known to have called them cilia (meaning eyelashes in Latin) was Otto Friedrich Müller, in his 1786 illustrated book on Infusoria (minute aquatic animals)[123]. Non-motile cilia are first thought to appear in literature in a 1867 paper by A. Kowalevsky[122,124]. They were first identified in humans by Zimmermann who found them in thyroid epithelial cells. Zimmermann, in his 1898 paper, suggested that they may have a sensory function. The prevailing view for a long time after this was that the non-motile cilia were vestigial and little further work was done for over half a century and it was not until 1968 that non motile cilia were named 'Primary Cilia' by Sorokin et al[125]. They had previously been referred to as rudimentary, modified or vestigial cilia.

In the 1990s and early 2000s, functional roles for the primary cilia were found, due to the identification of genetic 'ciliopathies' as the cause of numerous systemic diseases. The first discovery was that cilia were necessary for proper renal development and that mutations in genes controlling two ciliary proteins lead to polycystic kidney disease (PKD)[5]. PKD is a genetic disease which leads to large cysts growing on the kidneys and can be fatal. It was discovered that these genes were required for kidney cells to regulate cell function in response to changes in fluid shear. Thus in kidney epithelial cells primary cilia are required for correct mechanotransduction[5,126].

It is now known that there are a range of diseases involving genetic mutations to proteins associated with the cilium. These include Bardet-Biedl syndrome, Sensenbrenner syndrome, Joubert syndrome and Asphyxiating thoracic dysplasia[127–129]. Many of these ciliopathies are characterised by numerous systemic developmental disorders arising from the cilia's importance in regulating differentiation and migration in development[128].

1.6.2 Tubulin and Microtubules

Cilia are formed from an array of tubulin microtubules. Microtubules are one of the three types of cytoskeletal protein that control the shape, motility and life cycle of the cell as well as being important for intracellular transport[130]. They are long hollow tubulin tubes with an external diameter of 25nm, composed of multiple heterodimers of the proteins α-tubulin and β-tubulin[131]. Both α-tubulin and β-tubulin are small proteins, approximately 50kDa in size, that polymerise into αβ-tubulin dimers. At 37°C, when in the presence of GTP, the dimers polymerise sequentially forming a tight spiral tube as shown in Figure 6[132]. The dimers can only polymerise or depolymerize at the ends of the microtubule, and whether new dimers are added or removed is dependent on the concentration of free dimers. The two ends are different with one end assembling at a lower concentration of free dimer than the other.

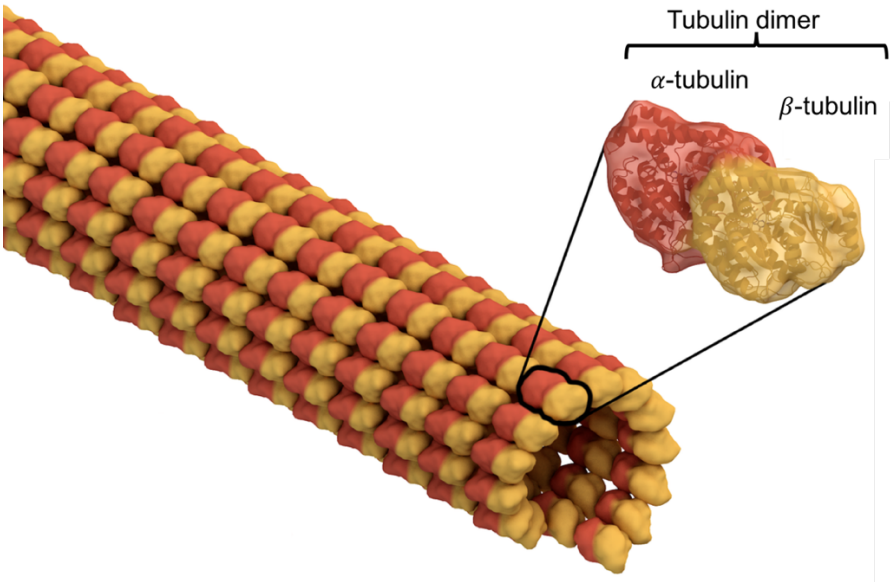

Figure 6: Tubulin microtubule, adapted from image by Thomas Splettstoesser[133]

Most microtubules are dynamic, however, some have been found to be very stable[132]. This is because once the microtubule is formed it is possible for the α-tubulin to be acetylated. Specifically, the lysine residues on the tubulin are acetylated, polymerizing

and stabilizing the entire microtubule beyond the end to end attachment of individual tubulin dimers and preventing the spontaneous disassembly of the tubulin dimers from the end of the microtubule[130]. Acetylation of α-tubulin is mediated by a protein called α-tubulin transferase (αTAT) which causes acetylation of the α-tubulin from the inside surface of the microtubule[132]. It is these acetylated microtubules which form the core structure of the primary cilium.

1.6.3 Ciliogenesis and Structure

The basis of primary ciliogenesis was developed by Sergei Sorokin using electron microscopy. Sorokin showed that the cilium grows from a mother centriole which then forms the basal body of the cilium[134]. Centrioles are part of the centrosome and consist of a tubular structure containing 9 bundles of microtubules. Most cells in G_0 or G_1 contain 2 complete centrioles[135]. The older of the centrioles is called the mother centriole and the younger is called the daughter centriole. The two centrioles are usually orthogonally aligned. Initially in ciliogenesis the centrioles migrate to the cell surface and dock to the actin cortex. The mother centriole then becomes a basal body which nucleates the primary cilium[135,136]. During ciliogenesis, 9 axonemal microtubule doublets (pairs) grow from the basal body. These microtubules protrude beneath a specialised extension of the cell membrane and this structure becomes the cilium. The α-tubulin in the microtubules is then acetylated as described above to provide greater stability[132]. The structural arrangement of 9 pairs of microtubule doublets is known as (9+0)[137]. In contrast, most motile cilia have 2 central microtubules, an arrangement known as (9+2). A schematic of cilia structure is shown in Figure 7.

Some exceptions to this structural distinction have been subsequently discovered, for example the non-motile olfactory sensory cilia has a 9+2 structure[138].

Elongation of the cilia axoneme is made possible by the movement of proteins to the tip of the cilium which increases the concentration of the tubulin required to lengthen the microtubules. This movement is driven by the process of intraflagellar transport, which is described in section 1.6.5[135].

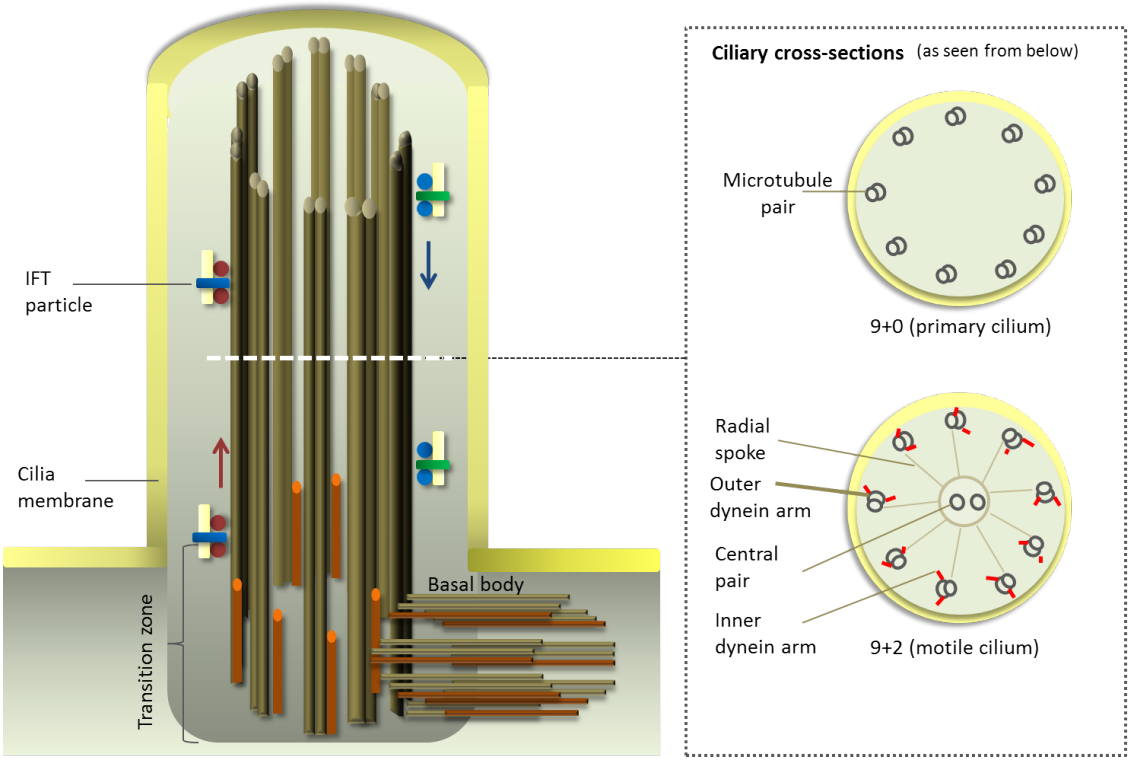

Figure 7: Cilia Structure by Miriam Schmidts

1.6.4 Cell Cycle and Disassembly

Reider et al showed that ciliogenesis is closely related to cell cycle and that cilia are disassembled and absorbed during cell division and reform after division has ended. During mitosis the centrioles detach from the cell membrane, which is not possible without first disassembling the cilia[135]. Upon reattachment of the centriole to the cell membrane after mitosis a new cilium can be nucleated as described above[136]. In terms of cycle, cells in G_0 and G_1 are most likely to express cilia. Cells in S or G_2 will sometimes

express cilia, but these will always be reabsorbed prior to the M phase. Figure 8 shows a diagram of cilia growth and resorption with cell cycle.

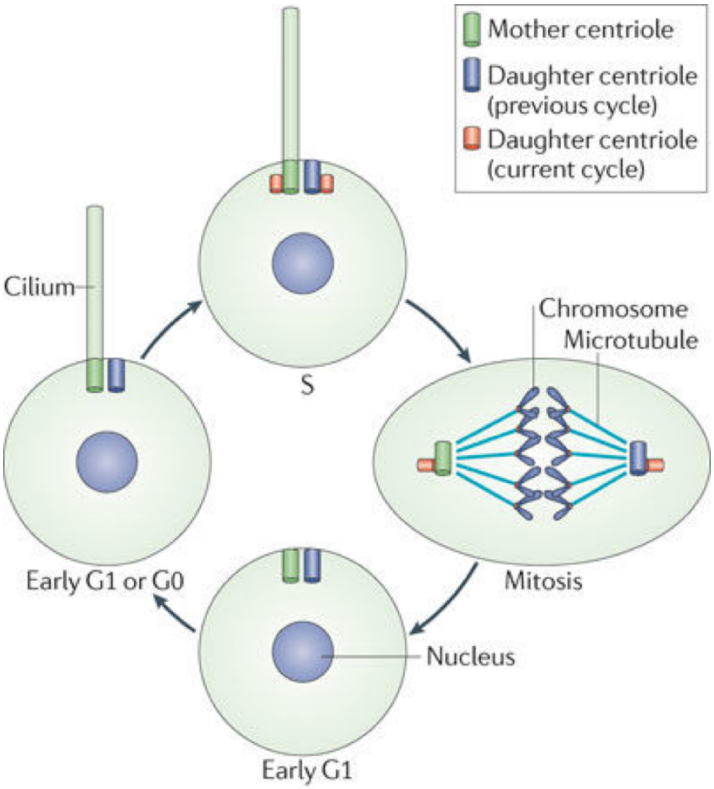

Figure 8: Cilia and the cell cycle, adapted from Ishikawa 2011 [135]

1.6.5 Intraflagellar Transport (IFT)

First described in 1993 by Kozminsky et al, intraflagellar transport (IFT) is the rapid bidirectional movement of particles along the microtubules of the flagella[139]. As cilia do not contain organelles for protein synthesis the vast majority of proteins required by the primary cilia, including tubulin, must be transported to the cilia axoneme via IFT[135]. Disruption of IFT may lead to missing or stunted cilium and disruption of cilia localised cell signalling pathways[6,140].

Intraflagellar transport can be thought to operate like trains travelling up and down the cilium. The role of the 'locomotive' pulling the trains along microtubules is performed by the protein motors dynein and kinesin[141]. Dynein is a large, 1,200kDa, protein that

operates via the breakdown of ATP and then uses the released energy to change the shape of the protein. Dynein has two 'heads' which bind to the microtubule. When dynein breaks down ATP, one of the heads unbinds from the microtubule, the whole molecule then twists round and the head rebinds in front of the other head. Repeating this process allows the molecule to 'walk' along the microtubule[142]. The kinesin family of proteins are a group of smaller microtubule motors, around 100kDa, that operate in a similar fashion to dynein. For trains travelling towards the tip of the cilium (anterograde) the driver is kinesin-2 whilst dynein-2 drives travel towards the base of the cilium (retrograde)[142]. Each 'locomotive' is attached to a protein 'carriage' which binds the proteins being transported. For anterograde transport this is done by IFT complex B with IFT complex A acting as the 'carriage' for retrograde transport. Each of these complexes is made up of around 20 individual IFT proteins with responsibilities for carrying different cargo proteins. The known proteins comprising each complex are shown in Table 4.

IFT Complex A	IFT Complex B
IFT144, IFT140, IFT139, IFT122, IFT43	IFT172, IFT88, IFT81, IFT80, IFT74, IFT72, IFT57, IFT52, IFT46, IFT27, IFT20

Table 4: Comparison of proteins in IFT complexes A and B

Many of the individual proteins and functions of IFT are not fully understood and it is not known whether the proteins carried by complex A and B are different. Complex B has been shown to be required for ciliogenesis, which seems intuitive since it brings proteins to the ciliary tip, while complex A does not appear to be required for cilia assembly[135]. Figure 9 shows a schematic of IFT along the cilium.

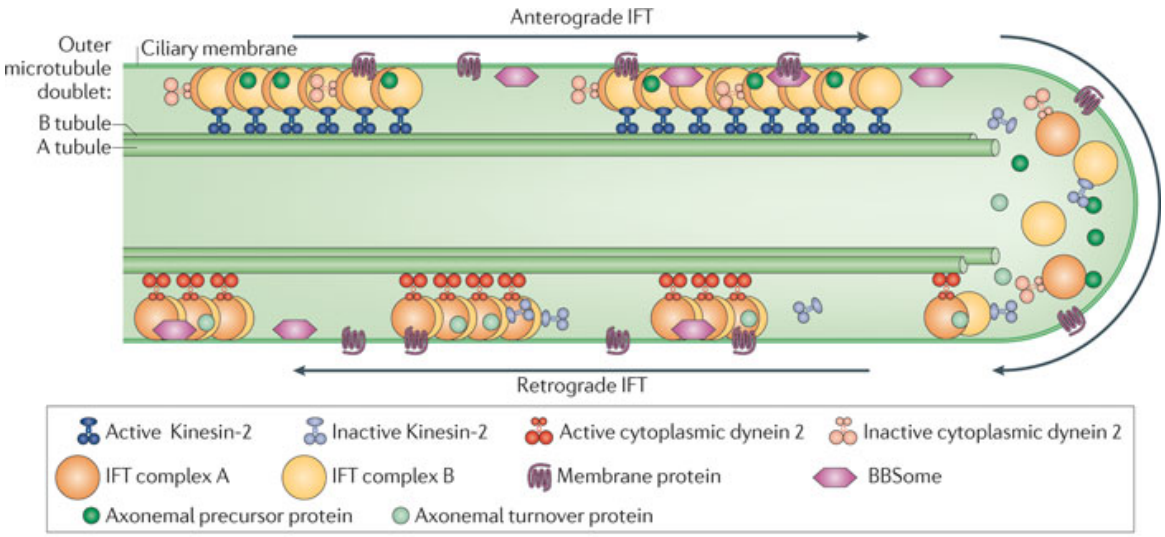

Figure 9: Schematic of retrograde and anterograde IFT. From Ishikawa et al 2011[135]

1.7 Role of the Primary Cilia in Signalling

1.7.1 Overview of Cilia Signalling

Signalling within the cell is called intracellular signalling and falls into two categories; intracrine signalling, in which the cell produces signal molecules which are trafficked to the relevant receptors within the cell, and autocrine signalling where signals are trafficked and bind to receptors on the outside of the cell that produced them[143]. Signalling between cells is known as extracellular signalling and takes three forms. Juxtacrine signalling, describes transmission of signals to adjacent cells via action potentials or gap junctions between touching cell membranes. Paracrine signalling relies on the diffusion of signal molecules (the largest group of which are known as cytokines) through the extracellular matrix to reach nearby cells. Finally, in endocrine signalling proteins (the largest group of which are known as hormones) are transported around the body via blood[143].

Primary cilia are a key centre for paracrine (and some autocrine) cell signalling, with primary cilia involvement in almost all of the major paracrine signalling systems including hedgehog(Hh), Wnt and growth factor signalling[144–146]. Hedgehog is the most established ciliary signalling pathway. During hedgehog signalling, Indian, Sonic and Desert ligands are produced and released from the cell. These ligands diffuse and bind to the hedgehog receptor Patched.[147] The binding of the ligand causes the protein smoothened (SMO) to be released from where it is stored at the tip of the cilia and transported into the base of the cell where it interacts with and causes the transcription of downstream proteins[148]. Hedgehog signalling is necessary for correct embryo development in humans and is highly conserved across species[149]. Hedgehog signalling has also been implicated in various diseases including cancer[150].

A second related signalling pathway group are the Wingless (Wnt) signalling pathways. There are at least two confirmed Wnt pathway groups and a number of others have been proposed. The first, known as the canonical pathway involves the binding of the Wnt ligand to the Fz and LRP5/6 receptors and controls β-catenin accumulation in the cytoplasm[144]. The second pathway group, known as the noncanonical pathways involves the binding of the wnt ligand to Fz without LRP5/6[144]. There are two verisons of this pathway, one that controls calcium signalling and one that controls planar cell polarity (PCP). Other proposed pathways include the integrated pathway involving the ligand Wnt5A that may involve both β-catenin and calcium, as well as a portential Wnt/GSK pathway[151]. Like Hh signalling, Wnt signalling is crucial for correct differentiation of cells in the embryo, specifically for developing the correct left-right axis as well as cell proliferation and migration[144]. Mutations in Wnt signalling have also been implicated in cancer and type II diabetes[144].

Thirdly, primary cilia are involved in a number of growth factor signalling pathways. Growth factors are a broad category of cytokines and hormones that influence growth and development. Receptors for both epidermal growth factor and platelet derived growth factor have been found to localise to the ciliary membrane[152,153]. Transforming growth factor beta (TGFβ) has been shown to be involved in cilia disassembly and will be discussed further in section 1.7.3[154].

Finally, cilia have also been shown to regulate a number of other paracrine signalling pathways via cytokine receptors and cilia localized ion channels including RTK, Notch and mTOR[155].

1.7.2 Role of Primary Cilia Mechanotransduction

It is well known that cells respond to changes in mechanical environment, be these externally applied forces or internally generated cytoskeletal tension. The latter may be regulated by the factors associated with the physiochemical environment such as substrate stiffness which is also known to control cell adhesion. The primary cilia has been implicated as crucial for mechanotransduction in a number of signalling pathways.

Nauli et al suggest that primary cilia act as mechanotransducers, sensing the flow of fluid through the kidney and thus regulating tissue morphogenesis[156]. They hypothesized that the cilia project into the extracellular environment and are deflected by fluid shear (or other forces in different models) which cause the cilia to bend. Previous studies support this, indicating that bending activated the mechanosensitive polycistin ion channel complex which is present on the axoneme, which may then lead to a Ca^{2+} signalling response. Indeed previous studies have shown that primary cilia are required for the activation of fluid shear induced calcium signalling in chondrocytes[6]. Further, Spasic et al showed that when osteocytes were exposed to cyclic fluid flow that cells with longer

cilia expressed more osteogenic markers, indicating that increased cilia length leads to increased mechanotransduction[157].

Studies by Wann et al have shown that cilia dependent calcium signalling is driven by mechanically induced ATP release[6]. However, recent research performed by directly bending cilia, has suggested that unlike in the initial hypothesis from Nauli et al, the primary cilia may not act as a direct mechanosensor[158]. Instead the cilium may be further downstream, a required component in the signalling chain from sensation to response, rather than the sensor itself.

1.7.3 Role of Primary Cilia in TGFβ Signalling

Transforming Growth Factor beta (TGFβ) signalling is vitally important for a number of cellular functions including growth, differentiation, homeostasis and apoptosis among others. TGFβ is one of many growth factors that has been shown to have ciliary involvement, and as discussed previously, it is specifically implicated in tendon mechanotransduction[80].

TGFβ has 4 similar isoforms, of which $TGF\beta_1$ is the most common. $TGF\beta s_{1,2, \text{ and } 3}$ all operate through the same signalling receptors. The signalling pathway begins with the binding of an activated TGFβ ligand to a TGFβ type II receptor[159]. Before they can bind to the type II receptor TGFβ ligands must be activated, either via cleavage by MMP-2 and MMP-9, activation by highly acidic conditions or activation by interaction with thrombospondin-1[160].

The binding of the TGFβ ligand to the type II receptor causes the phosphorylation of the type I receptor allowing it to phosphorylate the downstream SMAD proteins, activating them and causing many downstream effects, including changes in gene

expression[161]. The different SMAD proteins interact with a variety of other signalling systems, further changing which genes are expressed, thus the TGFβ signalling pathway cross-talks with a number of other signalling pathways forming part of the incredibly complex signalling network operating in each cell, a schematic summary of which is shown in Figure 10[162]. TGFβ has its own self-regulating feedback mechanism via SMAD7 which is activated by the TGFβ pathway and causes the breakdown of the receptors[163]. A schematic of the TGFβ pathway is shown in Figure 10.

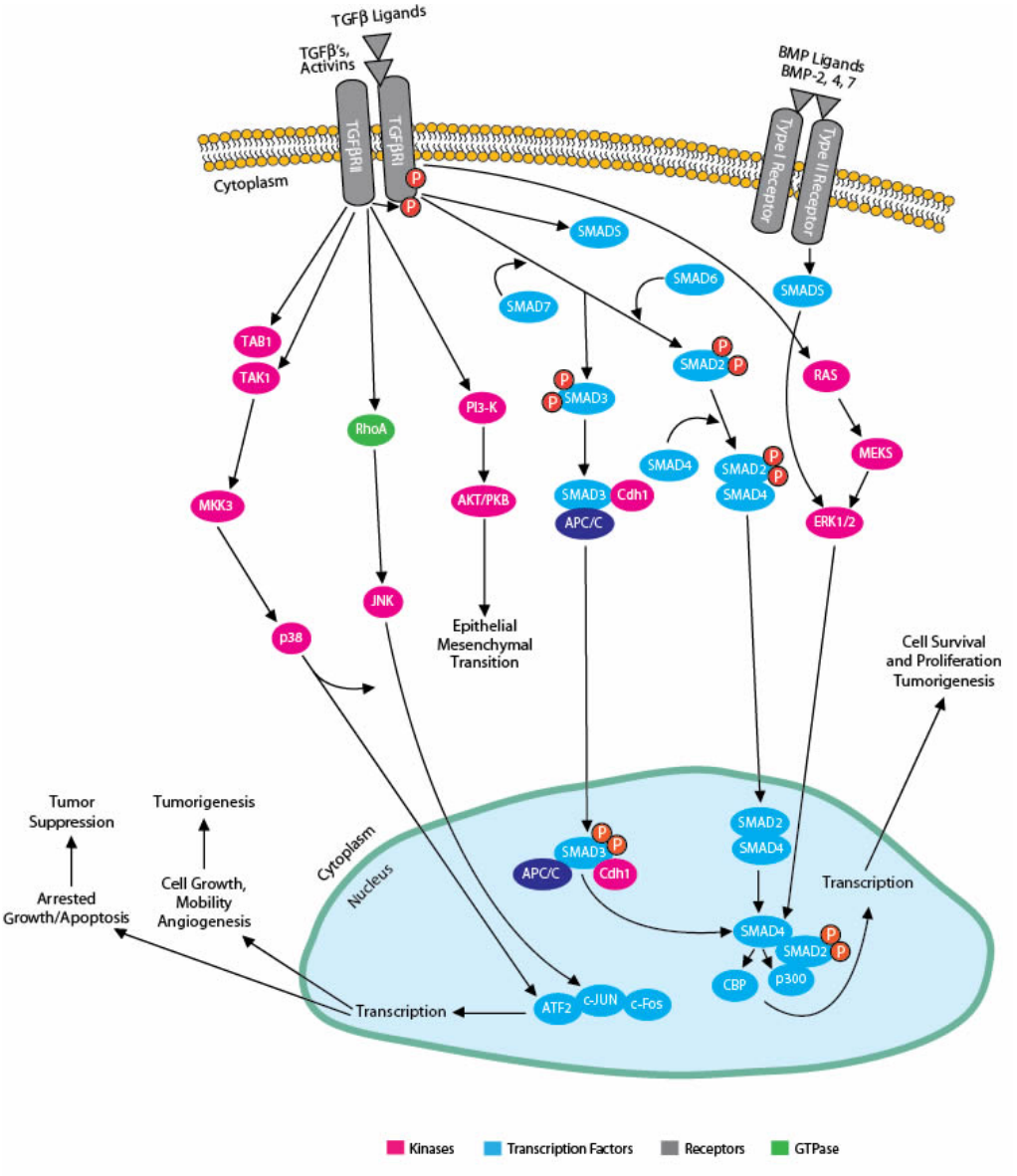

Figure 10: TGFβ signalling pathway. From Novus Biologicals

The primary cilium was recently shown to be involved in TGFβ signalling[154]. TGFβ receptors predominantly localise to the ciliary base with some also localising to the ciliary tip[164]. TGFβ_1 induced SMAD nuclear translocation was significantly reduced in ORPK mutant mice, a mouse mutant with a dysfunctional IFT88 gene leading to stunted or missing cilia[164]. Similarly, TGFβ transcription in response to increased intraocular pressure was abrogated in cells with mutated OCRL (a cilia localised protein involved in trafficking)[7]. Further, studies have shown that Clatherin Dependent Endocytosis, a method by which TGFβ receptors are protected from breakdown, requires a functioning cilium and is regulated by IFT[164]. Stimulation with TGFβ_1 was shown to lead to cilia disassembly in osteoblasts, and result in cells that were less mechanoresponsive[154]. These mechanisms are potentially linked, with TGFβ_1 leading to cilia disassembly and therefore a break in the mechanosignalling chain.

1.8 Effect of mechanical loading on primary cilia structure

1.8.1 Loading indirectly causes disassembly in some cell types

Loading has been shown to lead to cilia shortening and disassembly[165,166]. Cyclic loading of isolated chondrocytes from 0-10% strain at 0.33Hz for 1 hour led to a slight but significant decrease in cilia length[167]. Cyclic compressive loading, 0-15% strain at 1Hz, of chondrocytes in agarose constructs led to decreased cilia incidence at 48 hours, but prevalence was recovered after 72 hours subsequent unconstrained recovery[166]. In tendon cell cilia that had previously elongated in response to stress deprivation, 0.17Hz, 0-3% cyclic strain was found to return the cilia to their original length after 24 hours[9]. Further, primary cilia in trabecular meshwork cells were found to shorten in response to elevated hydrostatic pressure[7].

1.8.2 Theory of Tubulin Polymerisation and Acetylation as Regulators for Load Induced Cilia Disassembly

There are a number of mechanisms by which cilia disassemble. The cilium is constantly in flux, with new tubulin molecules being constantly added and removed at the tip[135]. Hence, whether the cilium increases or decreases in length depends on the rate of addition or removal of tubulin[135]. This behaviour is further complicated by the fact that the tubulin in the cilium is acetylated[132,135]. Because acetylated tubulin is very stable it cannot be removed without first being deacetylated[168]. The prime method by which tubulin is deacetylated is by means of the HDAC (histone deacetylase) family of proteins which, as the name suggests, are responsible for deacetylation. In particular HDAC6 has been found to be crucial in cilia disassembly[169]. There are a couple of proteins that are known to activate HDAC6 (by phosphorylation), and these work across a number of signalling pathways. The first protein is Aurora A, which is activated prior to mitosis and leads to phosphorylation of HDAC6 and thus cilia disassembly, which is necessary for mitosis[169]. Aurora A is activated via both calcium signalling and wingless[168]. The other protein known to activate HDAC6 is Plk1, which is activated as part of the wingless pathway[168]. The TGFβ pathway has also been shown to lead to cilia shortening and disassembly via HDAC6 activation, although whether TGFβ activates HDAC6 directly is unknown[154].

1.8.3 The Role of Actin in Regulating Cilia Length

Actin dynamics are another mechanism which affects cilia length[168]. It has been shown that treating cells with cytochalasin D (actin polymerisation inhibitor), or blebbistatin (myosin-II inhibitor, therefore reducing actin tension), leads to cilia elongation[170,171]. It is suggested therefore, that actin depolymerisation promotes cilia assembly and

increased actin polymerisation promotes disassembly. However, the mechanism by which this occurs is not fully understood[168].

There are a number of other processes, which may be associated with cilia disassembly, but in each case the mechanisms are unclear. These include protein methylation, protein ubiquination and regulation of IFT[168].

1.8.4 Effect of Cilia Length on Signalling

A number of papers have suggested links between cilia length and various cilia associated signalling pathways. The most obvious effect is that signalling pathways such as Hh and Wnt have been shown not to work in cells with absent cilia[153,167]. These pathways therefore require cilia to function and it seems likely that cilia length and prevalence influence signalling rate. With specific regard to Hh signalling, Thompson et al found in chondrocytes that primary cilia are required for mechanosensitive Hh signalling[167]. Further it was shown that increasing the strain magnitude led to cilia shortening and reduction of mechanosensitive Hh signalling. Treating cells with Tubacin to inhibit HDAC6 restored both cilia length and mechanosensitive Hh signalling[167]. There is also evidence from osteoblasts that TGFβ signalling requires functional cilia[172].

1.8.5 Tenocyte Primary Cilia and their Response to Loading

Tendon cells, like most other cell types, express primary cilia although their function in tendon has not been reported. Similarly, there is a lack of studies investigating tendon cilia structure. In fresh fascicles, cilia length has been measured a number of times with varying results. Donnelly et al found fresh rat tail fascicles to have cilia with an average length of 4.2 ± 2.2μm[173], considerable longer than the 1.35 ± 0.11μm, reported by

Lavagnino et al or the 1.1μm reported by Gardner et al (Table 5)[9,174]. These differences may be partially accounted for by differences in imaging techniques and the difficulty of imaging cilia in tissue, reconstructing 3D length from planar images. Further differences may arise from the state in which the tissue is kept prior to imaging. In addition, tendon is heterogeneous at the micro level, with two different material phases containing what are likely to be two different cell types, as described in Section 1.3.4. No studies have investigated differences in cilia expression between the FM and IFM regions of tendon, which may also explain some of the difference in cilia length in prior studies. Furthermore, studies in other cell types show how mechanical loading regulates cilia expression and hence it is possible that differences in the mechanical environment of the tendon preceding analysis may account for the differences in cilia length.

In tendon fascicles cilia have been found to align with the direction of the collagen fibres of tendon, which also reflects the alignment of tendon cells[173]. However, this was not found by Gardner et al, which may be due to the difficulty of measuring orientation for very short cilia[174].

Reference	Tissue	Reported Length
Donnelly et al	Rat tail fascicle	4.2 ± 2.2μm[173]
Lavagnino et al	Rat tail fascicle	1.35 ± 0.11μm[175]
Gardner et al	Rat tail fascicle	1.1μm[9]

Table 5: Summary of cilia length measurements in tendon tissue

Primary cilia in rat tail tendon fascicles have been shown to elongate from a mean length of 1.1μm to 3.0μm in response to stress deprivation. Further, this elongation has been shown to be reversible with 24 hours of low level cyclic loading (0.17Hz, 3% strain)[9].

A study by Lavagnino and co-workers in live rat tail fascicles showed that cilia appear to deflect under applied fascicle strain.[174]

However, beyond this little is known about the ciliary response to stress deprivation and loading in tendon. It may be the case that there is an association between cilia dependent mechanotransduction in tendon and tendinopathy. Further, it seems likely that the cilia are involved in some way in the cellular response to stress deprivation and load, although what that effect might be is unknown.

The lack of knowledge regarding the role of cilia in tenocyte mechanobiology, makes investigating cilia within tenocytes important for both tendon and cilia research as well as the filed of mechanobiology more generally.

1.9 Hypotheses, Aims and Objectives

1.9.1 Hypotheses

1) There are differences in cilia expression, specifically cilia length and orientation, between the cells of the FM and IFM.
2) There are zonal variations in the response of the FM and IFM to stress deprivation, in terms of both cilia expression and tissue mechanics.
3) The mechanical load environment regulates primary cilia length and prevalence in tissue and in isolated tenocytes.
4) Mechanical regulation of cilia expression is mediated via an HDAC6 dependent mechanism.
5) High levels of repeated strain (overload) lead to abnormal cilia regulation
6) The absence of cilia is associated with disruption of mechanoresponsive TGFβ related gene expression.
7) IFT88 siRNA knockdown leads to primary cilia disassembly and resulting inhibition of tenocyte mechanosignalling.
8) Pathological cyclic mechanical strain leads to localised damage shown by disruption of collagen organisation.

1.9.2 Objectives

1) Set up a method for reliably measuring primary cilia length and orientation within tissue.

2) Examine whether the different regions of the tendon (IFM & FM) show differences in cilia expression (length, orientation and prevalence) in situ.
3) Identify whether tendon stress deprivation regulates cilia expression (length and prevalence) in the different regions of the tendon (IFM & FM) in situ and whether this is associated with localised changes in tissue mechanics.
4) Quantify the effects of tenocyte isolation on primary cilia length, orientation and prevalence.
5) Examine the temporal effect of cyclic mechanical strain on primary cilia expression in isolated tenocyte cells and ascertain whether changes are recoverable with the removal of strain.
6) Identify the mechanism through which mechanical loads regulate cilia expression in situ and in isolated cells.
7) Identify whether the absence of cilia affects known mechanoresponsive gene expression in tendon.
8) Knockdown IFT88 using siRNA and determine resultant changes in cilia expression.
9) Develop a reliable method for assessing tissue damage in cyclically strained explants.
10) Measure changes in collagen organisation after the application of cyclic strain.

2 Protocols & Development

2.1 Cell and Tissue Culture Methods

2.1.1 Media

Cell culture media is a fluid containing nutrients required to keep cells and tissue alive in culture. Dulbecco's Modified Eagle Media (DMEM) (ThermoFisher, Waltham, MA) was used as the base for all experiments. Different DMEM products were used in different media formulations and the following components were added to the media depending on the requirements of the experiment, as described in Table 6:

Included in DMEM low glucose with pyruvate:

- Pyruvate – A supplement used as an additional source of carbon.

Included in DMEM Low glucose with pyruvate, GlutaMax and phenol red:

- GlutaMax – An essential nutrient for cell energy production, lower ammonia and carboxylic acid by-products than L-Glutamine.
- Phenol red – A pH indicator.
- Pyruvate – A supplement used as an additional source of carbon.

Further additives:

- Foetal bovine serum (FBS), (ThermoFisher, Waltham, MA) – provides a wide range of proteins and amino acids which are important for cell growth. Absence of FBS, known as serum starvation, inhibits growth and stops cells progressing through the cell cycle.
- Penicillin and streptomycin - antibiotics which are commonly added to media to prevent bacterial infections.
- L-Glutamine (ThermoFisher, Waltham, MA) – an essential nutrient for cell energy production.
- HEPES (ThermoFisher, Waltham, MA) – acts as a pH regulating buffer.
- NaCl – used to regulate osmolarity.

Components	Tenocyte Media 1	Isolation Media	Tenocyte Media 2	Serum Free Media 1	Serum Free Media 2
DMEM Low glucose with pyruvate	500ml	250ml	0ml	500ml	0ml
DMEM Low glucose with pyruvate, GlutaMax and phenol red	0ml	0ml	500ml	0ml	500ml
FBS	50ml	250ml	50ml	0ml	0ml
L-Glutamine 200mM	5ml	5ml	0ml	5ml	0ml
HEPES	10ml	10ml	0ml	10ml	0ml
Penicillin (10,000 I.U/ml) and Streptomycin (10,000µg/ml)	5ml	5ml	5ml	5ml	5ml
NaCl	1.85g	0g	0g	0g	0g

Table 6: Composition of the 5 different culture mediums used during experimental work.

2.1.2 Primary Bovine Tenocyte Isolation

Primary bovine tenocytes, used for a number of experiments, were isolated from the bovine digital flexor tendon (BDFT). The BDFT was dissected from the cow foot inside laminar flow cabinet, taking care to maintain sterile conditions. Cow feet were obtained from young but skeletally mature steers culled for meat. The tendon sheath was removed and small 5x5x2mm sections were cut from the mid portion (the area away from the insertion sites) of the tendon. The small tendon sections were placed into 6-well plate

wells, 3 sections per well. A small amount of high FBS Isolation media (Table 6) was pipetted onto each section to fully cover it but not so much that the section could float away from the plate. Plates were incubated overnight (37°C, 5% CO_2). Isolation media was then added to cover the tissue fully, taking care not to disturb the tissue. Plates were incubated for a further 24 hours, allowing time for cells to migrate from the explants. The tissue samples were removed once migrated cells were visible, media was removed and the cells incubated in tenocyte media 1 (Table 6) until confluent, during which time the media was changed every 24 hours. The wells were then passaged and combined. Cells were counted and the combined cells were moved to a flask as appropriate for the cell number and culture continued as appropriate for experiment or snap frozen in DMSO for cryostorage.

2.1.3 Rat Tail Dissection

Rat tail tendon fascicles used in this project were collected from rats killed for unrelated experiments. Rats used were either Wistar or Sprague-Dawley and were killed for unrelated purposes. Specifics of breed, sex, weight, skeletal maturity and ethical approval will be detailed in the relevant experimental chapters. Rats were all dissected and experiments begun between 9am-12pm.

Tails were removed from rats within 12 hours of death. All work post tail removal was performed in a laminar flow cabinet to maintain sterility. The skin was resected from one quarter of the rat tail from the proximal end to ½ way to the tip, exposing the tendon fascicles. 2 cuts were made across the tendon fascicles, approximately 1cm from the base and ½ of the way from the base to the tip. Groups of fascicles were then carefully removed from the sheath from the cut end in the middle of the tendon. Fascicles were carefully separated as required, into either individual or paired fascicles

as required. These were placed immediately into untreated sterile wells containing tenocyte media 1 (Table 6) or wrapped in PBS soaked blue tissue paper, depending upon downstream application, to prevent the fascicles from drying out. Once all fascicles had been removed from the first quadrant of the rat tail, the skin was removed from a further quarter of the tail and the procedure repeated until all the fascicles were removed from all 4 quarters of the tail.

2.2 Biomechanical Testing of Tendon

2.2.1 Mechanical Testing

The Instron ElectroPuls 1000 (Instron, Norwood, MA) was used for all mechanical property tests. A review of methods for testing samples and analysing data is produced here, with specific methods for individual tests covered as appropriate in the following experimental chapters. Samples were clamped at both ends using pneumatic grips. An air pressure of between 1 and 2 bar was used between grips as this was found to ensure that samples were gripped tightly enough to not slip but not so tightly as to cause fascicles to fail at the grip site. Further, sandpaper was attached to the grip surface to allow for increased lateral friction in the grips at lower air pressures, and a tare load (variable between experiments depending on the sample parameters) was applied to ensure samples were not slack before testing began. Tendon samples were misted with PBS immediately prior to and during testing to ensure that they did not dry out. Prior to testing, fascicle cross sectional area was calculated using a laser micrometer (LSM 501; Mitutoyo, Kawasaki, Kanagawa, Japan). This was done by measuring along the entire testing length of the tendon to identify the narrowest portion of the tendon, and calculating the cross sectional area with the assumption that the fascicle cross section is circular.

Testing protocols generally involved 10 preconditioning cycles to the same peak strain, followed by a quasi-static pull to failure test. Preconditioning is usually performed to make comparisons between different tendon tests more consistent primarily by controlling internal water. Further, the behaviour of the tendon during preconditioning tests can also be very interesting.

From the two stages a number of useful output measures can be determined as outlined below.

Quasi-static loading outputs:

- Failure stress – The stress at which the fascicle fails.
- Failure strain – The strain at which the fascicle fails.
- Tangent modulus – The rate of change of stress with respect to strain along the stress stain curve. This was calculated on a rolling basis for the entire stress strain curve.

Cyclic loading outputs:

- Hysteresis (Figure 11) – the energy dissipated between the load and unload phases of each loading cycle. Usually presented as a percentage, a material with a hysteresis of 0% would be perfectly elastic and a material with 100% hysteresis would be perfectly plastic.

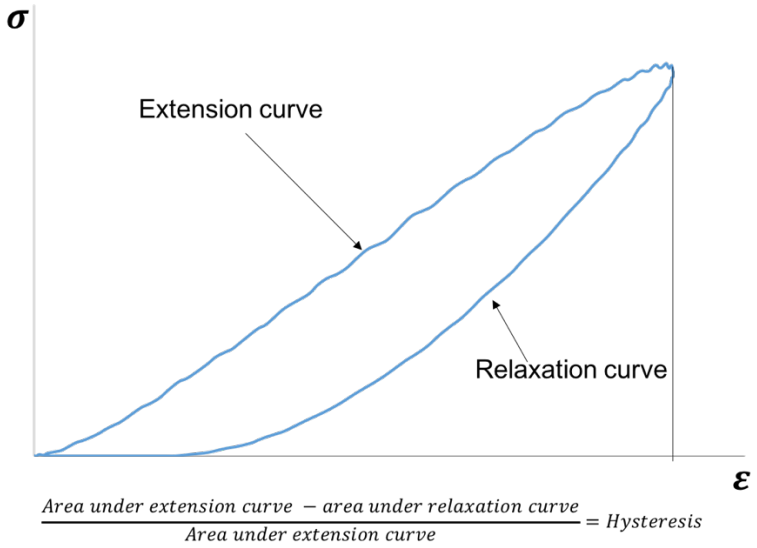

Figure 11: Schematic showing calculation of hysteresis

- Stress relaxation (Figure 12) – the drop in the peak stress measured across the multiple preconditioning cycles. This measure is similar to static stress relaxation and gives an indication of viscoelastic properties.

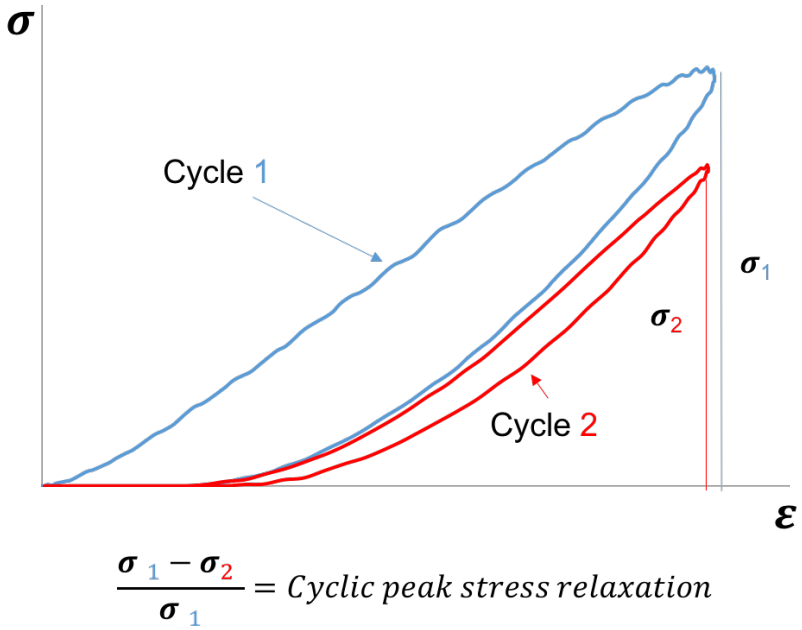

Figure 12: Schematic showing the calculation of stress relaxation over cycles.

2.2.2 Mechanical Testing of IFM

Testing the mechanical properties of the IFM presents a number of challenges. This is primarily due to its soft sticky nature and the challenge of dissecting a region of IFM without irrevocably damaging its structure. However, a method by which the shear properties of the IFM can be determined was developed by Thorpe et al[17] and is adapted for RTT testing here.

Fascicles were carefully separated into pairs, ensuring that the IFM binding the two fascicles together remains intact. The end of one of the paired fascicles was cut, after which the other end of the second fascicle was cut, leaving only a 10mm length of IFM connecting the two fascicles (Figure 13). The fascicle ends were clamped, after which mechanical testing will test just the IFM in shear.

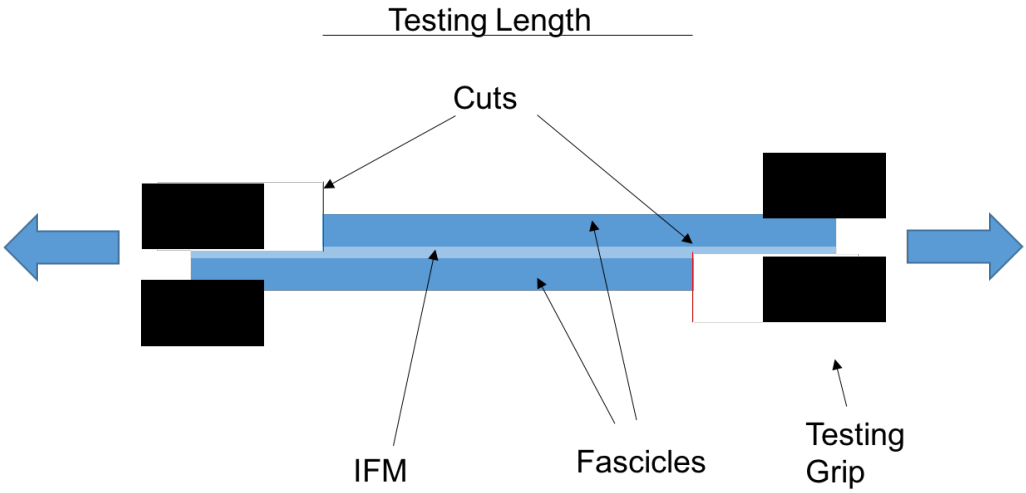

Figure 13: Schematic showing the IFM testing set up

2.3 Equipment and Validation for Mechanical Stimulation of Tendon Explants

Tendon explants were stimulated mechanically to investigate the cellular response to different types of loading. The different regimes investigated were stress deprivation,

static strain and cyclic strain. An introduction to the equipment used and preliminary data validating explant viability are provided in this chapter, with detailed methods covered in the relevant sections of the experimental chapters.

2.3.1 Loading Conditions

For stress deprivation, fascicles were maintained unconstrained in individual wells in a 6 well plate in tenocyte media 1 (Table 6), in an incubator at 37°C and 5% Co_2. The media was changed every third day. The number of fascicles and rats used depended upon the individual experiment.

To maintain the fascicles under static strain, custom built chambers were used (Figure 14). The tissue was clamped at each end and the desired strain was applied by hand using a micrometer. The chambers were filled with media as above and incubated at 37°C and 5% Co_2. Media was changed every third day.

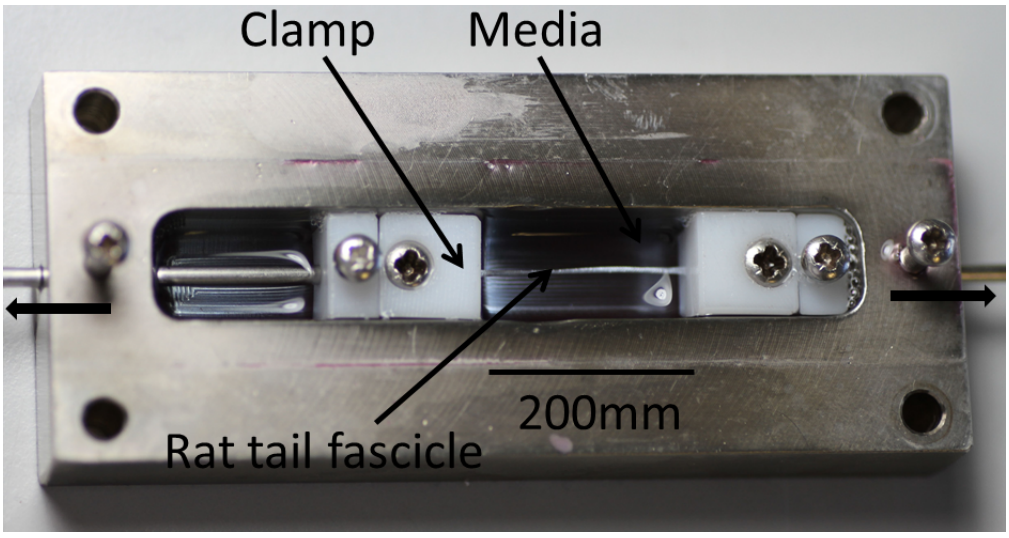

Figure 14: Custom static strain chamber

Cyclic strain was applied using custom made chambers (Figure 15). The chambers allow samples to be maintained in media during testing. The chambers can then be placed in

the Instron ElectroPuls 1000 mechanical testing machine or the Bose Electroforce cyclic tensile system (TA Instruments, USA).

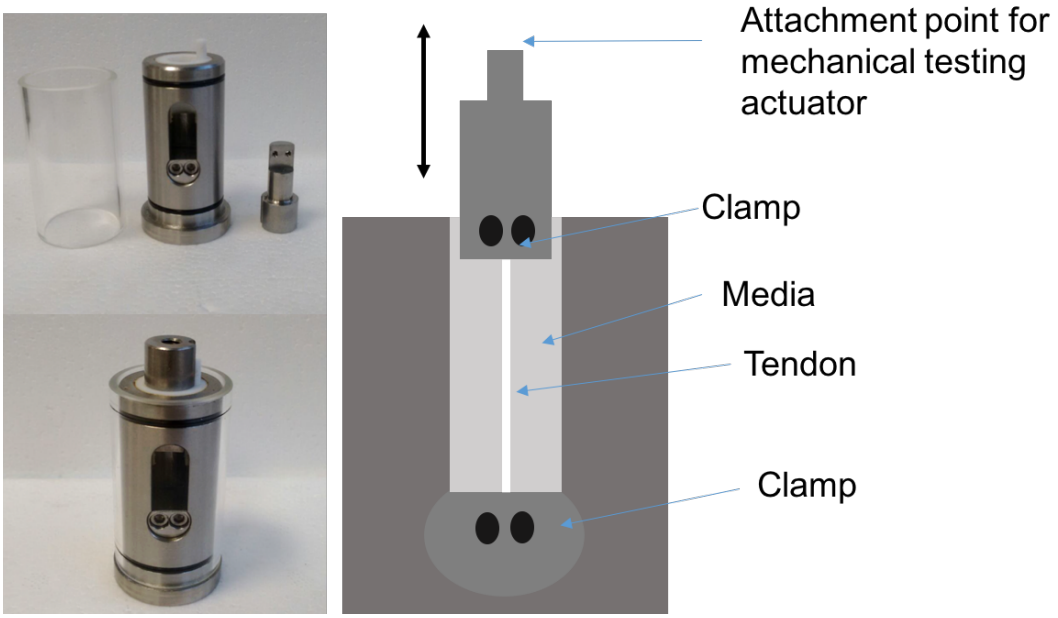

Figure 15: Custom cyclic strain chamber pictures and cross section schematic

2.3.2 Explant Viability During Loading Experiments.

For both stress deprived and statically strained explants, cell viability was required for up to 1 week. To validate that cell viability was maintained in explants for up to 7 days, cell activity was measured using the AlamarBlue (ThermoFisher, Waltham, MA) assay after 1, 2 and 7 days. The AlamarBlue assay is used to determine the metabolic activity of cells, through the addition of a non toxic dye which is reduced linearly by cell metabolic products and changes colour on reduction. 12 fascicles were dissected from a single rat tail, 6 fascicles were used for the stress deprived group and 6 for the static strain group. At each time point the media was changed immediately prior to testing to ensure no metabolic products were present, 100µl AlamarBlue was then added for every 1ml of media. Fascicles were incubated with the AlamarBlue for 1 hour at 37°C and 5% CO_2, after which 3x100µl samples of media were removed from each sample and

measured for absorbance at 570nm. 6 wells containing explant free media with the addition of AlamarBlue was incubated alongside the samples and was used as a control. After absorbance was measured AlamarBlue containing media was removed and replaced with fresh media. AlamarBlue is non-destructive and the same samples were tested at 0h (immediately after dissection), and after 24, 48 and 176 hours of incubation. Samples were compared with their respective cell activity at the 0h time point.

Data indicates a small increase in cell activity with incubation duration which may indicate cell proliferation. However, this was not significant at the $p<0.05$ level for either 4% static strain or stress deprived rat tail tendon fascicles at any time point (Figure 16), suggesting that both loading methods maintain cell viability over the 7 day testing period.

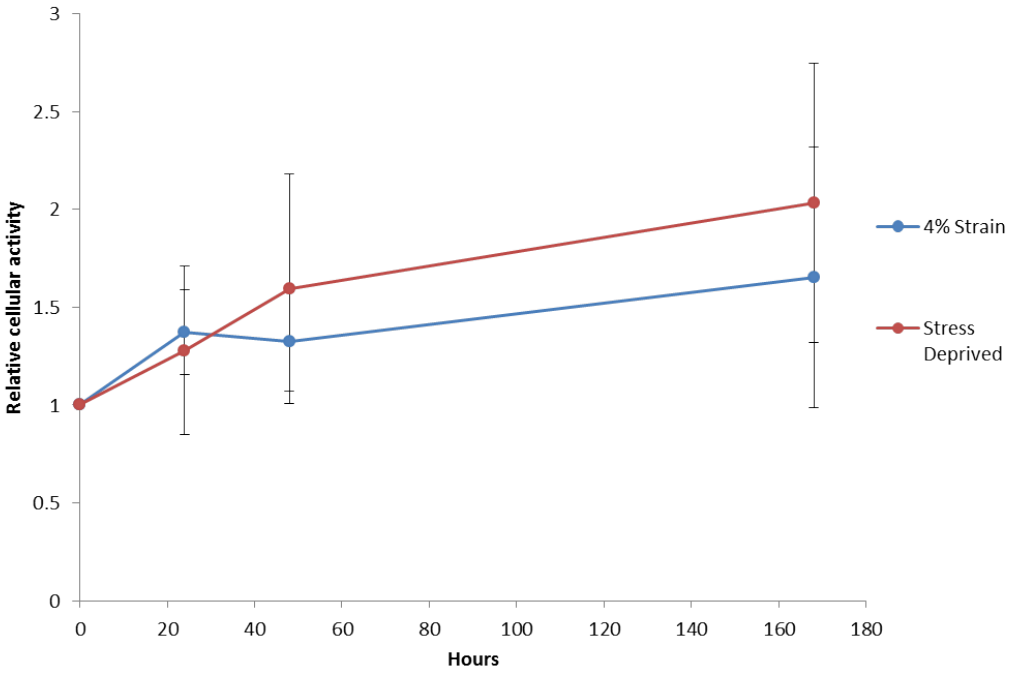

Figure 16: Relative cellular activity after 24, 48 and 168 hours for 4% static strain and stress deprived rat tail tendon fascicles. Error bars are standard deviation.

2.3.3 Cyclic Loading of Cells using the Flex Cell System

The flex cell system allows for the application of strain to isolated cells. This is accomplished by seeding cells into well plates with silicone membranes as bases, which

are then placed over 'posts' such that each well sits over a 'post'. A vacuum is then created underneath the well plate which pulls the silicone membrane down around the plate thus stretching the silicone membrane that rests on top of the post and stretching the cells as shown in Figure 17.

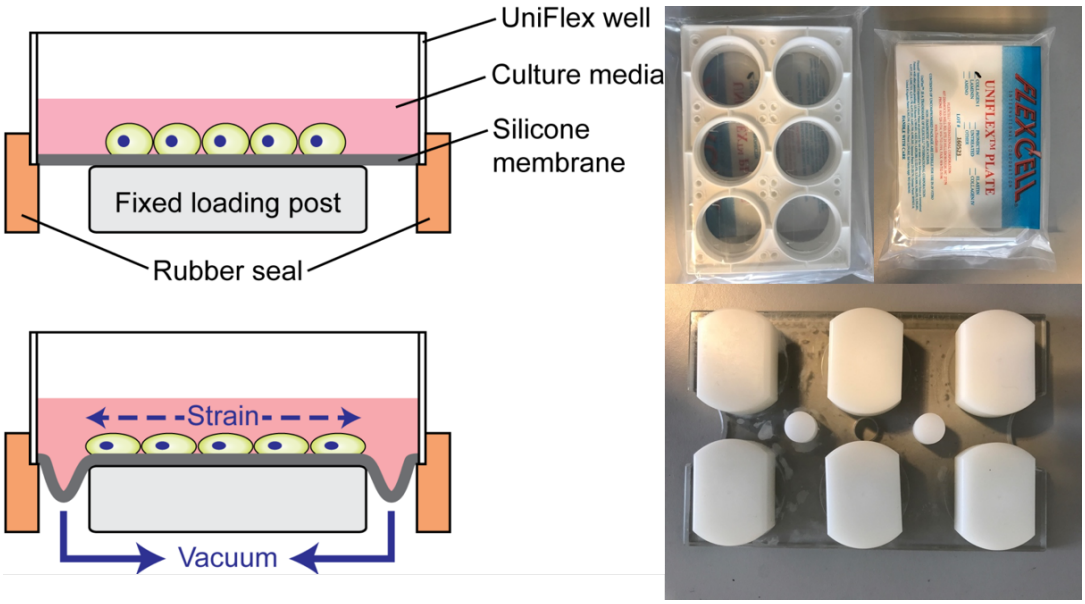

Figure 17: Figure showing cut-through schematic of the FlexCell system, collagen coated flex cell plates and 'arctangle' posts.

The amount of strain applied to the cells can be varied by changing the strength of the vacuum and varying loading patterns of static and cyclic strain are possible. Further, by changing the shape of the posts uniaxial or multiaxial loading can be applied. Since tendons experience strain in a primarily linear fashion 'arctangle' posts were used to apply uniaxial strain in all of the experiments in this thesis (Figure 17). Varying cell densities, incubation durations and loading protocols were applied to tenocytes using this system throughout this thesis.

2.4 Introduction to Immunofluorescent Imaging Techniques

The primary cilia can be imaged using a variety of techniques including TEM and multi-photon microscopy. However, the predominant method used in the last decade is

immunofluorescent confocal microscopy. The development of antibodies specific or localised to primary cilia has allowed imaging of the structural components of the cilium as well as protein trafficking into and out of the cilium[166,167,176]. Relevant literature concerning methods for cilia imaging is first addressed after which the developmental work to visualise tenocyte cilia is covered.

2.4.1 Confocal Imaging

Confocal laser scanning microscopy is a fluorescence microscopy technique which improves the resolution of fluorescence microscopy, particularly in the out of plane direction, by only illuminating and collecting a single voxel area at a time. Normal fluorescence microscopy works by illuminating the sample with light at the excitation frequency of the fluorescent label used. The fluorescent label then fluoresces and this is observed using optics such as would occur in an ordinary light microscope, possibly with filters to ensure that only light of the desired colour is transmitted to the collector.

In confocal microscopy the resolution of this technique is improved by the addition of a pinhole which ensures that only light from the focal plane of the lens can reach the collector, which replaces the traditional camera sensor or viewfinder. Since it is not an image being formed at the detector but just the light information from a single point, the confocal microscope relies on sequential illumination and detection of each region of the sample, usually by a photomultiplier tube (Figure 18). Because all out of focus light is eliminated, the confocal microscope has the property of optical sectioning, whereby only the information in the focal plane is seen.

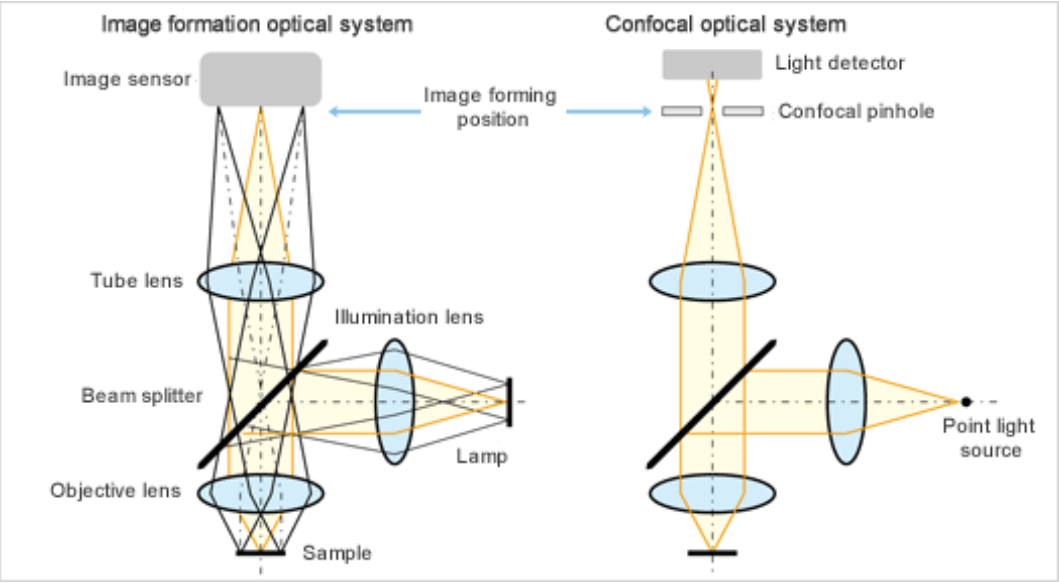

Figure 18: Schematic showing the operation of a confocal microscope compared with a standard flourescence microscope.

This is of particular importance for use in cilia imaging since cilia are structures that often project out of plane. It is also of vital importance for tendon tissue imaging since tissue samples can be thick, and the large out of focus components in epifluorescent microscopy makes accurate imaging difficult. With confocal microscopy it is possible to acquire multiple stacked images of the cilium at a range of depths which can be used to reconstruct the whole cilium length as opposed to only its 2D projection.

Two laser scanning confocal microscopes were used during this project, the Leica TCS SP2 (Leica, Wetzlar, Germany) and the Zeiss ELYRA (Carl Zeiss AG, Oberkochen, Germany).

2.4.2 Fixation

Two commonly used fixatives in immunofluorescence microscopy are paraformaldehyde (PFA) and methanol. PFA is a polymer of formaldehyde and is not actually a fixative, but works as a fixative when depolymerised into formaldehyde. It is

usually made as a solution from 4% PFA in PBS which can be denatured into formaldehyde by heating at 37°C for 2 hours[177,178].

Formaldehyde (like all aldehydes) is a crosslinking fixative, covalently binding carbon and nitrogen atoms in amino acids (primarily lysine) to each other via a number of reversible and irreversible reactions including the Mannich reaction[179]. This preserves the structure of large number of cellular proteins. However, not all the crosslinks are permanent and some proteins get cross-linked much less than others. Some disadvantages of PFA include cellular distortion and the loss of some cellular structures[178,179].

Methanol is another commonly used fixative. Methanol, like other alcohol fixatives, works by dehydrating the cells causing precipitation of protein and rendering them insoluble when water/PBS is reintroduced[178]. As a result of its dehydrating nature, methanol leaves gaps in the cell membrane, allowing for far better access of antibodies into the cell and does not require additional permeabilising[180]. One issue with methanol fixation is that it destroys the structures that the toxin phalloidin binds to. Phalloidin is a toxin that is commonly used to label actin. A further disadvantage of methanol fixation is that it destroys some membrane structures[178,181].

2.4.3 Immunofluorescent Antibodies for Visualising Primary Cilia

There are two commonly used antibodies for primary cilia immunofluorescent imaging. The first is anti-acetylated α-tubulin, which binds specifically to acetylated α-tubulin and not non-acetylated α-tubulin[182]. As the primary cilium is specifically composed of acetylated tubulin this antibody can differentiate the primary cilium from all the other

tubulin structures within the cell none of which contain as high a proportion of acetylated α-tubulin[182].

ADP-Ribosylation Factor-Like 13b (ARL13b) is a cilia specific membrane protein required for correct cilia formation. Since ARL13b is localised to the cilia[181] the anti-ARL13b antibody provides a good method of identifying the location of the cilium. However, ARL13b is not always uniformly distributed along the cilium and so gaps along the cilium can occasionally occur[183].

2.4.4 Other Useful Antibodies

A number of other antibodies can be used alongside acetylated α-tubulin and ARL13b to either assist in cilia detection or identify cell state to support data interpretation.

Pericentrin-B is a protein that localises to the centrosome, which forms the basal body of the cilia, thus making it very useful for identifying the location from which the cilium projects. However, care must be taken as the presence of pericentrin-B does not imply the presence of a cilium.

Ki67 is a protein associated with cellular proliferation and is exclusively located in the nucleus when the cell is in G_1 or G_2 states. Immunostaining for Ki67 is therefore important for determining whether the cell is quiescent[184]. Knowledge of cell state is important from a cilia length and prevalence perspective because cells do not express cilia when they are dividing.

Phalloidin is a toxin that binds selectively and specifically to F-actin. Fluorescently tagged phalloidin can be used to label actin for fluorescence microscopy. As mentioned in section 2.4.2 phalloidin can not be used with methanol fixed samples[185]. Phalloidin

was used in this thesis to investigate changes to the actin cytoskeleton, due to the potential link between actin tension and cilia structure.

2.4.5 Cilia Staining Protocol for Isolated Cells

Bovine cells from outgrowth as described in section 2.1.2. were seeded onto three 13mm diameter circular glass coverslips. Prior to seeding, coverslips were sterilised with UV overnight and immersed in FBS for 24 hours before being placed in 24 well plates. Cells were incubated in tenocyte media 1 (Table 6) for 3 days to adhere and proliferate after which point they were approaching confluence. Media was changed once after 48 hours. Cells were then incubated for 24 hours in serum free media 1 (Table 6) before media was aspirated and cells washed with PBS (ThermoFisher, Waltham, MA), prior to fixation with 4% PFA for 5 minutes at room temperature. Fixative was removed and cells washed with PBS, before incubation with 0.1% Triton-X (ThermoFisher, Waltham, MA) for 5 minutes at room temperature. Cells were washed with PBS again and then blocked using goat serum (Sigma-Aldrich, St Louis, MO) for 30 minutes at room temperature. Cells were incubated overnight at 4°C with both mouse anti-acetylated α-tubulin (Sigma-Aldrich, St Louis, MO) @ 1:1000 and rabbit anti-ARL13b (Abcam, Cambridge, UK) @1:1000 in PBS with 0.1% BSA (ThermoFisher, Waltham, MA). Cells were again washed 3 times for 5 minutes each time with PBS containing 0.1% BSA. Cells were incubated with anti-rabbit 488 (ThermoFisher, Waltham, MA) at 1:1000 and anti-mouse 555 (ThermoFisher, Waltham, MA) at 1:1000 for 1 hour at room temperature in darkness. Cells were washed 3 times for 5 minutes each time with PBS containing 0.1% BSA, and incubated with DAPI (Sigma-Aldrich, St Louis, MO) at 1:1000 for 5 minutes at room temperature. Cells were washed for a final time for 5 minutes with PBS containing 0.1% BSA. PBS was aspirated until the coverslip was as dry as possible without touching the cells, after which the glass coverslips were removed

from the wells and mounted onto microscope slides with prolong gold mountant (ThermoFisher, Waltham, MA) which was allowed to set overnight at room temperature.

Cells were imaged with the Leica SP2 confocal using a 63x oil immersion lens at a voxel resolution of 150x150x500nm. Cilia were found to be clearly visible with both ARL13b and acetylated α-tubulin staining. A representative image is shown in Figure 19.

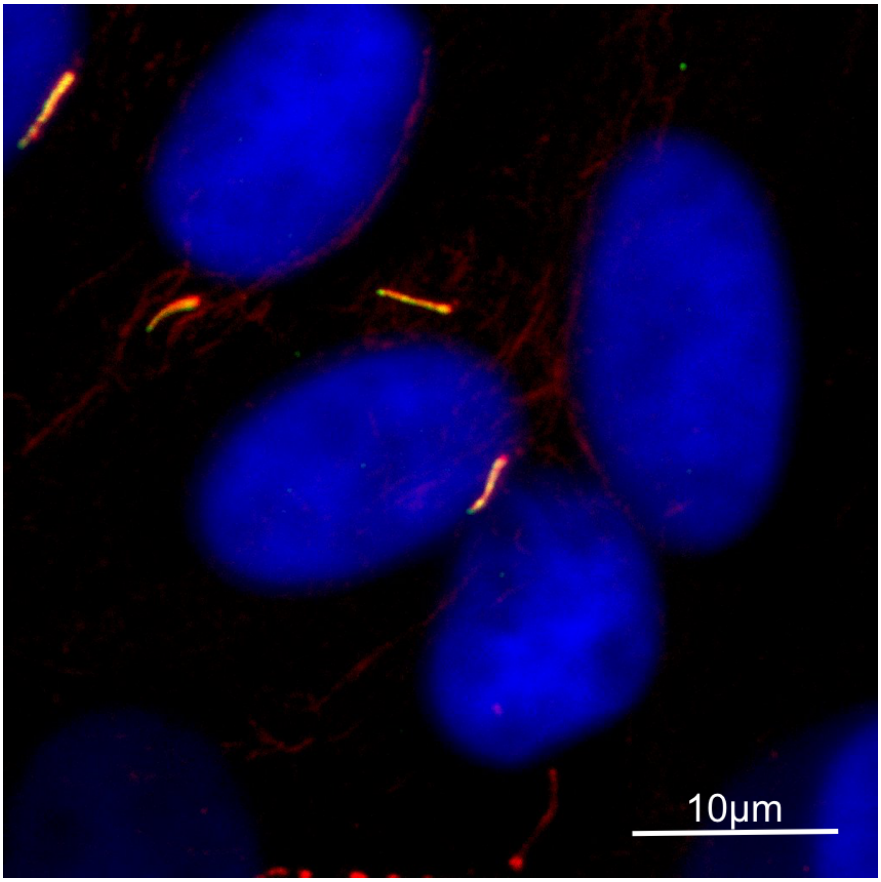

Figure 19: Bovine tenocytes with cilia. *ARL13b is labelled with green and anti acetylated α-tubulin is red. DAPI nuclear staining is shown in blue.*

2.5 Development of Primary Cilia Visualisation in Tissue

While it was verified that the staining protocol described above labelled cilia in isolated bovine tenocytes, it was also necessary to visualise cilia in explants, to investigate

regional differences in tendon cell cilia and relationships between matrix properties and cilia structure.

However, few studies have investigated cilia in tissue due to the challenge of identifying the cilium within the 3D structure of tissue. Further, appropriate sample preparation has proven difficult in many tissue types. Tendon is no different, with only a few studies looking at the primary cilium in tissue. The methods used varied between studies as shown in Table 7.

Author	Tissue Preparation	Fixation	Antibodies	Microscopy
Donnelly et al (2008)[186]	Micro-dissection	Methanol (2h @4°C)	Acetylated α-tubulin (overnight @4°C)	Multiphoton
Donnelly et al (2010)[173]	5μm paraffin sections	10% phosphate buffered formalin	Acetylated α-tubulin	Multiphoton
Gardner et al (2011)[9] **Lavagnino et al (2011, 2013)**[174,175]	Dissected Fascicles	Unfixed	Tubulin Tracker Green	Confocal

Table 7: Table of fixation and imaging methods used for tendon cilia imaging in previous papers.

The aim here was to develop a reliable protocol for staining primary cilia in tendon tissue.

2.5.1 Bovine Tissue Section Staining

The same protocol used to stain isolated bovine tenocytes was first investigated to determine if it would successfully stain tenocytes in situ within explants. 6 tissue

explants, roughly 1x5x5mm were dissected from bovine flexor tendons and immediately placed into 24 well plate wells and immersed in 4% PFA.

A range of different combinations of antibody concentrations and fixation times were investigated as outlined in Table 8 with 3 explants stained for each condition. The same antibody concentrations were used for both ARL13b and acetylated α-tubulin.

Fixation Length (4% PFA)	Antibody Concentration (both ARL13b and acetylated α-tubulin)
5, 20, 60 minutes	1:1000, 1:200

Table 8: Fixative lengths and antibody concentrations.

Samples were immunofluorescently stained using the protocol in section 2.4.5., but with the concentrations and fixation times described in Table 8. Secondary antibodies and DAPI were used at concentrations of 1:1000 regardless of primary antibody concentration. Samples were also placed directly in 24 well plate wells.

After staining samples were placed on glass slides and mounted with prolong gold under 13mm circular coverslips.

None of these tests resulted in visible staining with either antibody at any fixation time or concentration. DAPI nuclear staining was visible as were low levels of non specific secondary binding. However, staining was concentrated at the surface region of the samples. This suggests two problems; firstly, that the antibodies are not binding and secondly that penetration of dye into the sample is poor, either because of a lack of permeability, or because the samples are just too thick. Thickness of samples is also a problem due to the limited depth penetration of 63x confocal microscopy.

2.5.2 Bovine Cryosection Staining

To test the hypothesis that samples were too thick, cryosectioned samples were tested. Cryosectioning is a process whereby the sample is snap frozen in a protective medium, in this case 'optimal cutting temperature' (OCT) (Sigma-Aldrich, St Louis, MO), which does not form damaging crystals when frozen and remains frozen at cutting temperature, allowing thin biological sections to be cut. 1 explant was prepared and 12 sections were cut from each explant at a thickness of 20µm. Sections were placed on glass slides, 3 to a slide, giving 4 slides in total.

Each section was drawn around with a hydrophobic pen so that liquid could be placed in a bubble over the section and remain due to surface tension thus reducing spillage and wastage of resources. Samples were immunofluorescently stained using the protocol in section 2.4.5. with the variations in Triton-X permeabiliser concentration and duration shown in Table 9 as well as increased primary antibody concentrations of 1:100. DAPI and secondary antibody concentrations remained at 1:1000.

Fixation Time (4% PFA)	Antibody Concentration	Permeabiliser Concentration (Triton-X)	Permeabiliser Time (Triton-X)
5 minutes	1:100	0.1%, 0.5%	5 minutes, 30 minutes

Table 9: Shows fixation durations, antibody concentration, and permeabiliser concentrations and durations for the RTT staining test.

Samples were mounted with prolong gold under a single 40x22mm coverslip which covered all the sections on each slide.

As with the previous test no signal was observed from either the red or green channels in any of the conditions. The DAPI staining was clear throughout the whole sample

under all conditions although cell nuclei appeared more diffuse after 30 minutes at 0.5% Triton-X suggesting that the cells were overpermeabilised.

These findings indicate that the staining did not work due to the primary antibodies not binding. This is likely to be because some part of the tissue preparation method is destroying delicate cellular structures, or because of low bovine reactivity of the antibodies.

2.5.3 Rat tail Staining

To identify if species reactivity was the problem, rat tail tendon fascicles were stained with anti ARL13b and anti acetylated α-tubulin. Individual rat tail tendon fascicles were dissected and placed in 0.5ml Eppendorf tubes, which ensured they were fully immersed in minimal liquid volume, allowing the use of high concentrations without running out of consumables.

Staining protocol was as before, with primary antibodies used at a concentration of 1:100, and Triton-X at a concentration of 0.5% for 5 minutes. 4% PFA fixation was used for 5, 20 and 60 minutes as the rate of diffusion of PFA through RTT was not known. All conditions tested are shown in Table 10. DAPI and secondary antibodies were used at a concentration of 1:1000. A total of 9 RTTs were stained, 3 for each condition.

Fixation Time (4% PFA)	Antibody Concentration	Permeabiliser Concentration (Triton-X)	Permeabiliser Time (Triton-X)
5, 20, 60 minutes	1:100	0.5%	5 minutes

Table 10: Shows fixation durations, antibody concentration, permeabiliser concentration and duration for the RTT staining test.

After staining, fascicles were placed on glass slides and mounted with Prolong Gold under rectangular 40x22mm glass coverslips. Samples were left in the dark overnight for the prolong gold to harden prior to imaging.

Using this method, no signal was observed in either the red or green channels at any fixation duration, although the fascicles were thin enough that DAPI staining was observed through the whole thickness of the fascicle. This method also allowed for easy identification of the IFM surrounding the fascicle from the FM due to the clear difference in orientation and density of the cells in the two regions.

2.5.4 Rat Tail Staining with Methanol

With data indicating that 4% PFA fixing may be damaging cellular structures, alternative approaches were explored. Previous successful studies characterising tendon cilia have used methanol fixation and therefore fixation with methanol was investigated[186].

Rat tail tendon fascicles were fixed by immersion in 100% methanol (Sigma-Aldrich, St Louis, MO) inside 0.5ml Eppendorf tubes for 2 hours at 4°C and room temperature, after which samples were immunofluorescently labelled as in section 2.5.3, using primary antibody concentrations of 1:100. Samples were stained both with and without 0.5% Triton-X for 5 minutes, to test the effectiveness of methanol's permeabilisation properties. 12 RTTFs were used, 3 for each condition. Table 11 shows the range of conditions used.

Fixation Time (100% Methanol)	Antibody Concentration	Permeabiliser Concentration (Triton-X)	Permeabiliser Time (Triton-X)
120 minutes at 4°C, 120 minutes at RT	1:100	0.5%	0, 5 minutes

Table 11: Shows fixation durations, antibody concentration, permeabiliser concentration and permeabiliser durations for the RTT staining test with methanol.

While only minimal signal was observed with acetylated α-tubulin, clear signal was observed with ARL13b allowing cilia to be distinguished in all conditions tested. It is not clear why acetylated α-tubulin did not give a clear signal, as a recent study comparing fixative methods for cilia labelling found that both acetylated α-tubulin and ARL13b worked with methanol and PFA fixation[181]. Further, this acetylated α-tubulin antibody has been successfully used with human tenocytes fixed with both PFA and methanol in this thesis, which suggests that the issue may be species reactivity. However, the clear signal from the ARL13b was deemed acceptable for assessing cilia length and prevalence and was used henceforth for all rat tail cilia experiments.

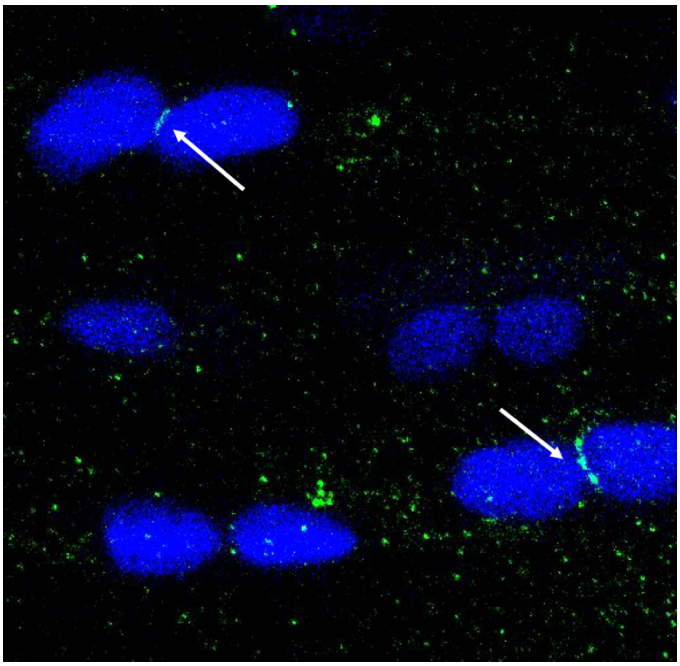

Figure 20: Figure showing cilia in stained with ARL13b in green and DAPI stained nuclei in blue.

There was no observed difference in explants fixed at room temperature and 4°C and no apparent difference with the addition of Triton-X. The final protocol for rat tail tendon tissue cilia fixation used throughout the project is as follows:

1. Fix fascicles with 100% methanol for 120 minutes at room temperature.
2. Wash 1 time with PBS.
3. Block cells using goat serum for 30 minutes at room temperature.
4. Incubate with rabbit anti-ARL13b @1:100 in PBS with 0.1%BSA overnight at 4°C.
5. Wash 3 times for 5 minutes with PBS with 0.1% BSA.
6. Incubate with anti-rabbit 488 @ 1:1000 for 1 hour at room temperature in darkness.
7. Wash 3 times for 5 minutes with PBS with 0.1% BSA.
8. Incubate with DAPI @ 1:1000 for 5 minutes @ RT
9. Wash 1 time for 5 minutes with PBS with 0.1% BSA
10. Place fascicles on glass slides, add 20µl of Prolong Gold and place rectangular 40x22mm glass coverslips over the top of each fascicle.
11. Leave to set in the dark overnight.

2.6 Image Analysis

2.6.1 Imaging and Measuring the Cilium (in Tissue)

One of the key ways of identifying cilia expression is by quantifying cilia prevalence and length[187]. This can be done through analysis of confocal image stacks. Confocal image stacks in tissue were taken so as to give high resolution images such that the cilia could be clearly visualised while also giving large enough fields that multiple cilia from a region could be identified and measured. A pixel size of 0.11x0.11μm was identified as appropriate, as this equates to approximately double oversampling when compared with the full width half maximum (FWHM) of 63x magnification confocal microscopy. Double oversampling is used as this fulfils the Nyquist criterion and further oversampling gives no further increase in resolution, while lower sampling rates lose resolution and can introduce low frequency aliasing. Confocal microscopy is less accurate in the z direction and therefore optical sections were taken at a separation distance of 0.25μm which equates to approximately half the FWHM in the z direction of approximately 0.5μm.

It is important to orientate the fascicle and standardise the plane in which images are taken so as to enable identification of different tendon regions. The plane in which images through whole rat tail fascicles were taken is shown in Figure 21 which shows a cross section of a fascicle as well as examples of the planes in which FM and IFM images are taken.

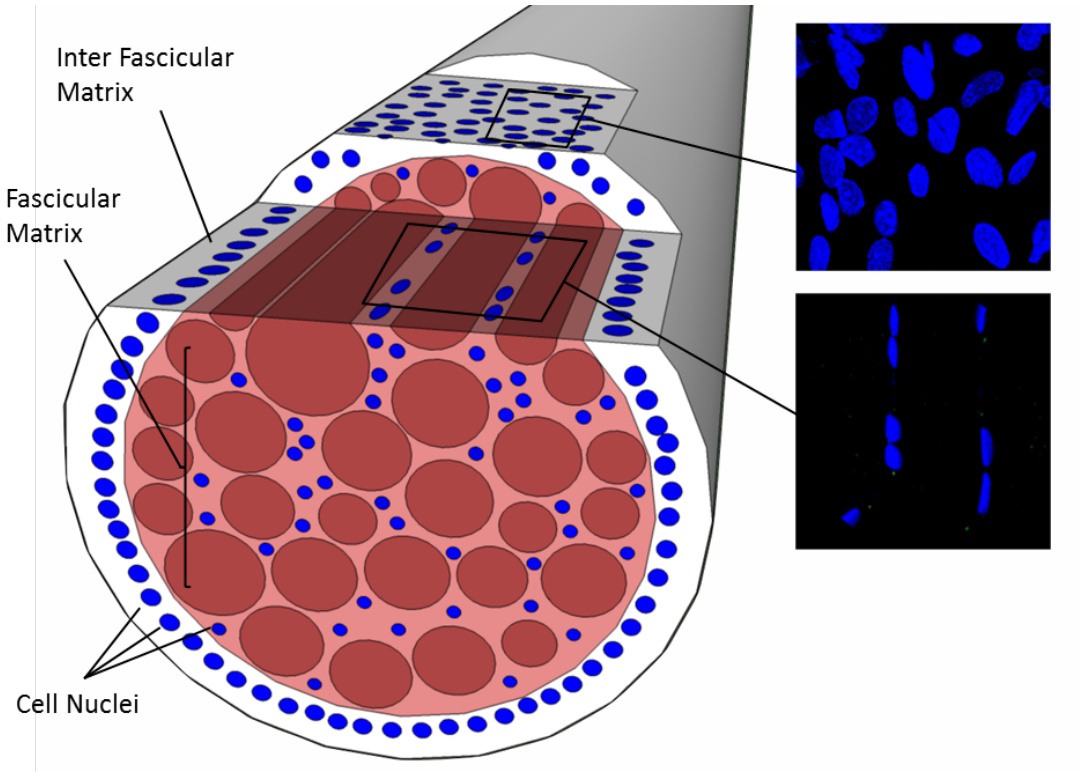

Figure 21: Schematic showing the plane in which confocal images of rat tail tendon fascicle were taken. *The top-right inset image shows DAPI staining of rounded nuclei in the IFM. The mid-right inset image shows DAPI staining of elongated nuclei further into the tissue, within the fascicle matrix.*

Separate stacks were taken for FM and IFM as taking a single image stack containing both FM and IFM would be too large. To visualise the entire field and full length of each cilium within a single image, stacks of between 10-15μm in depth are taken and then converted into a maximal projection, whereby the brightest pixel in each optical section is used as the value in the new flat image. The cilia can then be identified and measured in the maximal projection using ImageJ. This is much simpler than trying to measure them within the stack. However, since the cilia are highly unlikely to be oriented directly in the plane of imaging it is necessary to reconstruct the 3 dimensional orientation of the cilium to obtain the true length of the cilium. This is generally achieved by assuming that the cilia are straight, counting the number of sections the cilium occurs

in and then calculating the full length, as well as the deflection out of plane, using Equation 1. This is shown diagrammatically in Figure 22.

$$\text{Corrected Length} = \tan^{-1}\frac{(n-1)\Delta z - \delta z - t}{L}$$

Equation 1: Reconstructing Cilia Length from an Image Stack. *Where n is the number of section in which the cilium was observed, L is the cilia length in maximal projection,* Δz *is the distance between z sections, t is the thickness of the cilium which has been estimated at 0.2μm, and* δz *is the limit of the resolution of the objective lens out of plane based on the FWHM which is 0.5μm for the current set up.*

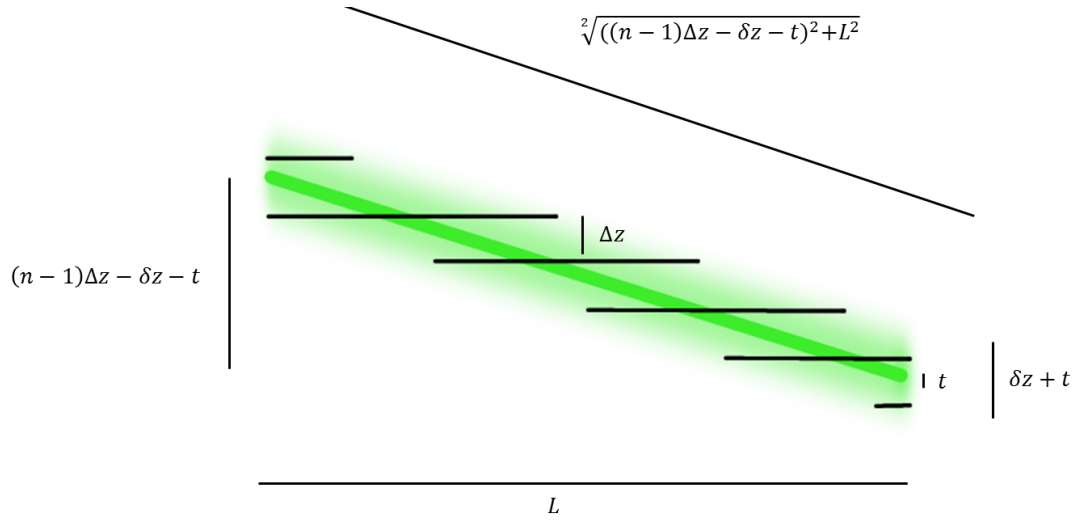

Figure 22: Diagrammatic visualisation of Equation 1. *The green bar represents the cilium and the faded green represents the area over which signal is picked up by the microscope. L is the cilia length in maximal projection,* Δz *is the distance between z sections, t is the thickness of the cilium which has been estimated at 0.2μm, and* δz *is the limit of the resolution of the objective lens out of plane based on the FWHM which is 0.5μm for the current set up.*

2.6.2 Nuclear Shape Analysis

As a proxy for cell shape, nuclear orientation and aspect ratio are calculated using maximal projection DAPI confocal images. The images were binary thresholded using the ImageJ IsoData iterative sorting method based on the algorithm by Ridler and Calvard[188]. The ImageJ plugin to fit ellipses was then used on the thresholded images.

All overlapping nuclei were discounted by manually comparing between original DAPI images and ellipse fitted images. For each ellipse the orientation and aspect ratio were outputted. This data gives an approximation of cell orientation and elongation.

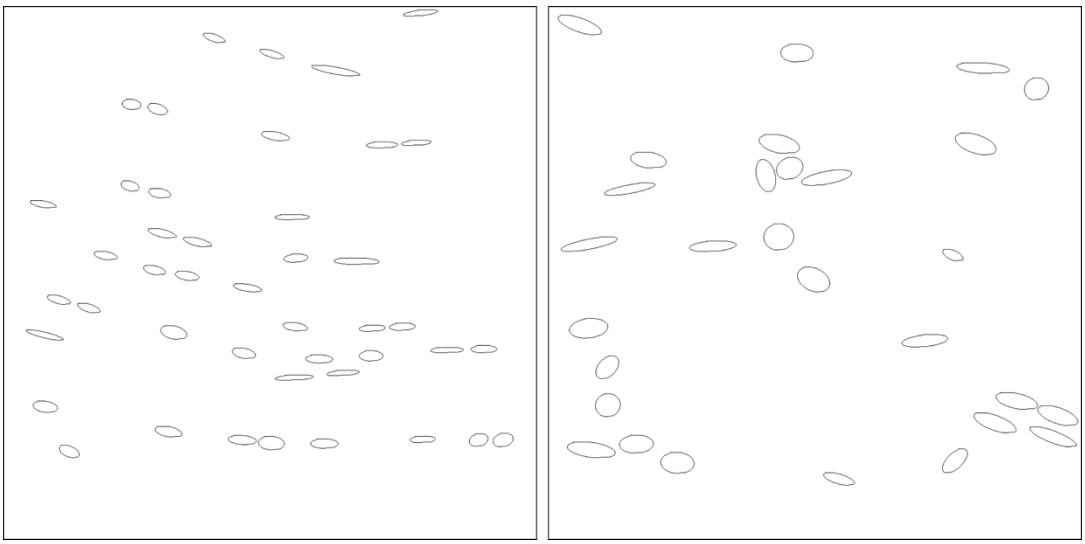

Figure 23: Example ellipses of tenocyte nuclei, FM on the left and IFM on the right.

2.7 Summary

The techniques described above are those that were used throughout this thesis in order to test the hypotheses described in section 1.9.1.

Mechanical testing techniques were used to apply strain to tendon cells in fascicles as well as in isolation in order to understand the cilia response to loading. Mechanical testing was also used to assess how the cellular effects of stress deprivation change the mechanical properties of tendon fascicles.

Imaging was used extensively to investigate cilia structure in tissue and isolated cells, and combined with the mechanical testing techniques, how cilia structure responds to mechanical stimulation.

A number of other techniques including RT-qPCR, SiRNA transfection and tissue damage analysis were used a small number of times at specific points during this thesis and are described and discussed in the relevant experimental chapters.

3 Zonal variation in primary cilia elongation correlates with localised biomechanical degradation in stress deprived tendon

3.1 Introduction

Tendons perform the primary function of transferring force from muscle to bone, undergoing regular cyclic loading and maintaining a constant pre-stress as a result of muscle attachment. Tendon has long been known to remodel its extracellular matrix (ECM) in response to changing loading condition. For example, the complete removal of external stress, also known as stress deprivation, results in degeneration of the tendon, including changes in collagen organisation and mechanical properties similar to the effects of tendinopathy[97,105,189]. Stress deprivation in tendon can occur due to a number of different pathologies, such as tumours, infection, congenital deformities, degenerative diseases and trauma[110]. It has also been hypothesised that the fibrillar micro damage resulting from overuse of tendon results in local areas of stress deprivation, and it is the subsequent stress deprivation conditions that are responsible for the development of tendinopathy[100].

Tendons are hierarchical structures, composed at the macro scale of collagen rich fascicles, bound together by a softer highly hydrated matrix called the endotenon or inter-fascicular matrix (IFM). Both the collagen rich fascicular matrix and the IFM contain tenocytes which synthesise and maintain the extracellular matrix. However, there are morphological and metabolic differences between the populations of cells in the FM and IFM, with rounder, more abundant and more active cells in the IFM[73]. In addition, recent work has shown that cyclic overloading of tendon tissue results in

increased expression of inflammatory markers and degradation proteins in the cells of the IFM, when compared with those in the fascicular matrix[74]. However, differences between these regions have not been investigated under stress deprivation.

Primary cilia are thin, non-motile, eukaryotic cellular organelles which project out from the cell, with almost every cell in the human body containing a single cilium[125]. Primary cilia are composed of an array of 9 microtubule doublets enclosed by a specialised cell membrane[125,134]. The length of cilia and the proteomal content are tightly controlled by intraflagellar transport and cilia are usually between 1-2μm in length in fresh tendon. First observed by Kowalevsky in 1867 primary cilia were mostly ignored for the next 100 years[122]. However, over the last 20-30 years a growing interest in their behaviour has led to the discovery of their role in autosomal dominant polycystic kidney disease (ADPKD) and an increasing range of so called ciliopathies[190].

Primary cilia are now known to function as a hub for various signalling pathways including mechanotransduction, as well as many pathways whose receptors are localised in the cilium such as Wnt and Hedgehog signalling[5,6,148]. More recent studies have shown involvement in growth factor signalling, differentiation and inflammation[153,191]. These pathways are important for development as well as healthy cell and tissue function[144].

Although cilia have been identified in tendon and shown to elongate in response to stress deprivation, the mechanism responsible for elongation, and the further consequences, are still unclear. Furthermore, no previous studies have investigated primary cilia expression or response to stress deprivation in the different regions of the tendon. Therefore, the aim of this study was to investigate how stress deprivation affects primary cilia in the fascicular and inter-fascicular tendon matrix. Changes in cilia were then evaluated to determine whether they are mediated by differential changes in the

mechanical properties in the two region. Finally, it was examined whether any localised changes in the cilia structure and tissue mechanics could be prevented by the application of static loading. Static loading was chosen to replicate the at-rest pre-strain found in tendon in vivo.

It was hypothesised that there are differences in cilia expression, specifically cilia length and orientation, between the cells of the FM and IFM. Further, that there are zonal variations in the response of the FM and IFM to stress deprivation, in terms of both cilia expression and tissue mechanics.

3.2 Methods

3.2.1 Stress Deprivation and Static Strain

Tendon fascicles were obtained from the tails of 200g (10 – 12 weeks old) female Sprague–Dawley rats, obtained from rats killed for unrelated purposes. Rats were euthanized by neck dislocation for extraction of dorsal root ganglia. Animal procedures were approved by the Animal Care Committee of Queen Mary, University of London, and the UK Home Office, and were in accordance with the UK Animals (Scientific Procedures) Act of 1986, and with the EU Directive 2010/63/ EU for the protection of animals used for scientific purposes. Fascicles were dissected as discussed in section 2.1.3.

18 fascicles were dissected from each of 3 rats. 6 fascicles from each rat tail were fixed and prepared for imaging immediately after dissection, as described in section 2.5.4. 6 fascicles from each rat were maintained stress deprived for 7 days, as described in section 2.3.1, and 6 fascicles from each rat were maintained at 4% static strain for 7 days, as described in section 2.3.1, before preparing for cilia staining and imaging. Cilia were

stained and imaged using the Leica confocal as described in section 2.5.4 and the method described in 2.6.1.

3.2.2 Time Course

To investigate the time frame over which cilia length changes occurred, twenty-four fascicles were dissected from a single tail. Six fascicles were prepared for imaging immediately. with further groups of six fascicles first subjected to 6, 16, or 24h stress deprivation prior to imaging preparation. Fascicles were imaged using the Leica confocal as above. The data was combined with that collected after 7 days stress deprivation from the previous experiment.

3.2.3 Mechanics

Fascicle mechanics in the fresh, stress deprivation, and static strain groups were tested using the Instron mechanical testing machine. Samples were prepared under fresh, stress deprived and 4% statically strained conditions with 8 fascicles per group.

Fascicle diameter was measured using a laser micrometer (LSM 501; Mitutoyo, Kawasaki, Kanagawa, Japan) with the lowest diameter across the test length recorded. Fascicles were secured in pneumatic grips at a gripping pressure of 4bar and a grip separation distance of 20mm. A tare load of 0.1N was applied to each sample, and the sample length established for strain calculations. Fascicles were preconditioned by applying 10 cycles between 0% and 4% strain at 1 Hz, followed by a strain to failure test at an extension rate of 1mm/s. Quasi static failure properties were calculated from the extension to failure test and hysteresis and cyclic stress relaxation were calculated from the preconditioning cycles as described in section 2.2.1.

IFM mechanics were investigated using the method described in section 2.2.2 using a separation distance of 20mm. The opposing fascicle ends were then secured in the pneumatic grips and a 0.05N tare load was applied to the samples. Samples were then strained to failure at 1mm/s. Fresh and stress deprived groups were both tested (n=6 fascicles per group). However, it was not possible to test 4% statically strained IFM samples since clamping and holding the fascicle pairs under static strain during sample preparation caused the IFM to tear and the fascicles to separate. Therefore, only the fresh and stress deprived test groups are reported.

3.2.4 Treatment with IL-1

18 fascicles were dissected from a single tail. 6 were fixed and stained fresh, 6 were stress deprived for 6 hours and 6 fascicles were stress deprived for 6 hours in the presence of 1ng/ml IL-1, before fixation and staining as in section 2.6.1. IL-1 has previously been shown to be associated with rapid <6h cilia length changes in other tissue types and may also be associated with applied tendon strain and tendinopathy[191–194].

3.2.5 Data Analysis

All data was assessed for normality with the Shapiro–Wilk test and then tested for significance with one tailed unpaired Student's t-tests. The full set of data collected is shown in Table 12.

Experiment	Conditions	Measurements
7 Day Cilia Length Experiment (Figure 24)	Fresh Stress Deprived 4% Static Strain	Cilia Length Cilia Orientation
Cilia Length Time Course (Figure 26)	Fresh Stress Deprived	Cilia Length
Fascicle Mechanics (Figure 27 & Figure 28)	Fresh Stress Deprived 4% Static Strain	Diameter Failure Stress Failure Force Failure Strain Hysteresis across 10 cycles Stress relaxation over 10 cycles
IFM Mechanics (Figure 29)	Fresh Stress Deprived	Failure Force
Effect of IL-1 on fascicle cilia	Fresh 6h Stress Deprived	Cilia Length

Table 12: Experiments performed during this study.

3.3 Results

3.3.1 Cilia Length and Orientation

Representative images of FM and IFM cells in all three test conditions are shown in Figure 24a, from which mean cilia lengths were calculated (Figure 24b). Confirming previous work, cilia in stress deprived fascicles were shown to significantly increase in length. However, data additionally showed that maintaining fascicles under static strain resulted in a significant reduction in cilia length relative to stress deprived tissue. Considering regional differences in cilia length, there was no significant difference in cilia length between FM and IFM cells in fresh samples. However, in the stress deprived

tissue, IFM cell cilia almost trebled in length and were significantly longer than the cilia of fascicular cells. Maintaining the samples under 4% static strain for 7 days lead to significantly reduced length increase compared with the stress deprived tissue for both the FM and IFM cells. However, there was still a significant increase in cilia length in the IFM relative to the fresh tissue. In fresh FM cells, cilia were predominantly orientated in the direction of normal axial tendon loading, which has been previously observed[173]. However, there was no predominant orientation observed in IFM cells (Figure 24c). While there did appear to be some loss of alignment of FM cilia with stress deprivation, this was not significant (data not shown). Furthermore, cell nuclei in the IFM were significantly rounder than those in the FM (Figure 25) potentially due to differences in the extracellular matrix structure.

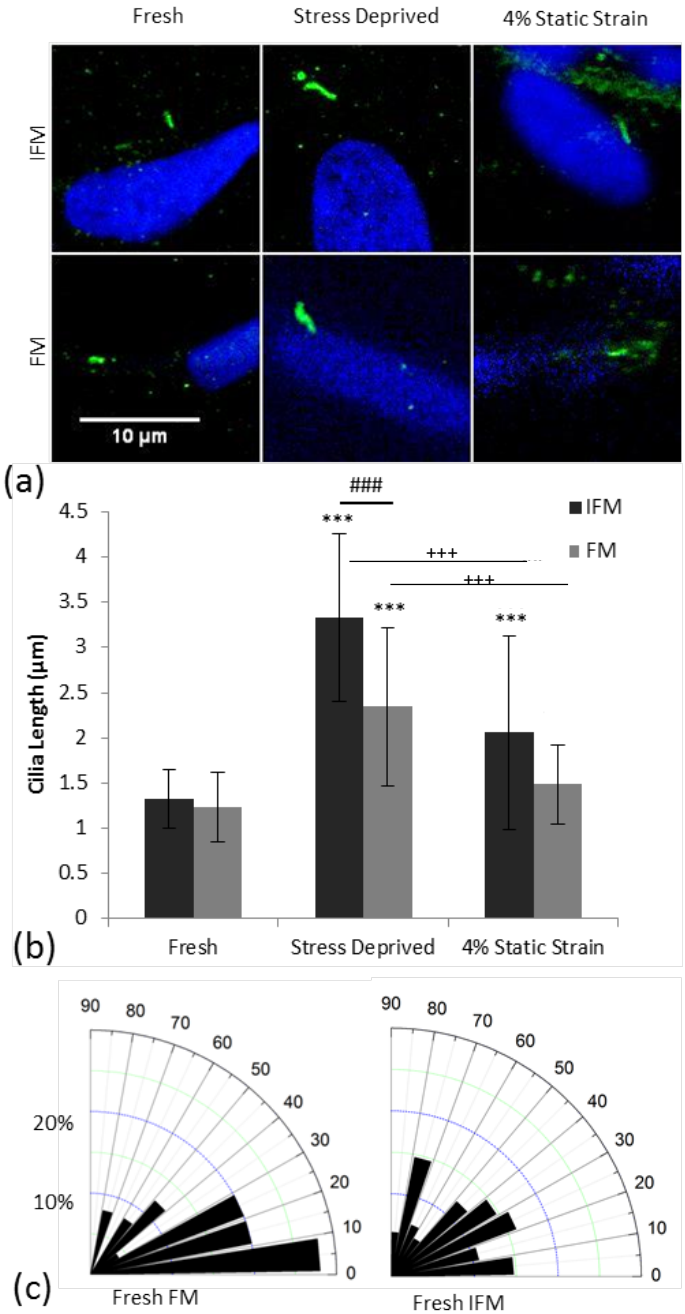

Figure 24: Under stress deprivation cilia length increases more in the inter-fascicular matrix than in the fascicular matrix. Under static strain the cilia length is partially conserved *. (a) Shows representative cilia for each condition. (b) Shows mean cilia length in each condition. Cilia measurements from three rat tails were combined. N=80±40 cilia measured per condition. Asterisks (*) show significance from the same region in fresh tissue. Crosses (+) show significance between stress deprived and static strain conditions for the same region of the tissue. Hashes (#) show significance between the two tendon regions at each condition. In all cases significance indicated at p<0.05 (*), p<0.01 (**) and p<0.001 (***). Error bars show ±1 standard deviation. Statistical analysis performed using 2 factor Anova (groups and interactions significant at p=0.001) with Tukey-Kramer post hoc testing. (c) Shows frequency distribution rose histograms of cilia angle with respect to the long axis of the tendon in fresh tissue.*

A time course was performed in order to gain some insights into potential lengthening mechanisms for the cilia of both regions (Figure 26). No increase in cilia length in either IFM or FM cells was observed after 6h of stress deprivation. However, by 16 h, stress deprivation had led to a significant increase in cilia length in both the fascicular and IFM cells. Data indicates that the increase in FM cell cilia length occurred gradually over the time course, while the majority of the IFM cell cilia length increase occurred after 24 h.

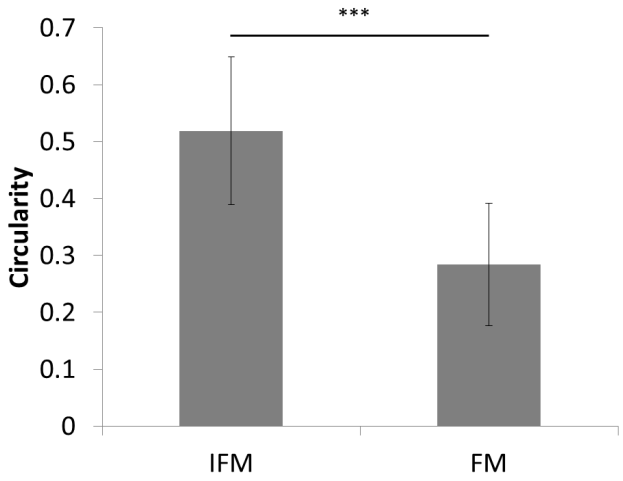

Figure 25: IFM cell nuclei are significantly rounder than those in the FM. *In all cases significance indicated at p<0.05 (*), p<0.01 (*) and p<0.001 (*). Data were analysed with a 2 tail Student's T-test.*

3.3.2 Fascicle and IFM Mechanics

Figure 27a shows representative preconditioning loops for fresh, stress deprived, and 4% static strain fascicles, from which hysteresis and stress relaxation were calculated. Hysteresis in cycle 1 is significantly higher in the stress deprived fascicles than in the other two conditions (Figure 27b). Furthermore, stress relaxation over the 10 cycles was significantly higher in the stress deprived fascicles than in either of the other two conditions (Figure 27c). However, a significant increase in stress relaxation was also seen in the 4% static strain condition relative to the fresh control.

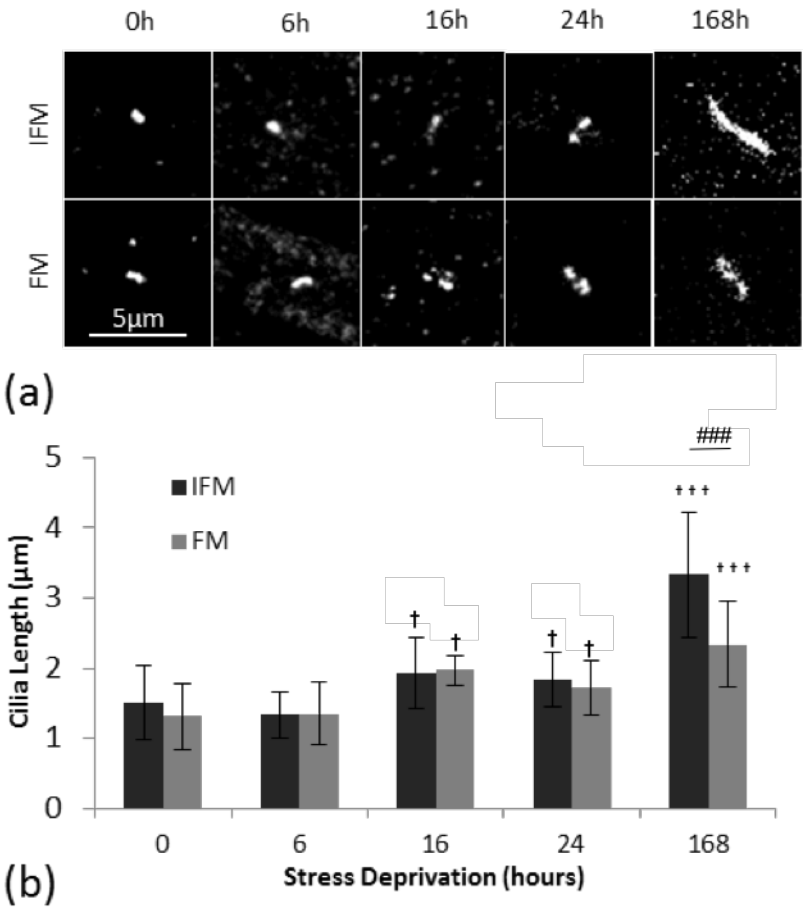

Figure 26: Stress deprivation time course shows that initially cilia length increases similarly in FM and IFM cells up to 24h but after 1 week IFM cell cilia are significantly longer than FM cell cilia. *(a) Shows representative cilia in the IFM & FM for each time point. (b) Shows mean cilia length in fascicular and IFM cells after 0, 6, 16, 24, and 168h of stress deprivation. N=60±30 cilia measured per condition. Data were analysed with 2-factorAnova (groups and interactions significant at p=0.001) and post hoc testing was performed using Tukey-Kramer. Crosses (+) show significance from the corresponding region in control (0h) tissue. Hashes (#) show significance between the two tendon regions for a given condition. #=p<0.05, ##=p<0.01, ###=p<0.001. Error bars show ±1 standard deviation.*

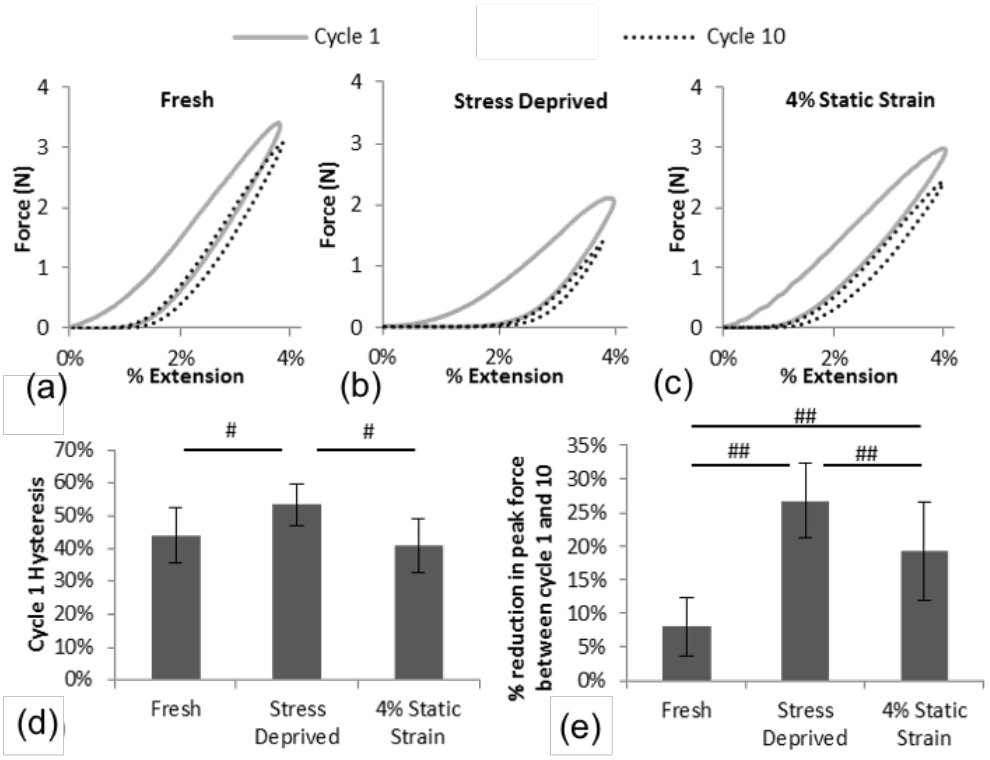

Figure 27: Under stress deprivation there is significant increase in viscoelastic behaviour. *(a–c) Show representative 4% cyclic preconditioning loops for fresh, stress deprived, and 4% static strained fascicles, respectively. Each figure shows preconditioning cycles 1, 2, and 10. (d) Shows the mean hysteresis in the first preconditioning cycle. (e) Shows the mean percentage reduction in peak force over the 10 preconditioning cycles. N=8 fascicles per group. Data were analysed with 1-factor Anova with post-hoc testing performed using Tukey HSD. In all cases significance indicated at p<0.05 (#), p<0.01 (##) and p<0.001 (###). Error bars show ±1 standard deviation.*

Quasi-static tests to failure of fascicles indicated little change in failure properties between test groups (Figure 28). While the failure stress was significantly reduced in stress deprived fascicles (Figure 28d), it is evident from the consistent failure force across groups (Figure 28b), that this was due to the increased fascicle diameter (Figure 28c) and not a change in fascicle mechanics. However, failure strain was significantly higher in stress deprived fascicles compared with the other two conditions (Figure 28e). Mechanical changes to the IFM with stress deprivation were also investigated using the IFM shear model described in section 2.2.2. Mechanical integrity of the IFM was reduced to such an extent that preconditioning was not possible for the stress deprived

samples. Therefore, all samples were only subjected to a quasi-static failure test, with typical curves shown in Figure 29a. After stress deprivation, the IFM fails at a significantly lower force, able to withstand only 50% of the failure force of fresh samples (Figure 29b). However, the effect on the IFM of static loading is not known.

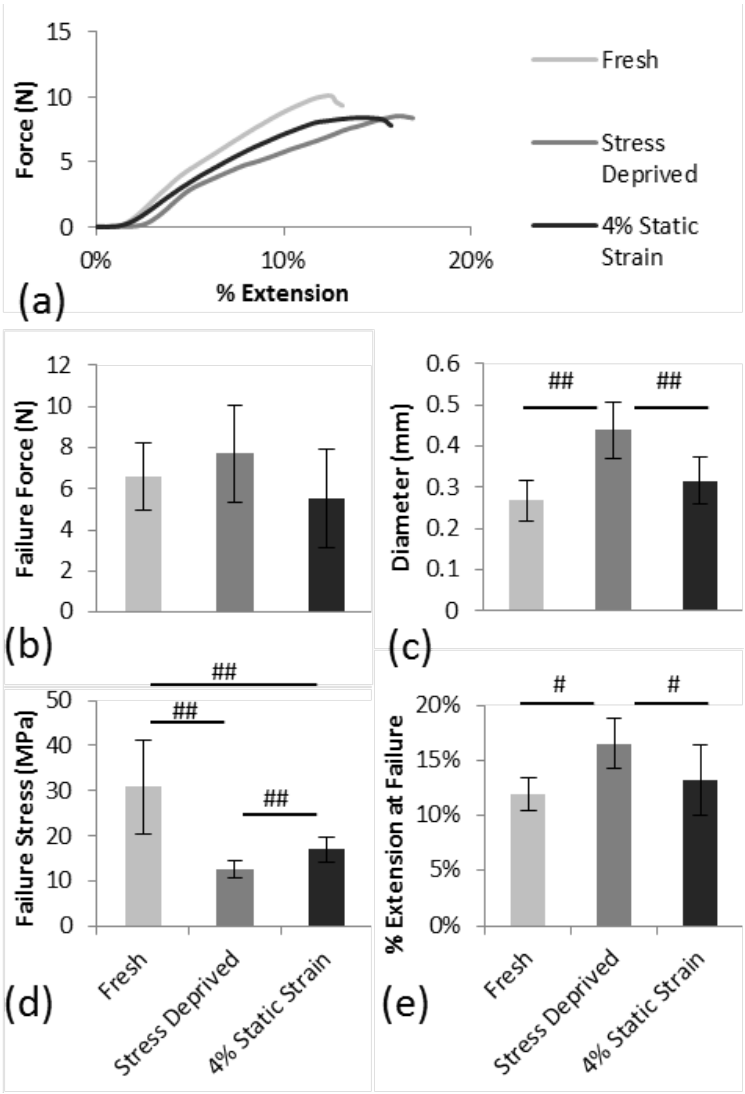

Figure 28: Stress deprivation does not cause significant loss of quasi static mechanical properties in fascicles. *(a) Shows representative failure curves for each condition, from which mean fascicle failure force, diameter, failure stress, and failure strain are determined. Failure force is not significantly different for any of the groups (b); however, failure stress is significantly lower for the stress deprived and statically strained fascicles, as a result of the significant increase in average fascicle diameter. Failure extension was significantly higher in the stress deprived samples. N=8 fascicles per condition. Data were analysed with 1-factor Anova with post-hoc testing performed using Tukey HSD. In all cases significance indicated at $p<0.05$ (#), $p<0.01$ (##) and $p<0.001$ (###). Error bars show ±1 standard deviation*

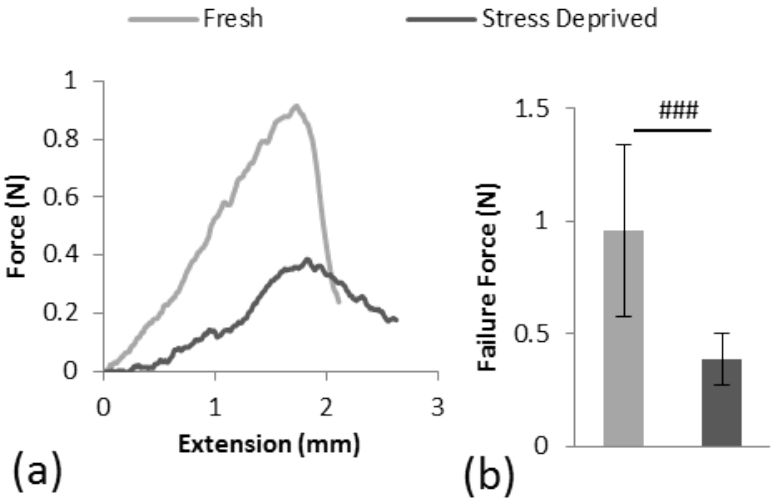

Figure 29: The inter-fascicular matrix shows a significant reduction in failure strength after stress deprivation. *This figure shows representative force-extension curves to failure for the IFM in stress deprived and fresh samples (a), alongside mean IFM failure force data (b). N=6 fascicle pairs per group. In all cases significance indicated at p<0.05 (#), p<0.01 (##) and p<0.001 (###). Data were analysed with a 2 tail Student's t-test Error bars show ±1 standard deviation*

3.3.3 Effects of Il-1

There was no significant effect observed on cilia length with the application of IL-1 in either the FM or IFM after 6 hours of treatment (Figure 30).

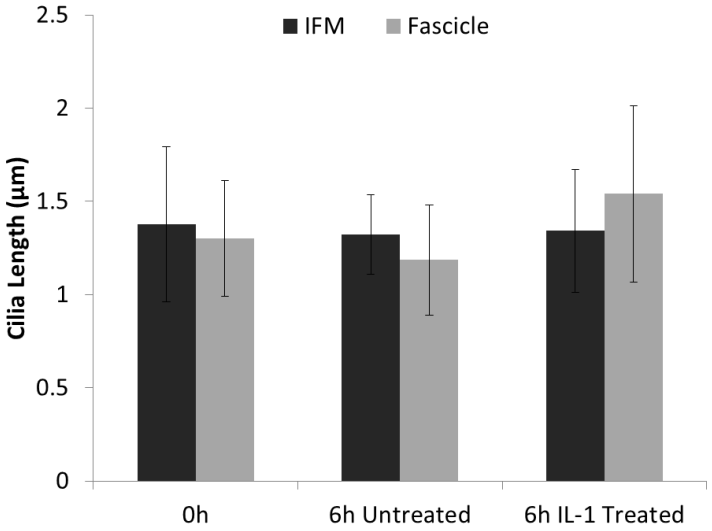

Figure 30: Treatment with Il-1 does not significantly change the length of fascicle or IFM tendon cell cilia. *N=6 fascicles per group. Data were analysed with 2-factor Anova (no significance).*

3.4 Discussion

It has been understood for some time that the tenocytes within functionally different tendons have different levels of metabolic activity[195]. However, recent work from Screen et al has shown that within a single tendon there are also metabolic and morphological differences between the cells in the fascicular matrix (FM) and the inter-fascicular matrix (IFM)[16,17,56]. These differences include increased metabolic activity in IFM cells, which are also rounder and more numerous for a given area. It is likely the IFM cell population is heterogeneous, but may contain a sub-population of more metabolically active Tendon Derived Stem Cells (TDSCs)[196].

This study is the first to show that the primary cilia response to stress deprivation is different in the inter-fascicular and fascicular matrix, and that this reflects differences in the biomechanical degradation of these regions. In particular, this shows that stress deprivation causes greater elongation of the primary cilia in the inter-fascicular matrix associated with a greater loss of biomechanical integrity in this region.

In fresh tendon, primary cilia length was the same in both the inter-fascicular matrix (IFM) and the fascicular matrix (FM) with most cilia between 1-2μm. Quantification of cilia prevalence was not attempted, as short cilia (less than 1μm in length) are difficult to identify in intact tissue, such that population estimates of cilia length tendon are biased towards longer cilia, and therefore any attempt to quantify cilia prevalence is likely to produce an underestimate of the true prevalence, particularly for samples with shorter cilia. In the fascicular region, cilia were oriented in the direction of the long axis of the tendon which is also the axis of applied mechanical load. By contrast, cilia in the inter-

fascicular region were distributed with no specific orientation. These differences in cilia orientation may reflect the differences in the local strain environment of the cells. Alternatively, cilia orientation may be determined by the structural organisation of the collagen matrix, as seen in previous studies, which have demonstrated that cilia alignment is associated with nanoscale topographical organisation of the substrate[197]. Indeed, in agreement with previous studies, under stress deprivation the highly aligned cilia in fascicular cells appeared to become more randomly orientated[174], potentially reflecting the loss of collagen organisation typically reported with stress deprivation[103].

While it has been previously shown that tenocyte cilia lengthen under stress deprivation in the FM [9], this study shows for the first time that after 7 days of stress deprivation, cilia in the IFM show a significantly greater elongation; 151% compared to only 90% in the FM. The mechanism responsible for this cilia elongation is unclear, although there are many regulators of cilia length including actin tension, the availability of soluble tubulin and direct physical stimuli[170,171]. Previous studies have reported that increased mechanical loading results in cilia shortening in chondrocytes via a mechanism involving the tubulin deacetylase, histone deacetylase 6 (HDAC6)[198] as also occurs in response to heat shock[199]. It is therefore possible that stress deprivation causes a reciprocal relationship, inhibiting the effect of HDAC6 thereby enabling cilia elongation.

The time course studies demonstrate that lengthening is not detectable until at least 6 hours of stress deprivation, with the majority of elongation occurring beyond 24 hours. This suggests that lengthening is not caused solely by the removal of mechanical load, since it has been previously demonstrated that cilia can disassemble or elongate within 3-6 hours of the removal of strain or other physicochemical stimuli[166,191,200]. Therefore, whether cilia elongation was mediated by the upregulation of inflammatory cytokines, such as IL-1β, was investigated. IL-1β has been shown to be upregulated in stress

deprived tissue and has been shown to cause rapid primary cilia elongation in chondrocytes[118,191]. However, in the current study no significant cilia elongation was observed after 6 hours of treatment with IL-1β in either the FM or IFM (Figure 30). Therefore, it seems unlikely that IL-1β is directly responsible for the stress deprivation induced increase in cilia length.

Having shown that cilia elongation was unlikely to be caused directly by the removal of mechanical load or by the associated increased expression of inflammatory cytokines, it was investigated whether cilia elongation may directly result from changes in the biomechanical and structural environment of the matrix. This was done by quantifying the changes in mechanics in both regions during stress relaxation. The lower shear strength of the IFM in the rat tail compared to that seen in other more functionally loaded tendons[16], does limit the applicability of the rat tail model for investigating FM and IFM mechanical changes. However, its extensive use over the last 50 years, and the importance of being able to prepare samples for both cilia imaging and mechanical characterisation without dissection damage to either the IFM or FM makes it the most suitable model for this particular investigation[19,201]. It was found that the biomechanical properties of the IFM and the FM change differently under stress deprivation. In the FM there was no significant loss in fascicular failure force although significant swelling of the fascicle occurred, which caused a reduction in failure stress due to increased cross sectional area. Swelling was probably also responsible for the increased failure strain and viscoelasticity of the fascicles, as more extensive fluid movement will increase the capacity for energy dissipation in the matrix during loading[202]. By contrast, much larger biomechanical changes were observed in the IFM where the failure force of the IFM in shear reduced significantly, by approximately 50%, after stress deprivation.

A number of previous studies, whilst not directly associating stress deprivation with IFM degradation, do strongly support such a finding. Stress deprivation has been shown to affect the transverse mechanical properties of tendon more substantially than the longitudinal properties[107], and also to affect whole tendon sections more than isolated fascicles[106], pointing towards the greatest stress deprivation changes occurring in the matrix between fascicles. Further, stress deprivation has been shown to more adversely affected non-collagenous that collagenous matrix components[203], which would also lead to a greater degeneration of the IFM, which is known to be proteoglycan-rich[56]. As has been shown recently it is possible to differentially dissect the FM and IFM for proteomics analysis which would be invaluable in further testing the differential degradation between IFM and FM[15].

Taken together, there is a clear correlation between biomechanical matrix degradation and the extent of primary cilia elongation. Thus the data indicates that mechanical degradation of the ECM may directly contribute to the cilia elongation associated with stress deprivation. Or else, that the cellular mechanisms causing matrix degradation also lead to increased cilia length. However, the precise pathways associating these parameters remain unclear. The matrix degradation occurring with stress deprivation is likely cell mediated. However, studies have reported some loss of mechanical properties even in acellular tendon samples subjected to stress deprivation, potentially due to changes in water content[117]. While not directly influencing cilia length IL-1β may still play a role in directly initiating tendon mechanical degradation. Treatment using IL-1β antagonists slightly reduces the biomechanical degradation of whole tendon samples during stress deprivation[120]. However, IL-1β antagonists did not significantly reduce degradation of individual fascicles, suggesting that IL-1β mediated degradation is primarily localised to the IFM. This correlates with studies showing that IL-6, MMP-3

and MMP-13 are all upregulated in response to tendon overload, but specifically in IFM cells, suggesting more pronounced metabolic changes are localised to the IFM region[74].

While the elongation of the cilia seems to be induced by, or at least associated with, matrix degradation, the consequences of this elongation are unclear. In other cell types cilia elongation is associated with increased mechanotransduction[8], reduced hedgehog signalling[204] reduced Wnt signalling[205] and increased inflammatory signalling[6,191,206]. As such, changes in cilia length caused by matrix degradation may subsequently influence cilia signalling pathways and further modulate the biomechanical degradation.

To further investigate the relationships between stress deprivation, matrix degeneration and cilia lengthening, prevention of both cilia elongation and biomechanical degradation was attempted by the application of a gross static strain over the same 7 day period. While it was unfortunately not possible to test the mechanical properties of the statically strained IFM, since the process of clamping and statically straining two attached fascicles caused them to separate over the 7 day culture period, maintaining the fascicles at 4% static strain was shown to minimise the viscoelastic biomechanical changes seen in the fascicles. Furthermore, static strain conditions significantly reduced the cilia elongation in both the FM and the IFM. This agrees with previous work that shows that tendon requires loading in order to properly function and that the loss of this stress causes tendon degradation[97,207].

In summary, this work shows for the first time that tendon stress deprivation explicitly leads to greater mechanical degradation in the IFM compared with the FM and that this correlates with a greater increase in primary cilia length. Further, this suggests that stress deprivation drives matrix catabolism, possibly partly through the up-regulation of inflammatory signalling, and that the resulting biomechanical and structural degradation

drives the primary cilia reorientation and elongation. The greater loss of biomechanical integrity with stress deprivation in the IFM is consistent with previous reports that the IFM turns over more rapidly than the FM in tendon[73], hence any cellular remodelling is likely to occur faster in the IFM. Furthermore, increased expression of MMPs and inflammatory cytokines are seen localised to this region with loading, again indicating a more active cell population[74].

The reported differential changes in cilia structure following stress deprivation are likely to produce differences in cilia signalling which may further modulate the differential degradation between tendon regions. Such zonal changes in cilia structure and function may therefore have important consequences in the aetiology of tendinopathy. Furthermore, in other connective tissues such as ligaments, intervertebral disks, articular cartilage or even blood vessels, similar biomechanical degradation induced by physicochemical or pathological stimuli may lead to similar alterations in primary cilia structure, thereby modulating cell behaviour.

4 Mechanical loading induces primary cilia disassembly in tendon cells via TGFβ and HDAC6.

4.1 Introduction

The cells within tendon, have long been known to remodel the extracellular matrix (ECM) in response to changing loading conditions. This cellular response to mechanical loading is critical for tendon health and homeostasis and the retention of biomechanical functionality[208]. Both too much loading as well as too little appear to be harmful and both lead to catabolism and degeneration of the tissue[97,105,189]. Excessive cyclic load in particular, is thought to lead to degenerative tendinopathy and while the exact mechanisms are unclear, degenerative tendinopathy is thought to be cellular mediated. In light of this, numerous studies have investigated the effect of mechanical loading on tendon cell behaviour, demonstrating changes in the expression of genes regulating matrix synthesis and catabolism[80,189]. In particular, studies have shown that cyclic loading causes up-regulation of gene expression for collagen I and the matrix metalloproteases, MMP1 and MMP3, via activation of the TGFβ signalling pathway[80]. TGFβ is a cytokine which regulates a number of vital cellular processes including proliferation, differentiation, growth and apoptosis. Application of TGFβ to tendon explants was shown to lead to increased production of collagen, mimicking the effect of loading[116]. TGFβ has also been shown to bind to and regulate proteoglycan synthesis in tendon[31].

Primary cilia are expressed singularly by almost every eukaryotic cell type in the human body[125], and function as a hub for various signalling pathways such as Wingless (Wnt) and Hedgehog (Hh) signalling as well as mechanosignalling[6,144,148]. In tendon, they have been measured at 1-2 μm in length[9,174], and orientated in the direction of collagen

fibres[173]. The work in chapter 3 of this thesis found that tenocytes in the FM had primary cilia orientated in the direction of the collagen fibres and the applied tensile loading. However, tenocytes in the IFM had a more random orientation in line with the local collagen organisation in this region[209].

Primary cilia have been shown to be affected by mechanical load in a number of cell types. In articular chondrocyte primary cilia length is reduced by compressive[166] or tensile loading[204]. In bone cells and epithelial cells, fluid shear forces also induce cilia disassembly and shortening[171]. Studies using tendon explants show that cilia elongate under stress deprivation and that this can be prevented by static loading[9].

The few previous studies on tendon primary cilia response to loading have only examined static loading, stress deprivation, or low levels of cyclic loading, and all studies have been performed in fascicle explants. Therefore, little is known about how cilia respond to cyclic tensile strain as experienced by tendon cells in vivo during normal activity, or the effect of higher magnitude cyclic strains likely to induce tendinopathy. Similarly, the mechanism by which mechanical loading regulates primary cilia length in tendon cells is also unknown. Finally, no studies have investigated cilia length in isolated tenocytes which provide a valuable model system for investigating tenocyte mechanosignalling.

While the exact mechanism for mechanical regulation of cilia length in tendon is unknown, there are a number of mechanisms known to be involved in cilia length changes in other cell types which may play a role[171]. Increasing actin tension is known to inhibit cilia elongation and it has been suggested that actin tension can be regulated by changes in loading[168]. The effects of cyclic loading on the cytoskeleton are investigated through changes in nuclear morphology, as nucleus morphology correlates

strongly with cell morphology, this allows nuclear shape to be used as a reasonable proxy for cell shape[210]. The more regular shape of the nucleus means that it can be more reliably and easily measured; therefore, to investigate the effects of loading on cell shape and orientation it is possible to use changes in nucleus shape to give approximations for what is occurring at the whole cell level. Furthermore, loading induced effects on nucleus morphology can be compared with those on cilia orientation and length.

It has been shown that $TGF\beta_1$ which is released by loading, leads to cilia shortening and disassembly in osteoblasts[154]. Other studies show that the tubulin deacetylase, HDAC6 also regulates cilia elongation, associated with modulation of tubulin acetylation and polymerisation[154,167]. Therefore, it is hypothesised that $TGF\beta_1$ may be involved in cilia length changes in tendon. The purpose of this study is to determine how cyclic strain affects cilia length in tendon cells, and what mechanisms may be responsible for any changes, specifically investigating $TGF\beta_1$ and actin tension.

4.2 Materials and Methods

4.2.1 Tendon and Tenocyte Culture

Tenocyte media 2 and serum free media 2 were used throughout this set of experiments. For experiments involving intact tendon tissue, rat tail tendon fascicles were dissected from a single female Sprague-Dawley tail between 10-12 weeks of age, within 24 hours of death following procedure described in section 2.1.3[209]. This tissue was obtained as waste from unrelated experiments. All isolated cell experiments were performed using human tenocytes obtained by digestion from young (18-21) healthy male hamstring tendons with full ethics approval (Collaboration with Graham Riley, University of East Anglia, REC 09/h0302/3). Isolated tendon cells were cultured in media with serum in flasks up to passage 2 (P2) prior to use in loading experiments.

For initial analysis of cilia expression in isolated tenocytes, cells at passage 2 were seeded onto glass coverslips and cultured until confluence. Media used was tenocyte media 2 during seeding and was switched to serum free media 2 24 hours prior to loading. Serum free media was used to ensure cells were not dividing and therefore not expressing cilia.

For mechanical loading experiments, cells were cultured in Flexcell 6-well loading plates. 50,000 cells were seeded per well and then cultured for 3 days in tenocyte media 2 before subsequent loading. To determine the mechanism(s) involved in mechanoregulation of cilia expression the following reagents were used: Blebbistatin, Tubacin (1 μM), TGFβ_1 (10 ng/ml) and TGFβ-Receptor Inhibitor SB 431542 hydrate (TGFβ-RI) (10 μM). All antagonists and agonists were prepared in serum free media 2. All reagents unless otherwise stated were purchased from Sigma (Sigma-Aldrich, St Louis, MO)

4.2.2 Mechanical Loading of Isolated Tenocytes and Tendon Fascicles

Uniform, uniaxial cyclic tensile strain (CTS) was applied to the isolated tenocytes using the Flexcell FX4000-T system with arctangle loading posts (Dunn Lab, Germany). All mechanical loading experiments were performed in serum free media 2.

To investigate the response of tenocytes to cyclic strain. Cells from 1 donor were subjected to 3% CTS for up to 24 hours at 1Hz. 3% strain was used to be consistent with other similar tests as well as to be within the physiological range. 24h of loading was used to simulate high levels of repetitive use, this was chosen instead of an intermittent loading regime to keep results more consistent with other studies as well reduce the overall duration of the tests. A further group of cells from the same donor were left to recover for 2 hours after the application of strain. 6 wells were seeded per condition, for a total of 24 wells (4 plates). For unstrained controls, isolated tenocytes

were cultured in an identical manner but without the application of strain (6 wells, 1 plate).

To determine the mechanism behind cilia length changes, to investigate actin tension, cells from 1 donor were seeded onto 12 flex cell wells (2 plates). 6 wells were strained (24 hours, 1Hz, 3%) and 6 unstrained. 3 unstrained wells and 3 unstrained wells were treated with Blebbistatin (10 μM).

To investigate the role of TGFβ in mechanically induced cilia length changes, cells from 3 donors were seeded onto flex cells wells. Cells were cyclically strained for 24 hours at 1Hz both untreated or with the addition of either Tubacin (1 μM), TGFβ (10 ng/ml) or TGFβ-RI (10 μM). Controls for each group were unstrained. For each donor and each condition 3 wells were seeded, for a total of 72 wells (12 plates).

Mechanical loading of intact rat tail tendon fascicles was conducted immediately following dissection using the Bose Electroforce cyclic tensile system (TA Instruments, USA). Fascicles were subjected to 4% CTS for 24 hours at 1 Hz in serum free media 2. Separate fascicles were maintained at 4% static strain, also in serum free media 2, using custom built loading chambers as previously described in section 2.3.1. 4% strain was used to be consistent with the static load used in Chapter 3, as well as to try and ensure that the cells were not under-loaded since cells experience lower strain than the gross strain applied to the fascicle. Unloaded stress deprived fascicles were treated in an identical manner and used as a control along with freshly dissected fascicles.

4.2.3 Immunofluorescence Labelling

Visualisation of the cilia axoneme in isolated tenocytes and intact tendon fascicles was performed by immunolabelling of acetylated α-tubulin and/or the cilia membrane protein, ARL13b.

Isolated cells were fixed with 4% PFA (5 mins, room temperature) and incubated overnight at 4°C in phosphate buffered saline (PBS) with rabbit anti-arl13b (1:1000, Abcam, Cambridge, UK) and mouse anti-acetylated α-tubulin (1:1000, Sigma-Aldrich, St Louis, MO). Samples were washed with PBS containing 0.1% bovine serum albumin (BSA) and incubated at room temperature in corresponding 488nm and 543nm Alexa secondary antibodies (1 hour, 1:1000, Molecular Probes, Invitrogen, Eugene, OR).

For the investigation into the role of actin in cilia length, Blebbistatin treated and control cells were stained with phalloidin-Alexa488 (ThermoFisher, Waltham, MA) instead of arl13b.

For visualisation of cilia in intact tendon, the fascicles were fixed in 100% methanol (2 hours, room temperature) and labelled with anti ARL13b as described in section 2.5.4.

In both isolated cells and intact tendon fascicles, the nuclei were counter stained by incubation at room temperature with DAPI (5 mins, 1:1000, Molecular Probes, Invitrogen). After a further wash in PBS (5 mins) cells or fascicles were mounted under glass using prolong Diamond mountant.

4.2.4 Confocal Microscopy and Analysis of Primary Cilia Expression

All imaging was done using a 63x/NA 1.4 objective with a Zeiss laser scanning confocal microscope (Elyra, Zeiss, Oberkochen, Germany). Confocal z series were captured with a format of 225 x 225µm and a pixel size of 0.11 x 0.11µm and a z-step size of 0.25µm.

Between 20 and 30 sections were used per stack covering the full range of cells on the slide. Measurements of cilia length and orientation were calculated from stacks using ImageJ as described in section 2.6.1. As described in section 2.6.2, the DAPI channel was thresholded and ellipses were fitted to the thresholded image. The orientation, size and aspect ratio of the ellipses was calculated. Nucleus aspect ratio was compared with cilia length, orientation and nucleus orientation. Nucleus area was compared with cilia length, and nucleus orientation was compared with cilia orientation. Lines of best fit were plotted and coefficients of determination calculated for each comparison at each time point. Pearson's correlations were calculated.

For experiments using isolated cells, 3 wells were used per condition with 2-4 random fields of view imaged per well, resulting in 40-160 cells measured per condition as indicated in the figure legends. This was repeated for up to 3 complete biological repeats per condition (N) as indicated above and in figure legends. For experiments based on rat tail tendon fascicles, 1 - 3 fields of view were imaged per condition with all comparable conditions based on fascicles from the same animal, resulting in 30-90 cells measured per condition as indicated in figure legends. In all cases, the resulting cilia length data were assessed for normality with the Shapiro–Wilk test and then tested for significance with two tailed unpaired unequal variance Student's t-tests. In isolated cells the number of cilia was counted for each field and cell number was based on the number of nuclei. The data across the fields was tested for normality and tested for significance with 2-factor Anova or two tailed unpaired unequal variance Student's t-tests as noted in figure legends.

Cilia prevalence for tissue was calculated as the percentage of cells with cilium of at least 1μm in length. This threshold was necessary due difficulty in correctly identifying cilia

below 1μm in tissue. Total cilia number across all fields was aggregated and significance was tested with chi-squared tests.

4.3 Results

4.3.1 Isolation of Tenocytes from Tendon Results in Primary Cilia Elongation and Loss of Orientation

Figure 31a shows representative confocal microscopy images of tenocytes and associated primary cilia in situ within the fascicular matrix (Left) and in the same cells following isolation and culture in monolayer (Right). Tenocytes within fascicles had elliptical nuclei with a median aspect ratio of approximately 0.6 (Figure 31c). The primary cilia were orientated in the same direction as the long axis of the nuclei which also reflects the local collagen orientation (Figure 31b). By contrast the nuclei of tenocytes isolated from the same tendon source displayed a statistically rounder morphology as shown by an aspect ratio of approximately 0.8 ($p<0.001$, Figure 31c). The cilia in isolated tenocytes consequently displayed no preferential orientation (Figure 31b). Primary cilia expressed in situ within the fascicular matrix were significantly shorter than seen in isolated cell culture in monolayer ($p<0.001$, Figure 31C) (Figure 31c). Within the tendon cilia had a maximum length of approximately 2μm whilst in isolated tenocytes the maximum length increased to approximately 9μm with a median length of 3.3μm.

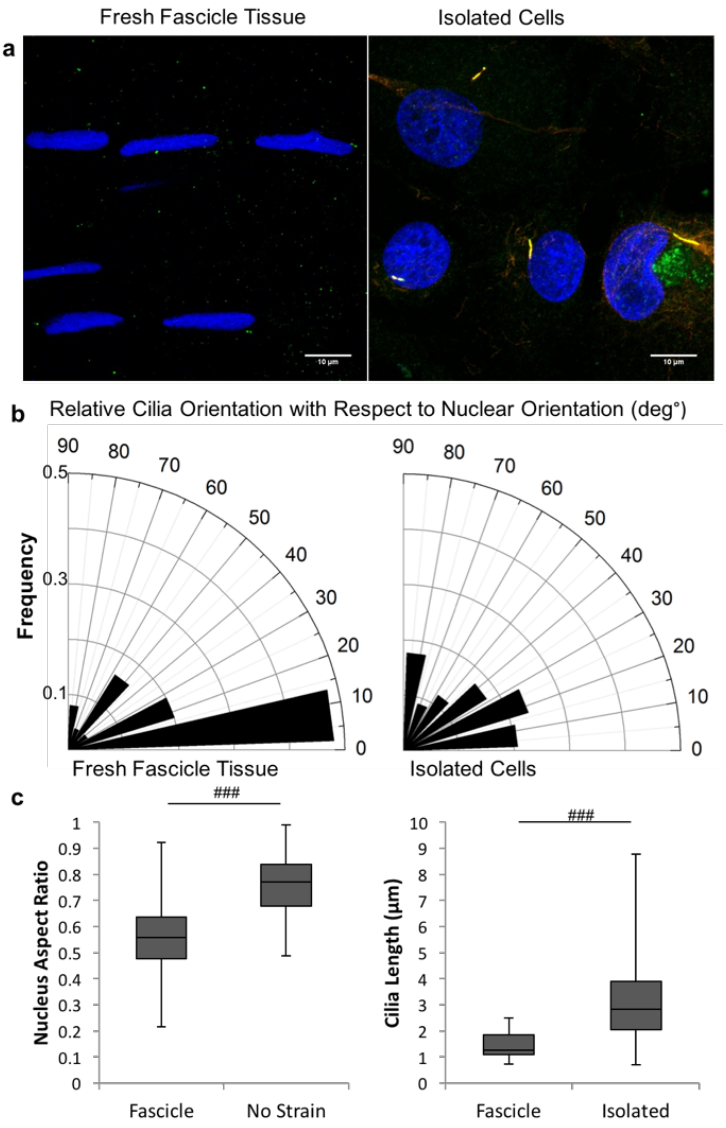

Figure 31: Isolated tenocytes express elongated cilia without any predominate orientation. *(a) Representative confocal images showing tenocyte primary cilia and nuclei in situ within rat tail tendon fascicles (left) and in isolated human cells cultured in monolayer (right). The cell nuclei are labelled with DAPI (blue) and cilia are immunolabelled for acetylated α-tubulin (red). In addition, cilia in isolated tenocytes have been immunolabelled for the ciliary membrane protein ARL13b (green). Scale bars represent 10 µm. (b) Rose plots showing orientation of tenocyte primary cilia parallel to the long axis of the corresponding nucleus in situ within tendon tissue (left) and the lack of any predominant relative orientation in isolated tenocytes (right). (c) Box and whisker plot showing nuclear aspect ratio indicating that nuclei in isolated human tenocytes are significantly rounder than those in situ in rat tail tendon fascicles. (d) Box and whisker plot showing longer primary cilia in isolated human tenocytes compared to in situ in rat tail tendon fascicles. N=120±20 cells and 60±20 cilia per group. In all cases significance indicated at p<0.05 (#), p<0.01 (##) and p<0.001 (###). Data were analysed with 2 tailed unpaired Student's t-tests.*

4.3.2 Cyclic Mechanical Loading Causes Rapid but Reversible Primary Cilia Disassembly in Isolated Tenocytes

The application of 24 hours cyclic mechanical loading (0-3%, 1Hz) to isolated tenocytes did not have any apparent effect on the random orientation of either the cell nuclei (Figure 32a) or the primary cilia (Figure 32b). However, loading did induce progressive cilia disassembly. There were no significant differences observed after 5 hours of loading, but by 8 hours there were significant reductions in both cilia prevalence ($p<0.05$, Figure 33a) and cilia length ($p<0.05$, Figure 33b and c). There was further cilia disassembly after 24 hours with only 35% of tenocytes expressing cilia compared to 80% of unloaded control cells ($p<0.001$, Figure 33a). Similarly, for those cells that did still express a cilium, there was a significant reduction in length of more than 50% with median values of 1.5μm ($p<0.001$, Figure 33b and c). Despite this dramatic cilia disassembly, the removal of mechanical loading led to a complete recovery of both cilia prevalence (Figure 33a) and length (Figure 33b) within 2 hours, such that neither parameter was significantly different from values in unloaded controls.

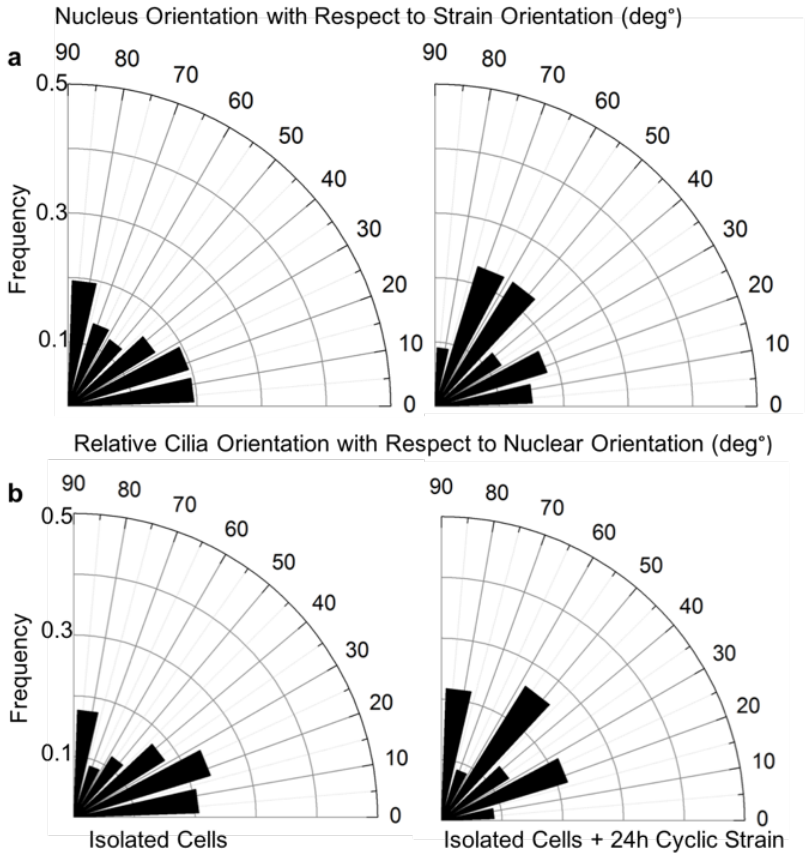

Figure 32: Cyclic tensile strain (24 hours 3%, 1Hz) does not cause cilia or nucleus reorientation in isolated human tenocytes. *(a) Rose plots showing lack of any predominant nuclear orientation before and after loading. (b) Rose plots showing lack of any predominant cilia orientation relative to nuclear orientation before and after loading. N=120±20 cells and 60±20 cilia per group.*

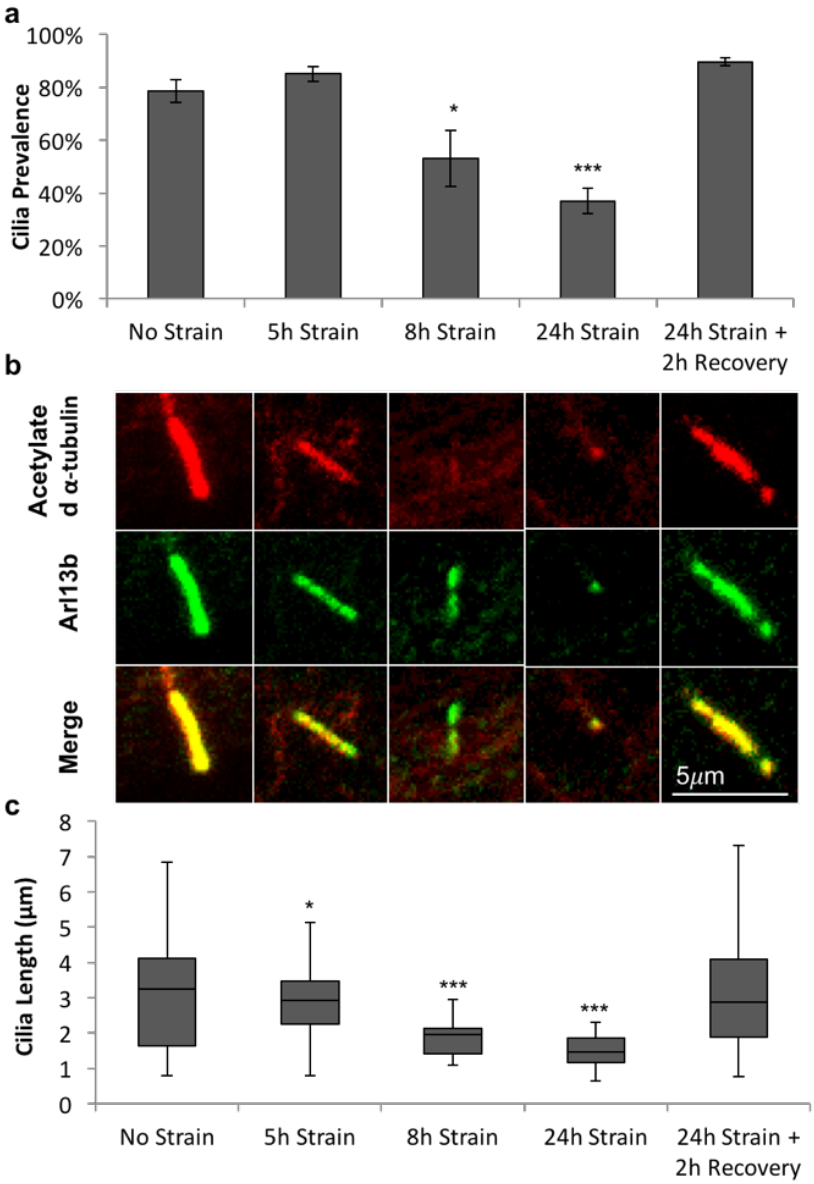

Figure 33: Cyclic tensile strain of isolated human tenocytes leads to progressive disassembly of primary cilia over time. *(a) Time course showing the effects of cyclic tensile strain (3%, 1Hz) on cilia prevalence measured after 5, 8 and 24 hours of loading and following a 2 hour recovery period after 24 hours of loading. Values represent mean prevalence with error bars showing standard error (n=6 fields of view per condition). (b) Representative confocal images of primary cilia in unloaded cells and loaded cells. Cilia have been labelled with anti-acetylated α-tubulin (red) and anti-ARL13b (green). Scale bar represents 5 μm. (c) Box and whisker plots showing corresponding cilia length (n=40-80 cilia per condition). Statistically significant differences relative to unstrained control indicated at p<0.05 (*), p<0.01 (**) and p<0.001 (***). Significance was tested using 1 factor Anova with post hoc testing using Tukey-Kramer.*

4.3.3 Cell Morphology Does Not Correlate with Cilia Length or Orientation in Cyclically Loaded or Unloaded Cells

Nucleus aspect ratio was found to decrease slightly but significantly in the loaded conditions, 5h, 8h and 24h, cyclic strain (Figure 34). However, the aspect ratio of cells that had been strained for 24 hours and left to recover for 2 hours without strain was not significantly different from that of the control cells (Figure 34). For each time point where cells were evenly distributed across the entire angular spectrum, there was no significant difference in nucleus orientation with respect to the axis of strain at any time point (Figure 34).

For each condition, correlations of cilia length and orientation with nuclear aspect ratio, area and orientation were performed. No significant correlations were observed in any of the compared groups as shown in Figure 35, Figure 36, and Figure 37.

The highest coefficient of determination was 0.44. However, the slope of the line for this correlation was close to 0 and the correlation was not significant at the $p=0.05$ level. It is possible there was a small correlation between nucleus aspect ratio and length in cyclically loaded cells, as all of the loaded groups had subtle downward trends, with R^2 values between 0.16 and 0.31. However, none were significant and the trend did not appear in either the 0 strain controls or the 2h recovery samples. Plots of all variables compared are shown in Figure 35, Figure 36, and Figure 37.

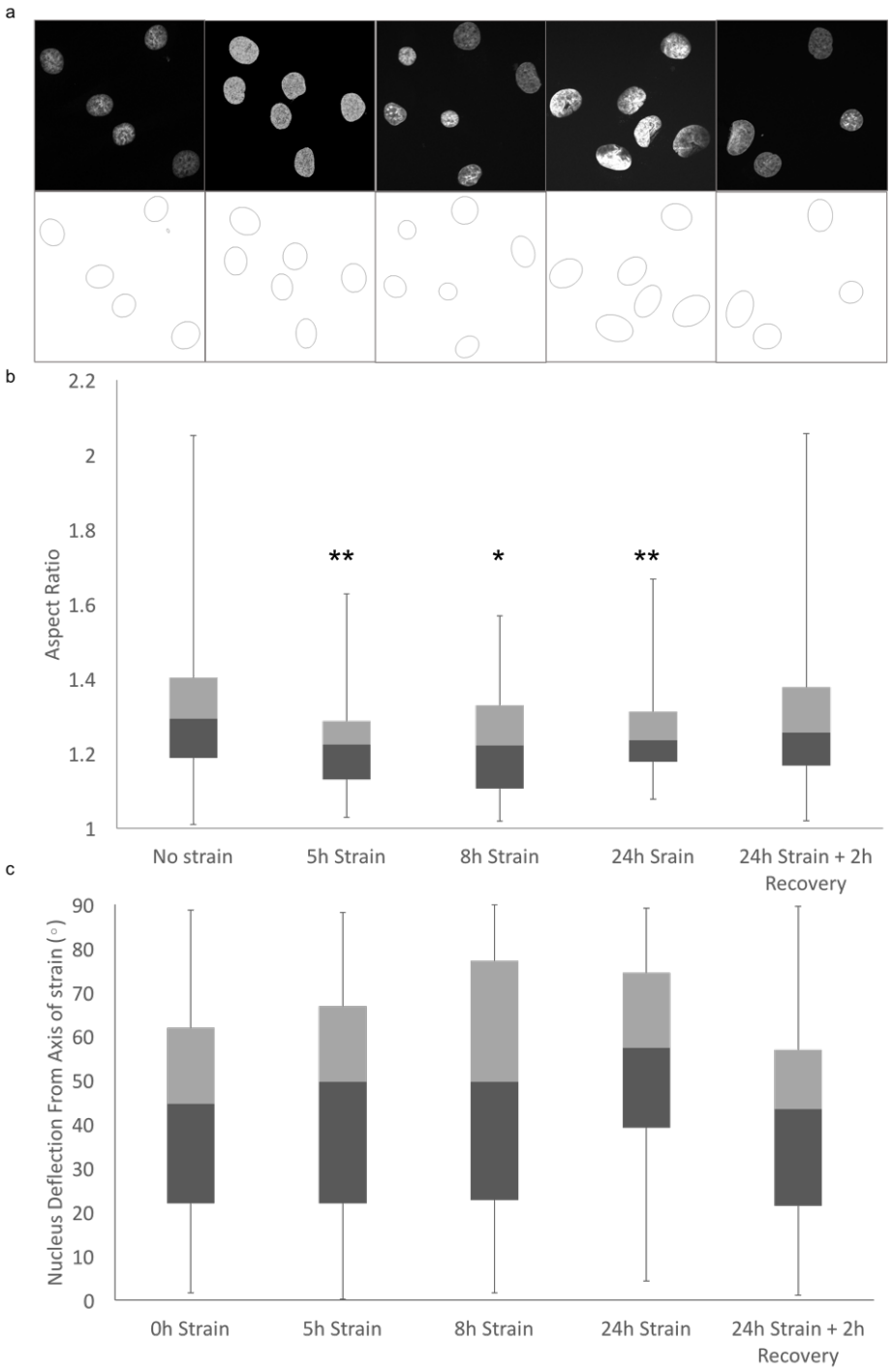

Figure 34:Cyclic strain leads to increased nuclear roundness. *(a) representative images of DAPI stained nuclei for each condition and ellipses fitted to those nuclei. (b) box and whisker plot showing nucleus aspect ratio after increasing durations of cyclic loading as well as after 24 hours of loading followed by 2 hours unstrained recovery. (c) Shows box and whisker plots of the deflection away from the axis of strain for each time point. N=80-120 nuclei per condition. In all cases significance indicated at p<0.05 (*), p<0.01 (**) and p<0.001 (***). Significance was tested using 1 factor Anova with post hoc testing using Tukey-Kramer..*

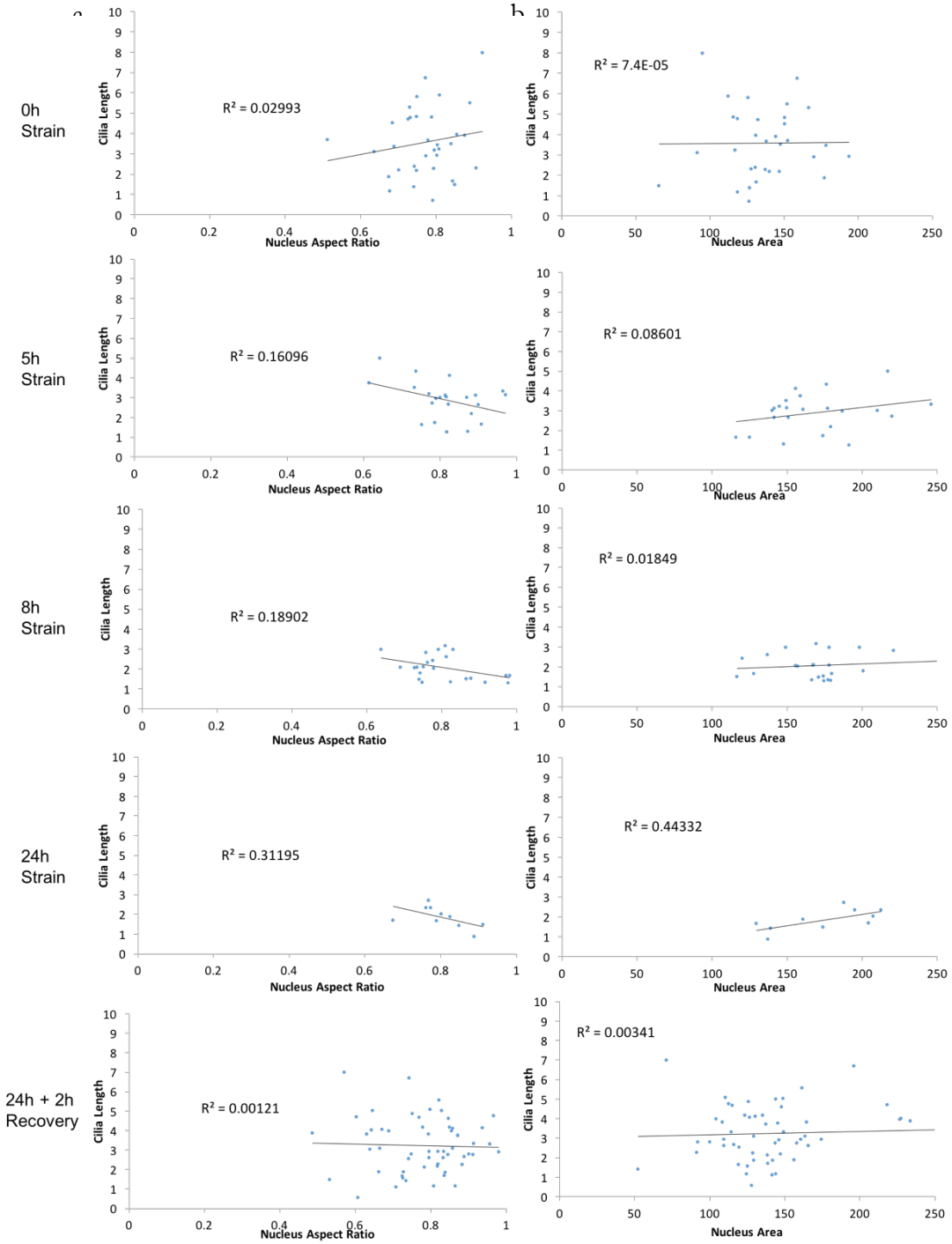

Figure 35: There is no correlation between cilia length and nuclear aspect ratio or area regardless of strain duration. (a) shows scatter plots of nucleus aspect ratio against cilia length at increasing cyclic strain durations as well as after 24h strain followed by 2h recovery. No notable correlation between length and aspect ratio is observed at any time point. (b) shows scatter plots of nucleus area against cilia length for the same time points as (a), no notable correlations are observed at any time point. Correlations for each plot are shown as R2 values on the plots.

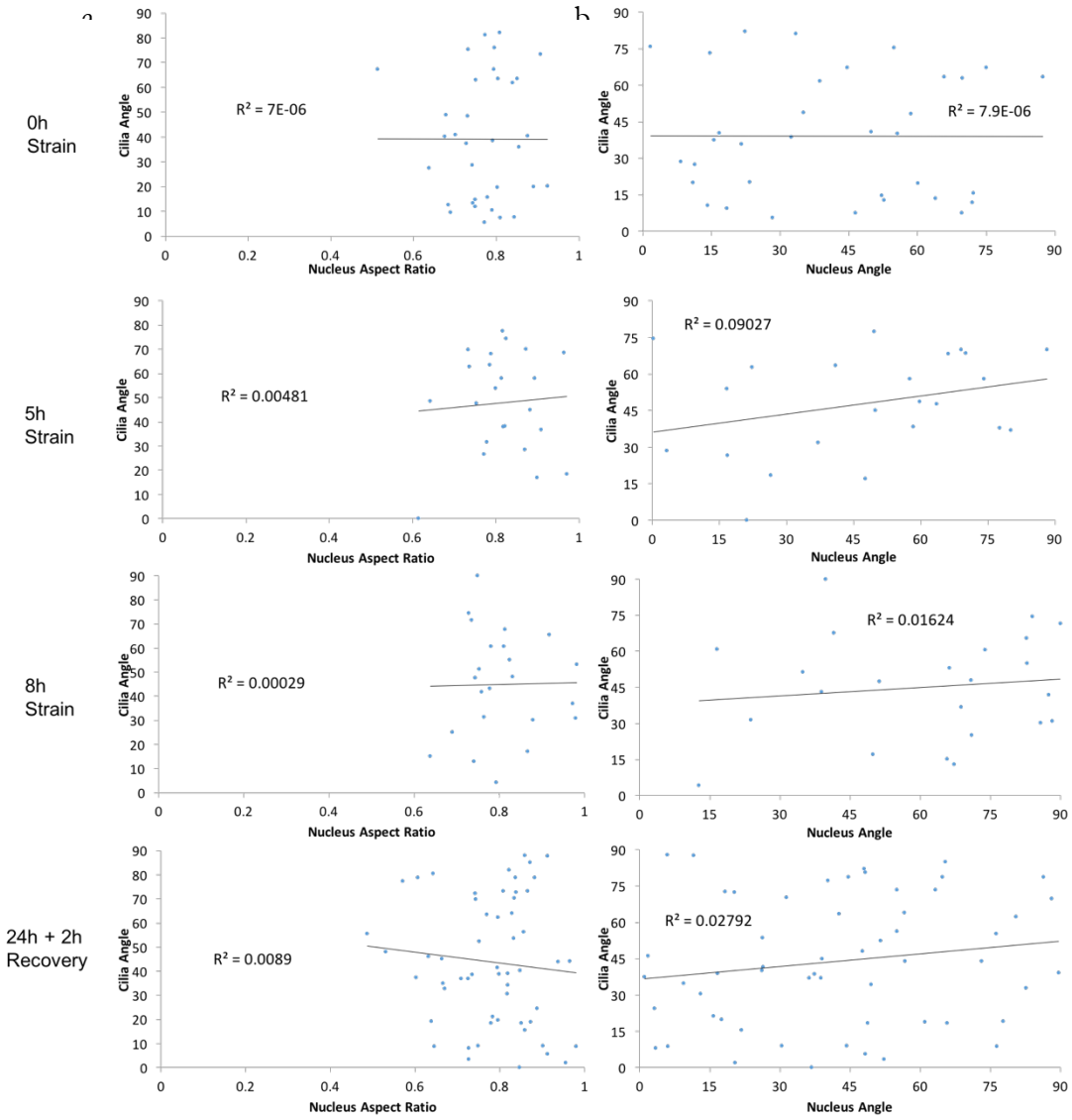

Figure 36: There is no correlation between cilia orientation and nuclear aspect ratio or orientation, regardless of strain duration. (a) shows scatter plots of nucleus aspect ratio against cilia angle at increasing cyclic strain durations as well as after 24h strain followed by 2h recovery. No notable correlation between length and aspect ratio is observed at any time point. (b) shows scatter plots of nucleus angle against cilia angle for the same time points as (a), no notable correlations are observed at any time point. Correlations for each plot are shown as R2 values on the plots.

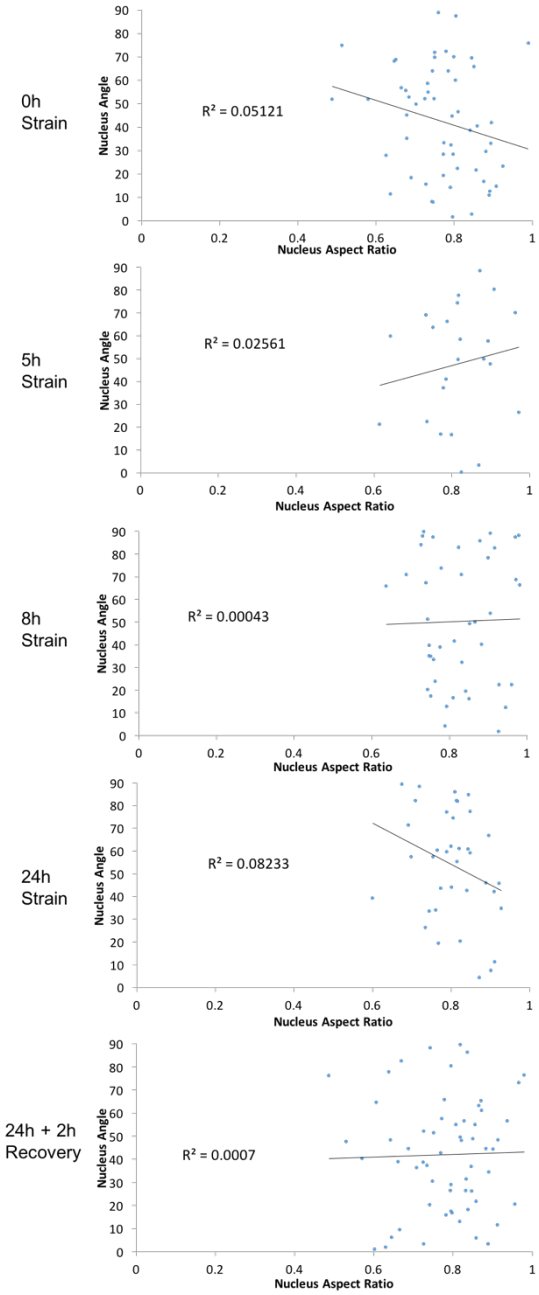

Figure 37: There is no correlation between nuclear orientation and nuclear aspect ratio, regardless of strain duration. *shows scatter plots of nucleus aspect ratio against nucleus angle at increasing cyclic strain durations as well as after 24h strain followed by 2h recovery. No notable correlation between length and aspect ratio is observed at any time point. Correlations for each plot are shown as R2 values on the plots.*

4.3.4 Cyclic Mechanical Loading Causes Cilia Disassembly in the Fascicular Matrix Region of the Tendon

It was investigated whether mechanically induced cilia disassembly was also present following cyclic mechanical loading of intact tendon fascicles. These studies examined the effect of loading on cilia within both the fascicular matrix (FM) and interfascicular matrix (IFM). Similar to behaviour in isolated tenocytes, 24 hour cyclic loading (0-4%, 1Hz) led to significant reductions in both cilia prevalence ($p<0.001$, Figure 38a) and cilia length ($p<0.05$, Figure 38b) for tenocytes within the fascicular matrix compared to fresh tendon sample. By contrast, no significant reduction in length or prevalence were observed for cells in the interfascicular matrix (Figure 38a and b). Data from Chapter 3 from stress deprived fascicles was used as a control. In these stress deprived tendons, cilia prevalence increased in both the fascicle and interfascicular matrix by more than 2-fold compared to values in fresh tendon samples ($p<0.001$, Figure 38a). Similarly cilia length also increased with stress deprived tendons in both the FM and IFM regions with median lengths of 2.5μm and 2.6μm respectively ($p<0.001$, Figure 38b). These values of cilia length in stress deprived rat tail tendon fascicles are similar to those for isolated human tenocytes in unloaded conditions. In contrast to the response to cyclic loading, the application of static strain (4%, 24 hours), induced no difference in cilia prevalence compared to fresh tendon in both the FM or IFM regions (Figure 38a). However, there was a small but significant increase in the length of cilia in the IFM region ($p<0.05$, Figure 38b).

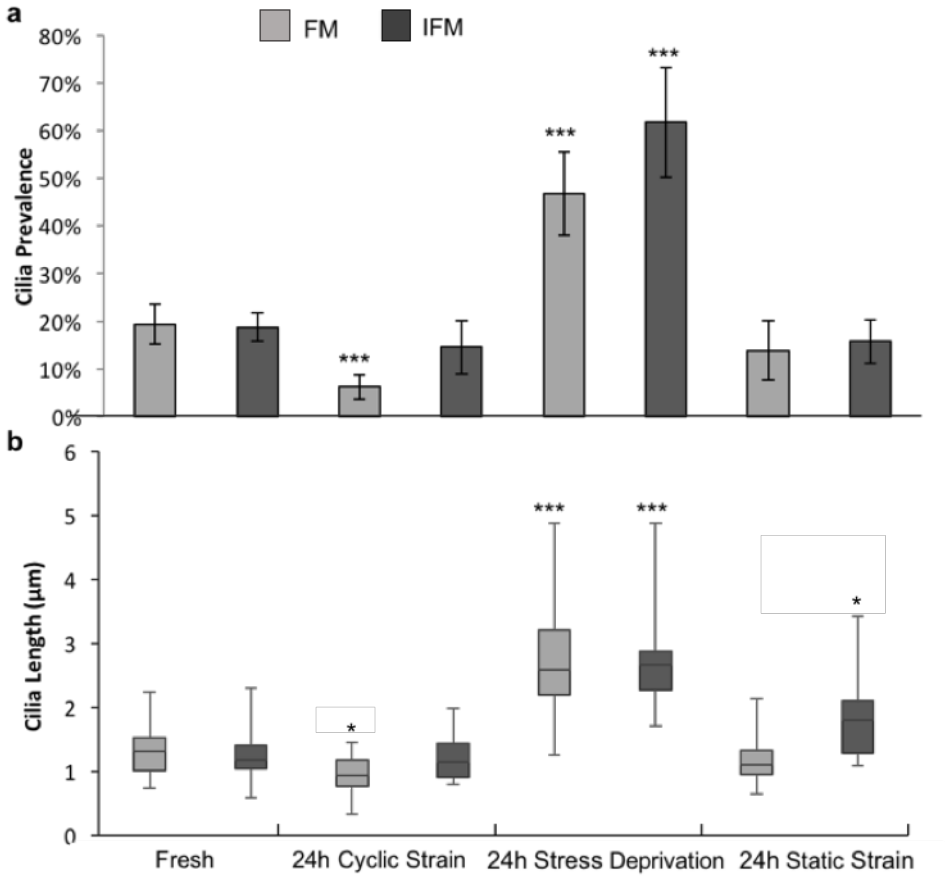

Figure 38: Cyclic tensile strain leads to cilia disassembly in situ within tendon tissue. Primary cilia (a) prevalence and (b) length in the FM and IFM region of fresh rat tail tendon fascicles and following 24 hours of either cyclic tensile strain (4%, 1 Hz); stress deprivation or static tensile strain (4%). Prevalence values represent mean with error bars indicating Poisson standard error. N=10-50 cilia per condition from 90±30 observed cells. Box and whisker plot show cilia length. Significance for prevalence data was calculated using chi-squared tests. Length data were analysed with 2-factor Anova (significance at the 0.001 level was found for both tissue region and treatment type but interactions were not found to be significant at the 0.05 level.) Post hot testing was done using Tukey-Kramer. Statistically significant differences indicated between FM and IFM and relative to corresponding values for fresh fascicles, $p<0.05$ (*) and $p<0.001$ (***).

4.3.5 Mechanically Induced Cilia Disassembly in Tenocytes is Mediated by TGFβ and HDAC6, Independent of Actin Changes

Mechanical loading has been shown to increase actin tension and stress fibres perpendicular to the direction of strain organisation in fibroblasts[211], whilst further studies show that changes in actin tension can regulate cilia expression in various other cell types[212,127]. To investigate whether reorganisation of the actin cytoskeleton was

responsible for the mechanically induced cilia disassembly, cells were treated with blebbistatin to reduce actin tension. Confocal visualisation of F-actin in isolated tenocytes demonstrated that with the loading conditions used in this study (0-3%, 1Hz, 24 hours), cyclic tensile strain had minimal effect on actin organisation (Figure 39a). Furthermore, although blebbistatin significantly reduced the presence of actin stress fibres (Figure 39a), this had no significant effect on cilia prevalence (Figure 39b) or length (Figure 39c) in either the unloaded control or cyclic loaded conditions. Together these data indicate mechanical loading did not induce cilia disassembly via actin reorganisation.

Next, the role of TGFβ in mechanically induced cilia disassembly was investigated since TGFβ has been shown to mediate mechanosignalling in tendon[80]. Mechanically loaded (0-3%, 1Hz, 24 hours) and unloaded cells were treated with TGFβ or the receptor inhibitor (SB 431542 hydrate TGFβ-RI) prior to analysis of cilia expression. In addition, previous studies have demonstrated that mechanically induced cilia disassembly and shortening in chondrocytes is mediated by the histone deacetylase, HDAC6[167,171,172]. Therefore, separate groups of loaded and unloaded cells were treated with the HDAC6 inhibitor, tubacin, and results compared to untreated controls. Treatment with TGFβ led to a significant reduction in cilia prevalence ($p<0.05$, Figure 40a) and length ($p<0.001$, Figure 40b) in unloaded cells. Indeed the effects of TGFβ were similar to that induced by mechanical loading with no significant differences between the two groups. In loaded cells, the presence of TGFβ did not further enhance cilia disassembly in terms of cilia prevalence or length. In unloaded cells, TGFβ-RI had no effect on cilia expression. However in loaded cells, inhibition of the TGFβ receptor completely prevented mechanically induced cilia disassembly such that there were no significant

differences between loaded+TGFβ-RI and unloaded control cells. These results demonstrate that mechanically induced cilia disassembly in tenocytes is mediated by activation of TGFβ receptors.

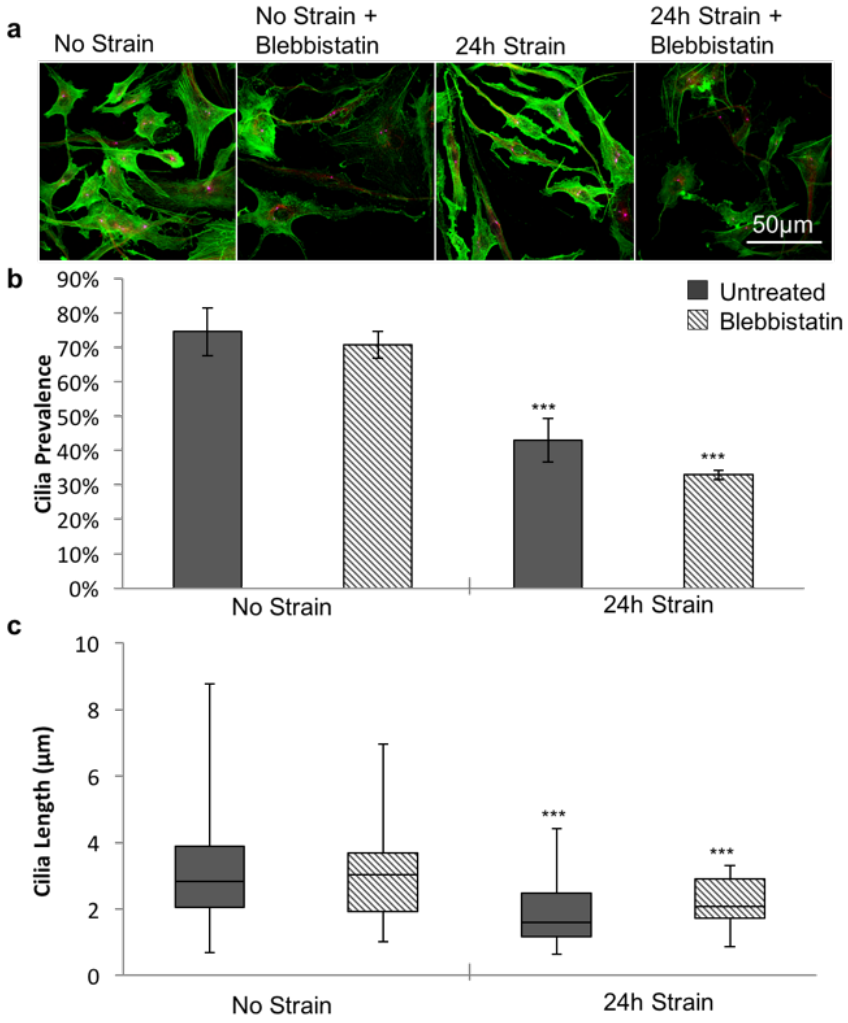

Figure 39: Cilia disassembly induced by cyclic strain is not caused by changes in actin tension. *(a) Representative confocal images showing F-actin in unstrained isolated human tenocytes and following a 24 hour period of cyclic tensile strain (3%, 1 Hz) with and without treatment with 10μM Blebbistatin. Actin labelled with Alexa-Phalloidin. Scale bars represent 50 μm. (b) Corresponding cilia prevalence (values represent mean with error bars indicating standard error for n=4 fields for each condition). (c) Box and whisker plots showing corresponding cilia length for each condition (N=40±20 cilia per condition). Data were analysed with 2-factor Anaova (for both length and prevalence, significance was observed at the 0.001 level between strain and no strain, However, no significance was observed between blebbistatin and no blebbistatin nor was any significance noted between the interactions). Post hoc testing was performed using Tukey-Kramer. In all cases significance indicated at p<0.05 (*), p<0.01 (**) and p<0.001 (***)*

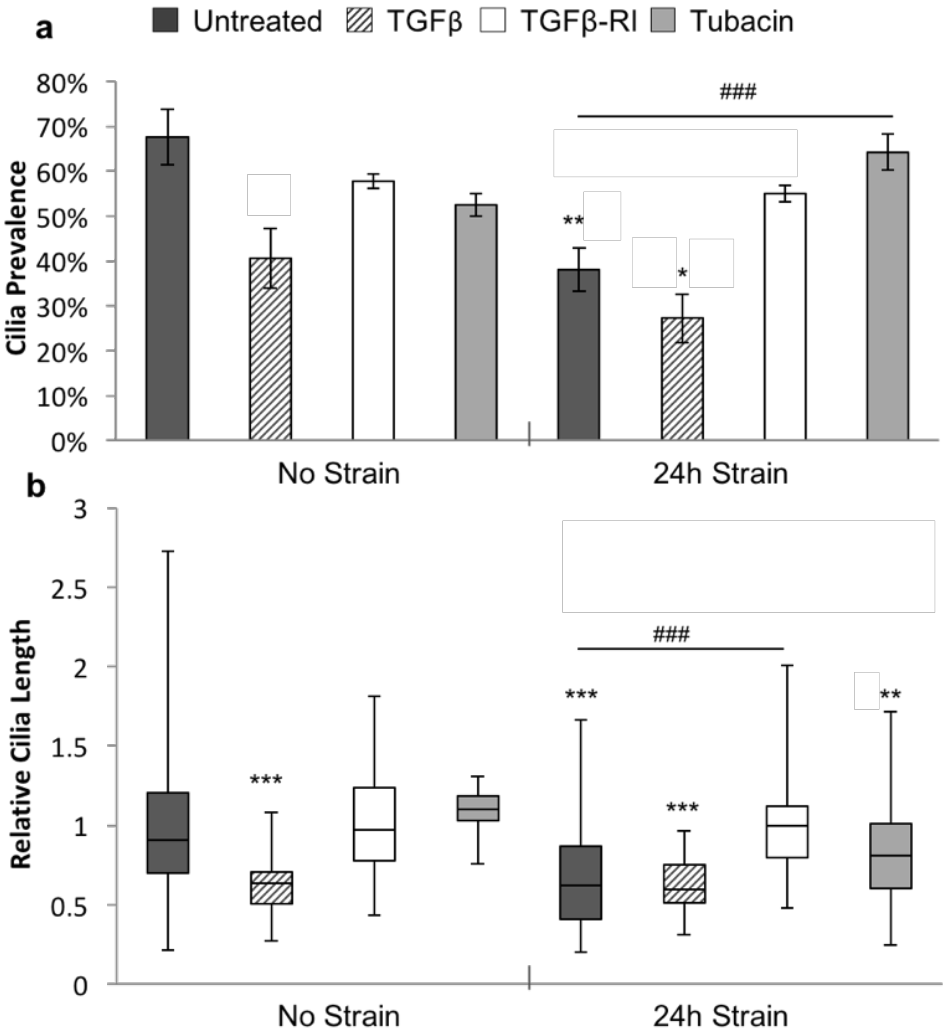

Figure 40: Cilia disassembly induced by cyclic strain is caused by activation of TGFβ receptors and HDAC6. *Primary cilia (a) prevalence and (b) length in unstrained cells and cyclic strained cells (24 hours, 3%, 1 Hz) for cells treated with either TGFβ; TGFβ receptor inhibitor (TGFβ-RI) or tubacin. For comparison across different experiments cilia length has been normalised to the corresponding unstrained control. Prevalence data represent mean values with error bars indicate standard error for n=8±4 fields of view from up to 3 biological repeats. Corresponding relative lengths are shown as box and whisker plots for N=120±60 cilia. Data analysed using 2-factor Anova (groups and interactions significant at p<0.001 for both length and prevalence) post-hoc testing performed using Tukey-Kramer. Statistically significant differences are indicated relative to unstrained control at p<0.05 (*), p<0.01(**), p<0.001 (***) and between groups p<0.05 (#), p<0.01(##), p<0.001 (###).*

In the absence of strain, inhibition of HDAC6 with tubacin had no significant effect on cilia prevalence or length (Figure 40). However, in loaded cells, tubacin rescued the mechanically induced reduction cilia disassembly, such that values were significantly different from untreated, loaded conditions ($p<0.001$) for both cilia prevalence and

length). Cilia prevalence was completely restored to levels in unstrained, untreated cells, however, cilia length remained slightly shorter.

4.4 Discussion

The work in chapter 3 as well as other previous studies have described the response of tenocyte primary cilia to mechanical loading of tendon tissue[9,174,209]. This study is the first to examine primary cilia in isolated tenocytes and the effect of mechanical loading as well as the underpinning mechanism. By studying isolated cells, it is possible to identify the direct effect of mechanical loading in isolation from factors associated with loading or remodelling of the extracellular matrix. Isolated tenocytes from human tendon, cultured in monolayer in the absence of mechanical loading exhibited primary cilia that were significantly longer than those in intact rat tail tissue (Figure 31). Interestingly the cilia set length in unloaded isolated tenocytes is similar to that previously reported in stress deprived tendon[9,209]. Although species-to-species variation cannot be ruled out, these results suggest that cilia elongation in response to stress deprivation *in situ* is directly due to the absence of loading rather than any indirect effect caused by remodelling of the surrounding matrix.

Primary cilia expressed by isolated tenocytes had no predominant orientation compared with cilia within the tendon fascicular matrix (Figure 31). Furthermore, no obvious reorientation of either cilia or nuclei was observed in isolated cells after 24 hours of cyclic tensile strain. This is in contrast to other cell types where nuclei have been observed to reorient perpendicularly to the axis of applied strain depending on confluence, loading frequency and duration[213]. The lack of orientation in isolated cells suggests that the orientation observed in tendon fascicular matrix is due to constraint by the collagen fibres of the fascicle which are orientated parallel to the applied strain,

rather than the strain itself. This also explains the lack of orientation reported in the interfascicular matrix where the collagen fibres are more randomly orientated relative to the axis of loading.

Cyclic loading at 3% strain of isolated tenocytes induced a marked reduction in cilia prevalence and set length with increasing loading duration. 3% strain was used as it is likely within the physiological range and is consistent with a number of previous studies of tenocyte mechanobiology thus making it more directly comparable. This response to loading was replicated in tendon fascicles after 24 hours of cyclic loading (4% 1Hz). Significant reductions were not observed in the interfibrillar matrix region which may be due to lower strains in this region of the tendon compared to the fascicle itself[214]. 4% strain was used to be consistent with the previous rat tail tissue experiment from Chapter 3. Further, the strain experienced by the tenocytes is likely to be lower than the gross applied strain[215].

Cyclic load was found to slightly but significantly reduce nuclear aspect ratio, after 2 hours of recovery aspect ratio was not significantly different from unstrained controls. Other than this, cyclic strain had no significant effects on either nucleus morphology or cilia orientation. Further, no correlations were observed between cilia length and orientation, and nucleus morphology. The lack of large changes to nuclear morphology suggest that the regular cell orientation and long thin structure seen within the fascicle, as well as the less consistently orientated and rounder cells seen within the IFM are due to matrix constrains rather than a response to cyclic strain. The fact that strain alone did not cause cilia reorientation and there was no correlation between nuclear morphology and cilia orientation suggests that the differences in cilia orientation observed in the FM and IFM must be due to other factors, most likely the different matrix compositions of the FM and IFM. This further suggests that cilia length and orientation in tenocytes are

not primarily controlled by processes controlling cell shape, such as actin tension. Despite this, it is still possible that tenocytes do have a morphological response to higher levels or longer durations of strain.

Following this, the mechanism for mechanical regulation of cilia expression was investigated. Previous studies have reported that loading modulates actin organisation in other cell types[211] and that increased actin tension inhibits cilia elongation[171]. In light of this cells were treated with Blebbistatin to reduce actin tension as indicated by confocal imaging of cells labelled with Alexa-phalloidin (Figure 39). Despite this alteration in actin organisation, Blebbistatin had no significant effect on cilia prevalence or length (Figure 39). Similarly, there was no correlation between cilia length and the nuclear aspect ratio, which indicates the level of actin tension within individual cells (Figure 36). Furthermore, Alexa-phalloidin imaging demonstrated that cyclic strain had no obvious effect on actin organisation. These results therefore suggest that alterations in actin are not involved in the mechanism of mechanical regulation of cilia expression.

Next an alternative mechanism involving TGFβ was examined. TGFβ is known to be activated by mechanical loading of tenocytes[80]. Further, previous studies have reported that TGFβ reduces cilia expression in mesenchymal stem cells and osteoblasts[216,172]. It was found that application of $TGF\beta_1$ to unloaded isolated tenocytes induced a significant reduction in both cilia prevalence and set length similar to that observed with loading. Furthermore, treatment of cyclically loaded cells with TGFβ receptor inhibitor (SB 431542) blocked mechanically-induced changes in cilia expression without affecting unstrained cells. It has previously been shown that mechanical loading of chondrocytes induces cilia disassembly and shortening via the activation of histone deacetylase 6 (HDAC6) which is enriched on the cilium[167]. This shows that treatment of tenocytes

with the HDAC6 inhibitor (Tubacin) prevented mechanically-induced reductions in cilia prevalence and length. Together, these results demonstrate that mechanical regulation of cilia expression in tenocytes is mediated by activation of $TGF\beta_1$ receptors and HDAC6.

The consequences of this response in tenocytes are unclear. In chondrocytes, mechanically-induced cilia disassembly inhibits hedgehog signalling[167,187]. Previous studies have also shown that cilia set length regulates, intraflagellar transport as part of the balance point model first proposed by Marshall[217]. Thus mechanical loading may effect a variety of cilia signalling pathways by $TGF\beta_1$-mediated regulation of cilia length. Interestingly, studies in mesenchymal stem cells show that TGFβ receptors localise to the ciliary base, and that TGFβ signalling is attenuated in the absence of cilia[164]. Thus loading-induced changes in cilia expression may regulate TGFβ signalling as part of a negative feedback mechanism. This mechanism may be protective to ensure that $TGF\beta_1$-activated genes, such as MMP1, MMP13 and Col1A1, are not continually upregulated if loading continues for a long period of time and would explain why cyclic loading induces transient activation of these genes. A schematic demonstrating this hypothesis is shown in Figure 41.

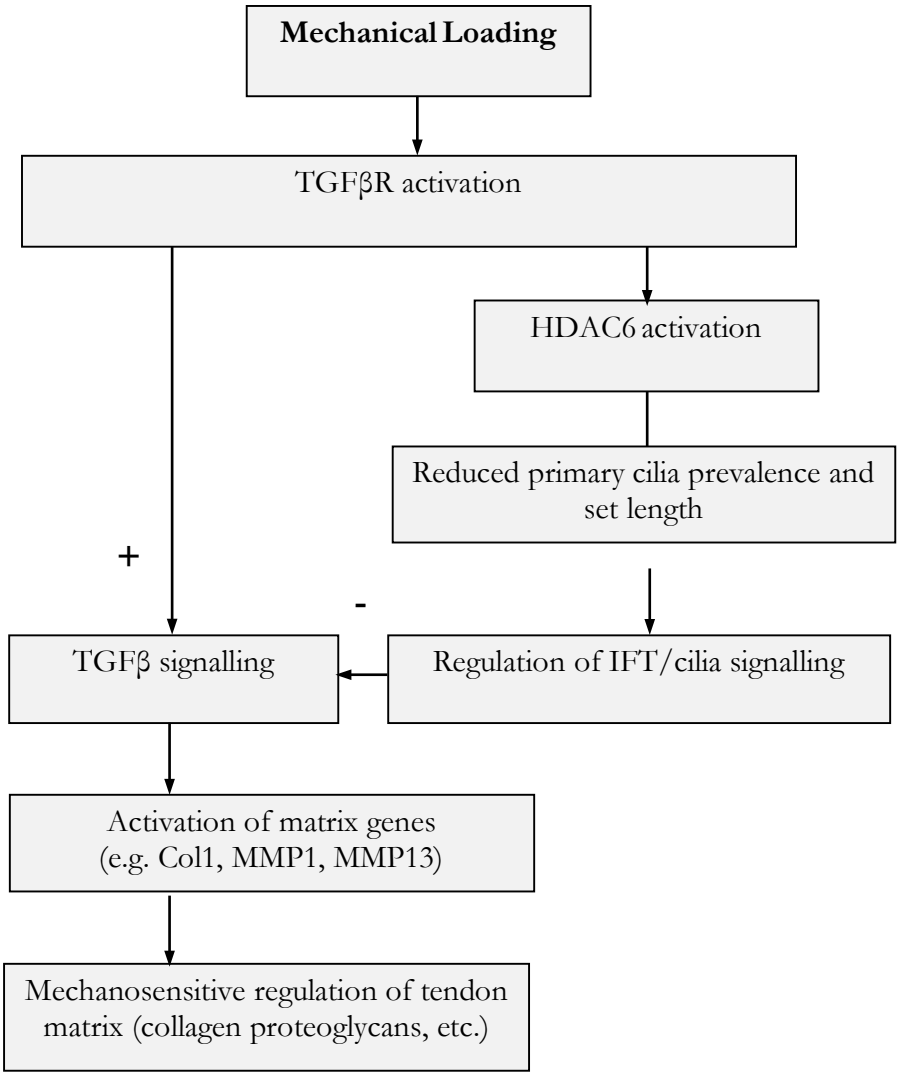

Figure 41: Schematic diagram showing proposed pathway through which cyclic mechanical loading regulates primary cilia expression to control tendon matrix turnover. *Mechanical loading disrupts primary cilia expression via TGFβR and HDAC6 activation. This in turn may modulate cilia signalling, including supersession of TGFβ signalling as part of a negative feedback mechanism regulating tendon matrix turnover in response to mechanical loading.*

5 Role of primary cilia and mechanically-induced cilia disassembly in tenocytes

5.1 Role of Mechanically-induced Cilia Disassembly on Mechanosignalling

5.1.1 Introduction

The previous chapters have shown how mechanical loading results in disassembly and shortening of primary cilia within tendon and isolated tenocytes. Other studies have reported that primary cilia are involved in mechanosignalling although this has not yet been shown in tenocytes[157,167,187]. Numerous studies have looked at the effects of cyclic loading on tenocyte gene expression showing a characteristic upregulation of genes regulating the synthesis and turnover of the tendon extracellular matrix[80,189,218]. This chapter therefore set out to examine whether this characteristic metabolic response to loading was mediated or modulated by mechanically induced changes in primary cilia expression. The study set out to examine the effect of mechanical loading on gene expression with and without inhibition of cilia disassembly as identified in the previous chapter.

A number of extracellular matrix related genes have been found to be often affected by cyclic strain in tenocytes, including ADAMTS5, MMP1 and COL1A1. In particular, Col1A1 has been found to be upregulated in cyclically loaded cells and tissue, while MMP1 and ADAMTS-5 have been found to be both up and down regulated depending on the cell source and precise loading regime[113,114,80].

The purpose of the study described in this chapter was to investigate loading-induced changes in the expression of these genes in the presence and absence of the HDAC6

inhibitor, Tubacin and the TGFβ receptor inhibitor, both of which inhibit mechanically-induced cilia disassembly. It was hypothesised that the inhibition of TGFβ leads to changes in mechanoresponsive gene expression. Of course it should also be noted that tubacin and the TGFβ receptor inhibitor may also have other cilia-independent effects on gene expression.

5.1.2 Methods

50,000 cells were seeded on 6 separate 6 well flex cell plates, one for each condition as shown in Table 13. For full details of this methodology and associated cell culture and media preparation see section 2.3.3. Mechanical loading was applied in the form of 0-3% cyclic tensile strain at 1 Hz for 24 hours using the flex cell system as described previously in section 2.3.3. Cells were subjected to mechanical loading both with and without the addition of 1μM Tubacin (Sigma-Aldrich, St Louis, MO) or 10μM TGFβ receptor inhibitor (Sigma-Aldrich, St Louis, MO). Mechanical loading conditions and the concentrations of Tubacin and TGFβ receptor inhibitor were identical to those used in previous chapter examining the effect of loading on cilia expression.

	Unloaded Control	Mechanically Loaded (0-3% CTS, 1Hz)
Untreated	X	X
Tubacin (1μM)	X	X
TGFβ receptor inhibitor (10μM)	X	X

Table 13: Showing the conditions used to examine the role of mechanically induced cilia disassembly on tenocyte mechanosignalling.

RNA extravtion was performed using the TRIzol method (acid guanidinium thiocyanate-phenol-chloroform extraction). Cells were lysed with TRIzol reagent

(Invitrogen, Carlsbad, CA) and the RNA containing aqueous phase obtained. RNA was precipitated with isopropanol, centrifuged and supernatant removed. The RNA pellet was washed 2 times with 75% ethanol. After the second ethanol wash the supernatant was removed and the pellet air dried for 10 minutes. The pellet was resuspended in 0.5% SDS solution and incubated for 15m minutes at 55-60°C. RNA quality and amount was assessed with a NanoDrop spectrophotometer. RNA was converted to DNA for RT-qPCR using Quantitect reverse transcription kits (Qiagen, Hilden, Germany).

Reverse transcription quantitative polymerase chain reaction (RT-qPCR) is a technique whereby gene expression can be determined. The reverse transcription refers to the process of converting RNA (which is what needs to be measured for expression levels) into DNA (which can be measured using PCR). The method can be quantified by the use of a dye which binds preferentially to double stranded DNA over single stranded and thus quantifies the amount of double stranded DNA created by the PCR.

All RT-qPCR was performed using Fast SYBR Green Mastermix (ThermoFisher, Waltham, MA). A total of 6 repeats were done for each condition with 3 technical replicates per condition. GAPDH was used as a house keeping reference gene, it is considered invariant to cyclic strain and is commonly used in cyclic strain experiments[80,219]. ROX was used as a normalizing reference dye. Genes tested for were MMP1, Col1A1 and ADMTS5, all primers were acquired from Life Technologies (Carlsbad, CA) details of the primers used can be found in Table 14. RT-qPCR was done in triplicate and 384 wells were used run on one plate. All RT-qPCR data was analysed using the ΔΔCt method. Significance was calculated from ΔΔCt values. All ΔΔCt values shown are with reference to untreated unloaded samples. Stats were calculated using 2-factor ANOVA with the factors being strain and treatment.

Target Gene	Primers	Sequence	Amplicon Size (bp)	Location (bp)
GAPDH[220]	Forward	5'- TTT TAA CTC TGG TAA AGT GGA TAT TGT TG -3'	97	240-337
	Reverse	5'- TGA CGG TGC CAT GGA ATT T -3'		
COL1-A1[220]	Forward	5'- CGC ACG GCC AAG AGG AA -3'	66	185-251
	Reverse	5'- CAT GGT ACC TGA GGC CGT TCT -3'		
MMP1[80]	Forward	5'- AAG ATG AAA GGT GGA CCA ACA ATT -3'	59	587-646
	Reverse	5'- CCA AGA GAA TGG CCG AGT TC -3'		
ADAMTS5[221]	Forward	5'- AGG AGC ACT ACG ATG CAG CTA TC -3'	53	1796-1849
	Reverse	5'- CCC AGG GTG TCA CAT GAA TG -3'		

Table 14: Showing details of the primers used for each gene tested in this experiment.

5.1.3 Results

RT-qPCR was performed to determine the effect of Tubacin and TGFβ receptor inhibitor on ECM gene expression in unloaded and cyclically loaded tenocytes (Figure 42). In the absence of mechanical loading, neither Tubacin nor the TGFβ receptor inhibitor had any effect on expression of ADAMTS5, MMP1 or COL1A at the concentrations tested (Figure 42, a-c respectively). Mechanical loading of untreated cells produced no statistically significant change in any of the three genes measured. However it should be noted that there was considerable variability in the replicates (n=6) for MMP1 in the cyclic strain, no treatment condition, as indicated by the SEM values

(Figure 42). Further, no significant differences were observed due to treatment in any of the three genes investigated.

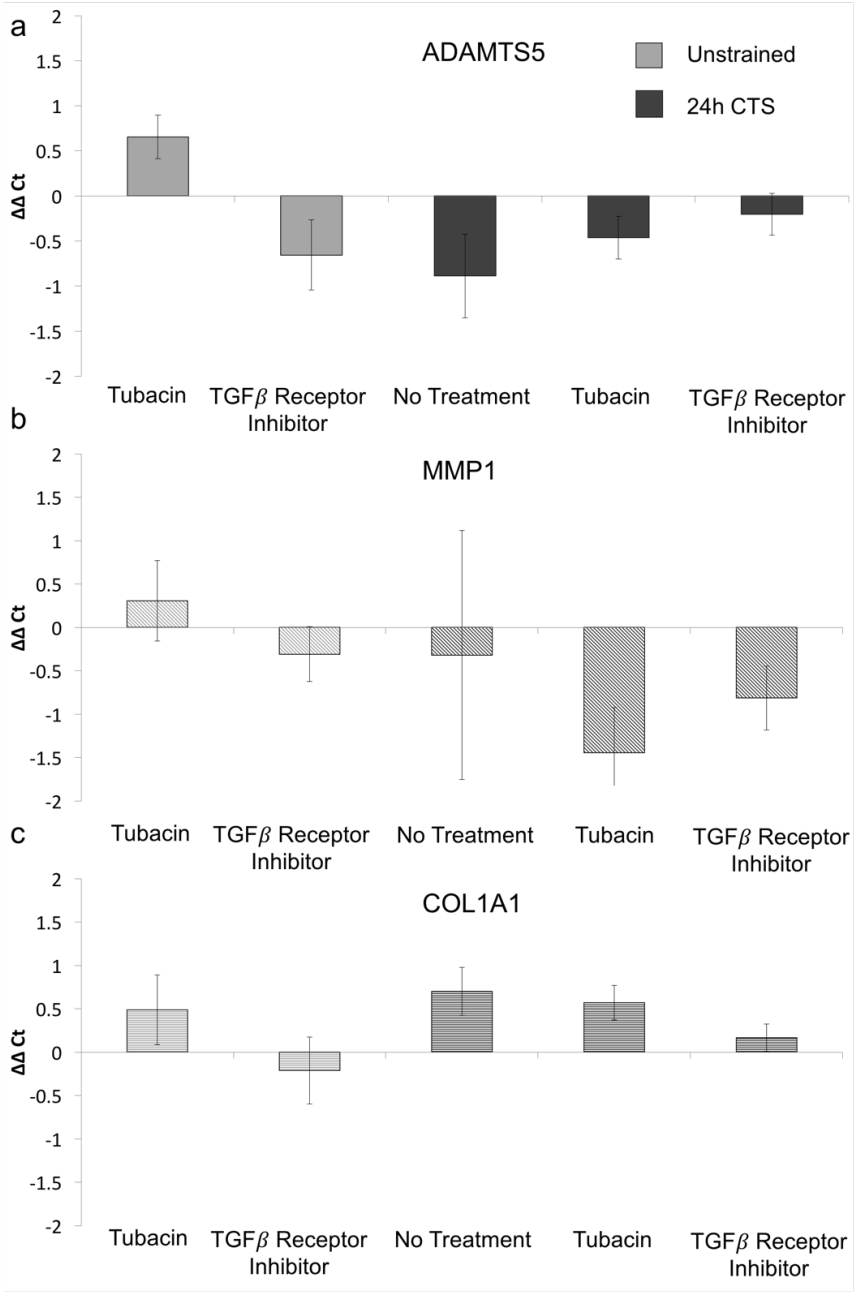

Figure 42: Gene expression ΔΔCt with respect to untreated unloaded controls, for (a) ADAMTS5, (b) MMP1, (c) Col1A1 for tenocytes treated with Tubacin or the TGFβ receptor inhibitor over a 24h period with and without cyclic strain. Cyclic tensile strain was applied at 1Hz, 0-3%. Cells were treated with the HDAC6 inhibitor, Tubacin or TGFβ Receptor Inhibitor as described in the text. Untreated cells were used as a control. Values represent mean for n=6 wells of cells per condition. No significant differences were found for any group using 2 factor ANOVA.

5.1.4 Discussion

Previous studies have reported that mechanical loading in the form of cyclic tensile strain regulates expression of extracellular matrix genes such as those examined here[80,113,115]. However, the present study found no statistically significant changes in expression of COL1A1, MMP1 or ADAMTS5 using the loading regime of 1Hz, 0-3% uniaxial strain with this tenocyte model. This may be partly due to high variability in gene expression. Other studies have also used the same magnitude and duration of strain and shown significant changes. However, previous results are not all consistent suggesting that mechanosensitive expression of these genes is also dependent on other factors which contribute to variability. Interestingly, Tubacin treatment was found to induce a statistically significant down regulation of MMP1 expression relative to untreated, unloaded controls. It is possible that the high variability in the untreated, loaded cells hides a similar reduction in MMP1 expression as previously reported[80]. Further analysis requires a better understanding of the factors contributing to variability of tenocyte mechanosensitive gene expression and an increased sample size to aid precision in the face of this variability.

5.2 Role of IFT88 on Tendon Cilia Expression and Mechanosignalling

5.2.1 Introduction

Previous studies in chondrocytes[187], osteocytes[157] and epithelial cells[5] have shown that cilia are involved in mechanosignalling. This typically involves disrupting expression of cilia and measuring the metabolic or signalling response to mechanical loading. Cilia disruption may be achieved by chloral hydrate treatment which disrupts all microtubules causing a loss of primary cilia. However cytoplasmic microtubules reform faster than cilia such that by carefully timing experimental interventions post chloral hydrate treatment it is possible to mechanically stimulate cells with normal microtubules but without primary cilia[222]. Although this approach has been used in several studies it is now considered a relatively crude and unreliable method of regulating cilia expression. Alternatively a more specific disruption of cilia structure and function may be achieved by disrupting intraflagellar proteins using small interfering RNA (siRNA) or genetic mutant cell lines[140]. For example the involvement of cilia in chondrocyte mechanosignalling was first demonstrated using a chondrocyte cell line derived from the oak ridge polycystic kidney (ORPK) mouse model in which cells express a hypomorphic mutation of IFT88[6,153,198,212]. This results in stunted or absent primary cilia and a corresponding loss of mechanosignalling compared to wild type cells[6,198]. However, the degree of disassembly seems to vary depending upon cell type[140,223]. Furthermore, it is increasingly apparent that disruption of IFT may lead to non-ciliary effects which influence cell function. For example hypomorphic mutation of IFT88 leads to increased acetylation of cytoplasmic microtubules[224] and altered actin organisation and cell biomechanics[140,225]. Interestingly, no studies have yet used any of these techniques with tenocytes to elucidate the role of primary cilia in tendon.

This chapter describes functional studies to examine the role of cilia in tenocyte mechanosignalling for the first time. Studies attempted to use siRNA to disrupt IFT88 expression and cilia expression followed by analysis of mechanosensitive matrix gene expression. It was hypothesised that IFT88 siRNA would lead to short or absent cilia.

5.2.2 Methods - IFT88 siRNA Transfection and analysis of cilia expression

Small interfering RNA (siRNA) transfection was performed to silence the IFT88 gene in order to try and disrupt intraflagellar transport and prevent cilia assembly. A similar approach has successfully been used to examine the role of cilia and IFT in mechanosignalling in various other cell types[140,226]. The present study used the dharmafect system (ThermoFisher, Waltham, MA) to transfect cells with either human IFT88 siRNA (ThermoFisher, Waltham, MA); a scrambled siRNA (ThermoFisher, Waltham, MA) negative control to determine nonspecific effects of transfection or a Green Fluorescent Protein (GFP) labelled siRNA (SiGLO) (ThermoFisher, Waltham, MA) to serve as a positive control. An additional control group consisted of cells treated with transfection reagents in the absence of siRNA.

Isolated human tenocytes at P2 were seeded onto glass coverslips in 24 well plates and cultured for 3 days in tenocyte media 2 as described in section 2.1.1. Cells were treated in 4 different transfection/siRNA groups as described above with 6 coverslips per group. Transfection was performed according to the manufacturer's instructions. To review briefly, cells were washed with PBS. Dharmafect reagent was prepared with 1 μl in 100 μl of antibiotic-free tenocyte media 2. A total of 5 μl of either IFT88 siRNA (5μM), scrambled siRNA (5μM) or SiGLO (5μM) were added to 100 μl of antibiotic-free tenocyte media 2 and incubated for 5 mins at room temperature. SiRNA and

dharmafect solutions were combined 100µl:100µl and incubated for a further 20 minutes at room temperature. Each solution was mixed with 800 µl of serum and antibiotic free media. Media on cells was replaced with this transfection mixture with 1ml per 24 well plate well. Cells were incubated for 48 hours prior to further PBS washing and fixation.

For untreated, negative control and IFT88 siRNA treated cells, cells were stained with ARL13b and acetylated α-tubulin as per isolated cell protocol previously described (Sections 2.4.5). Cilia expression was then visualised by epifluorescence and confocal microscopy as previously described (Section 2.6.1). Positive control cells were imaged using epiflouorescent microscopy to determine transfection efficiency.

The protocol was repeated and a western blot performed after 48 and 72 hours after transfection. Western blot control was β-tubulin. To perform the western blot, protein was extracted using TRIzol method (acid guanidinium thiocyanate-phenol-chloroform extraction) and protein concentration was calculated using the Bradford assay with BSA as a standard. Protein was diluted in 0.1%SDS solution such that it was at a concentration of 0.5µg/µl. For loading on to gels the protein containing solution was mixed 1:1 with 2x Laemmli buffer (4% SDS, 10% 2-mercaptoehtanol, 20% glycerol, 0.004% bromophenol blue, 0.125 M Tris HCl). Gels were immersed in migration buffer (25 mM Tris base, 190 mM glycine, 0.1% SDS) and placed into the electrophoresis machine. 20µl protein solution was loaded in each well of the gel and a loading control was added for each experiment. The gel was run at 120V until the bromophenol blue dye approached the bottom of the gel. Protein was then transferred under wet conditions to membrane using the previous running buffer minus SDS with the addition of 20% methanol. Membrane was stained with Ponceau red to ensure protein has been transferred. Membrane was then blocked with 5% BSA for 30 minutes. Primary

antibodies, mouse anti-IFT88 and rabbit anti-β-tubulin were incubated with the membrane at a concentration of 1:100 for 1 hour at room temperature. Membrane was washed with TBS containing Tween 3 times for 10 minutes each time. Secondary antibodies anti-rabbit Alexa 488nm and anti-mouse Alexa 555nm were incubated for 1 hour at a concentration of 1:1000 at room temperature. Membrane was washed a final time in Tris buffer without Tween for 10 minutes prior to imaging using Li-Cor Odyssey.

5.2.3 Results

Using the SiGlow treated cells transfection efficiency was measured as a percentage of cells with green nuclear fluorescence as determined by routine epifluorescence microscopy. Cell number was calculated from corresponding bright field microscopy images (Figure 2). Results indicate transfection efficiency with primary human tenocytes of above 80% for all 3 slides measured.

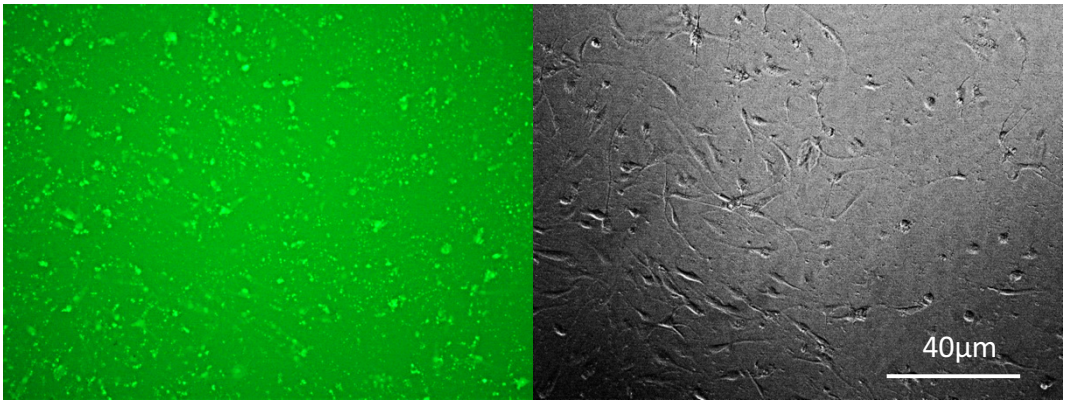

Figure 43: Representative images of human tenocytes treated with SiGlow to quantify transfection efficiency. *Left image shows SiGlow fluorescence as captured using epifluorescence and right image shows corresponding brightfield image of the same cells.*

Cilia length was not significantly reduced in the IFT88siRNA group, although there was a greater number of cells with short cilia (Figure 3) this is likely due to a low number of cilia observed in the control sample as many cilia in the range 1-4μm were observed in prior control experiments with isolated cells. There was an increase in prevalence from 64% for control (n=14 cells) to 82% for IFT88 SiRNA transfected cells (n=28 cells). However, this was not statistically significant and was within the range of 60-90% prevalence seen across fresh isolated tenocytes in prior experiments. A scramble control was performed but not analysed since there were no differences between the transfected cells and the control.

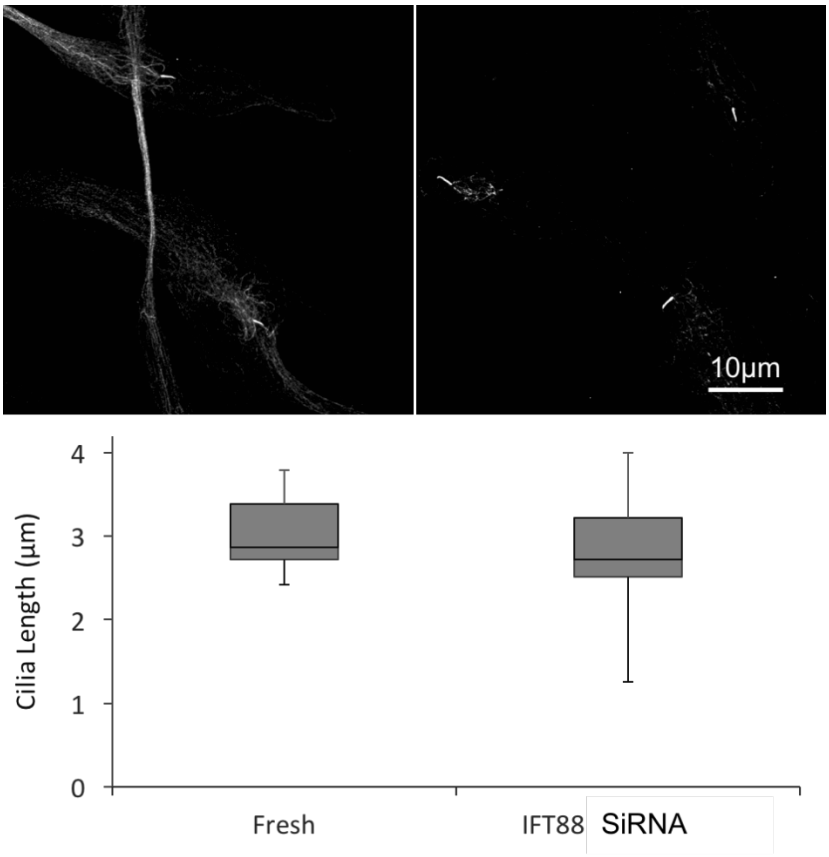

Figure 44: Primary cilia length does not change with IFT88 transfection. *(top) representative images showing cilia in untreated (left) and IFT88 SiRNA treated (right) isolated cells. (bottom) shows box and whisker plots for cilia length in untreated and IFT88 SiRNA treated cells. N=9 cilia fresh control and N=23 cilia for IFT88 transfected samples. Significance was tested with a two tailed unpaired student t-test, no significant differences were found p>0.25.*

Western blot analysis was performed to determine the efficacy of siRNA treatment to reduce expression of IFT88 protein measured 48 and 72 hours post transfection. The band for β-tubulin is very faint but can be seen in all groups and conditions. However the results of the western blot were not conclusive as the protein bands for IFT88 were not clear for any condition, including the controls (Figure 45).

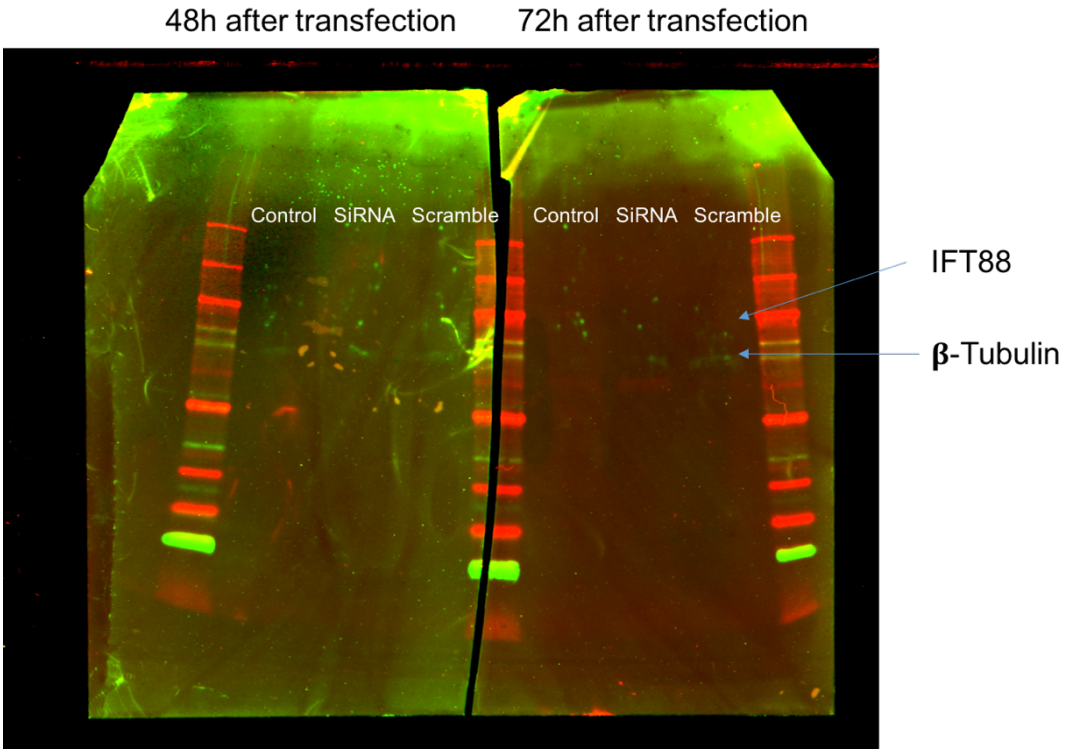

Figure 45: Western blot showing IFT88 levels 48 and 72 hours after transfection for control, SiRNA transfection and scramble. β-tubulin is faintly visible in all conditions. However, no clear IFT88 band was discernible for any condition.

5.2.4 Discussion

The high proportion of cells illuminated by SiGlow, the positive control, suggests that the SiRNA was able to get into the human tenocytes. The data shows a trend towards a reduction in both cilia length and prevalence with IFT88 siRNA. However, these changes are not statistically significant which probably reflects the inherent variability in cilia expression and the small sample size used for these experiments. Previous studies

in other cell types have reported more dramatic reductions in cilia length and prevalence with disruption or loss of IFT88[140,226]. Unfortunately, the western blot performed to determine whether protein levels of IFT88 had decreased was inconclusive. Therefore, it is unknown whether the siRNA transfection successfully reduced IFT88 expression. Interestingly, unpublished observations in other cell types indicate that IFT88 knockdown does not always prevent cilia assembly. This may also explain the complete lack of functional knockdown cilia studies in tenocytes despite the activity of several research groups in this area[9,173,175].

6 Effects of Cyclic Loading on Tendon Fascicle Collagen Structure

6.1 Introduction

This thesis has focussed on the properties of cilia in different regions of tendon and how they are affected by different loading conditions. Cyclic loading was shown to progressively decrease cilia length, even at relatively low strains. Relating cilia behaviour to the structural integrity of tendon tissue is important for interpreting whether the cells are exhibiting an injurious response. Damage quantification is typically done by investigating changes in fascicle mechanics or collagen organisation. However, while the extent to which cyclic strain causes reduction in mechanical properties in fascicles is well studied[18], the effects on collagen organisation are less well understood. This chapter focusses on developing and validating methods to support such analysis. It was hypothesised that cyclic loading would lead to changes in collagen organisation measurable with the two methods developed in this chapter.

To date most research into collagen damage has focussed on diseased tissue and on assessing disease progression[227], and from this a number of techniques to assess collagen damage from images have been developed, including Fast Fourier Transforms (FFT) and Fractal Dimension (FD) analysis. The aim was to develop a method based on these that can be used to assess the damage induced by explant loading experiments and thus potentially investigate the link between tissue damage and cell mechanobiology.

6.1.1 Fast Fourier Transforms

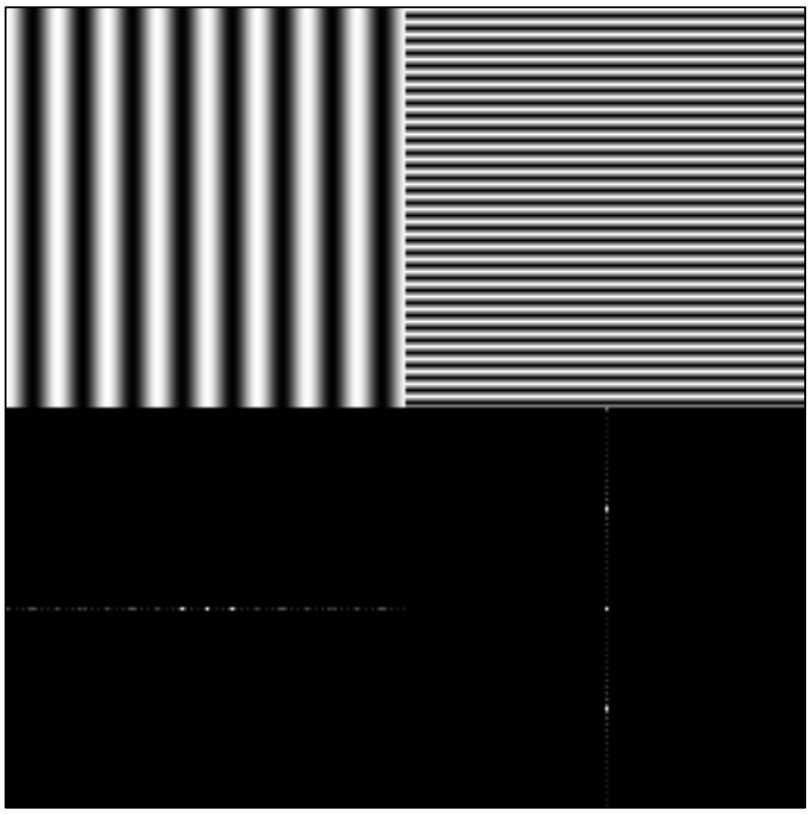

Figure 46: Representative examples of FFTs of sine waves. *Left shows a horizontal cosine wave above its FFT. Right shows a higher frequency vertical cosine wave above its FFT. As can be seen, the FFT picks out the frequency information. The primary frequency on the left image is low (8) and the FFT shows frequency components close to the origin. The primary frequency on the right image is higher (32) and the FFT shows frequency components much further from the origin. From 'Introduction to Fourier Transforms' by University of New Mexico*[228]

The FFT is a process that converts an image from the spatial domain to the frequency domain. FFT decomposes the information in an image into its component sine waves in every orientation. In Figure 46, the top two images are sine waves of different frequency and orientation, and below them are their respective FFTs. The dots in the FFT images represent the individual sine waves required to make the original images. The FFT images have vertical and horizontal symmetry and the origin is at the centre of the image. The brightness of each dot represents the amplitude of the wave and the location of the dot represents the frequency and orientation of the wave. In polar

coordinates the radius represents the frequency of the wave and the angle shows the orientation.

This is useful for looking at collagen organisation because one can see a clear visual difference between well aligned and disorganised collagen. With organised collagen being decomposed into sine waves with similar angles and disorganised collagen being decomposed into sine waves with widely varying angles. This can be seen in Figure 48 where the FFT of the organised collagen on the left shows bright points predominantly aligned perpendicular to the collagen fibres while the FFT of the disorganised collagen on the right has bright points that are more evenly distributed about the origin.

6.1.2 Fractal Dimension

Fractal dimension provides a statistical index of complexity and is the property of objects to have non-integer dimension. As David Harte explains, there are complex structures that are too complex to be a line but too simple to be a plane[229]. Fractal dimension is calculated as the ratio of how the shape-filling capacity of a pattern changes with the scale of measurement. This can be seen in the example shown in Figure 47.

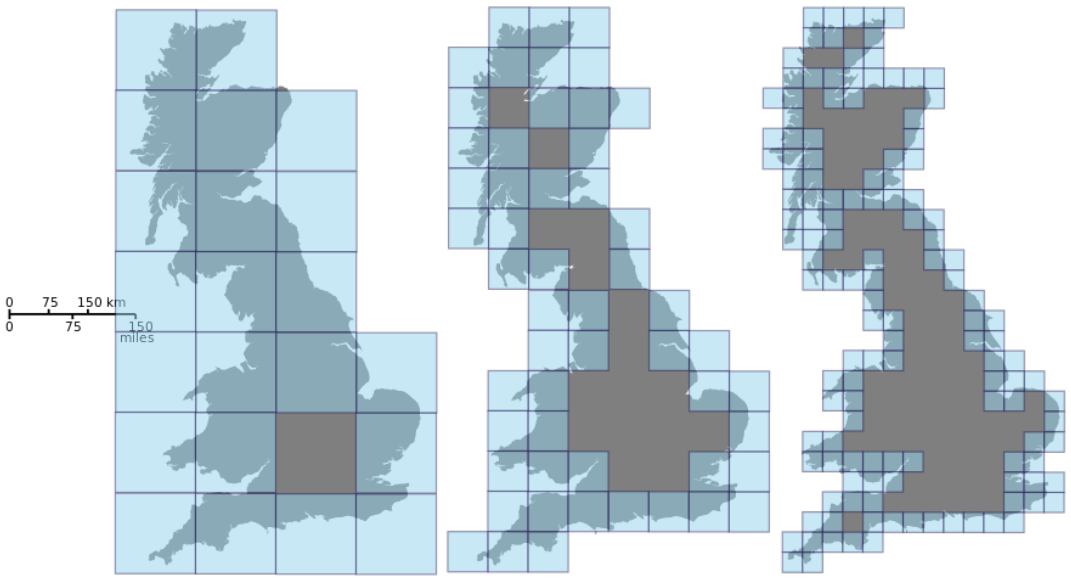

Figure 47: In this illustration the coast of Great Britain is assessed for dimension using the box-counting method. This is done by counting the number of boxes required to cover the coast at decreasing sizes. (Created by user 'Prokofiev' for Wikipedia, Creative Commons)[230].

While structures such as patterns of interlaced collagen fibres are not truly infinitely complex, and the resolution of imaging is a limiting factor, the fractal dimension can still be approximated. This is useful because calculating an approximate fractal dimension for an image of collagen gives a measure of the organisation of the collagen. A method utilising fractal dimension to assess collagen damage was developed by Frisch et al, and the work on fractal dimension in this chapter is based on this[231].

Fractal dimension can be calculated by using the box-fitting method. The box-fitting method works by calculating the number of boxes of different sizes that would be needed to cover an image. By comparing the number of boxes needed to cover a non regular area using different sizes of box, not only can the non-integer nature become clear but a measure between 1 (one dimension) and 2 (two dimensions) can be calculated. For example, if 4 boxes of size 128x128 are needed, 16 boxes of size 64x64 and 64 boxes of size 32x32 are needed then the trend implies the object is 2 dimensional. i.e. the number of boxes needed increases in direct proportion (squared) to the change in size. If 4 boxes were needed at 128x128 but only 8 at 64x64 and 16 at 32x32 then the image is 1 dimensional. i.e. the number of boxes needed increases in direct proportion (simple multiples). If the trend is between 1 and 2 then the image has a non-integer dimension. An illustration of how boxes are fitted using the British coastline is shown in Figure 47.

The aim in this study was to use these techniques to develop a robust method to characterise damage caused by cyclically loading rat-tail fascicles.

6.2 Methods

6.2.1 Sample Preparation

12 fascicles were obtained from a single rat killed for unrelated purposes. 6 were loaded to 5% strain for 1800 cycles at 1Hz before fixation with 4% PFA for 30 minutes at room temperature. The remaining 6 were immediately fixed upon dissection (fresh group). Loading was carried out in the Instron ElectoPuls 1000 in custom chambers (Section 2.3.1) filled with tenocyte media 2. It has been previously shown that this amount of strain causes observable tissue damage[74].

After fixation samples were stained using FITC labelled (5-(4,6-Dichlorotriazinyl) Aminofluorescein) (DTAF). DTAF stains protein, which in tendon is primarily collagen. Samples were immersed in 200μg/ml DTAF in PBS for 1 hour at room temperature. After staining, samples were washed in PBS before being mounted with prolong diamond mountant under glass coverslips on glass slides. For method development one cyclically strained sample and one unstrained sample were imaged using 40x confocal microscopy from the exterior IFM through to the fascicle to a depth of roughly 40μm, taking images at 1μm intervals.

6.2.2 Fast Fourier Transforms

To develop a method for quantifying collagen fibre disorganisation, an image of FM and another of IFM were selected for analysis. FFT was performed on each of the images (Figure 48). However, the Fourier transforms were too complex to analyse easily. Further difficulties were encountered due to horizontal and vertical artefacts (seen in Figure 48), formed because FFT assumes an infinite repeating image and there is therefore a discontinuity where the edges meet.

In order to overcome these limitations, a second method was attempted. This utilised a procedure whereby the image was split into 100, 100x100, pixel images, and an FFT performed for each of these smaller images. Each Fourier-transformed image was then thresholded before an ellipse was fitted to the resulting thresholded image. From the resulting data, 100 ellipses, an orientation of the long axis of the ellipse was calculated which represents the predominant orientation of the sub image the ellipse was generated from. Further, from each ellipse an aspect ratio was calculated which corresponds to the strength of alignment of collagen within the sub image. However, this method proved inconsistent across images with varying stain intensity. Furthermore, whilst every thresholding method built into ImageJ was used none could consistently and reliably threshold all the sub-images. Finally, as with FFT of whole images, edge artefacts were still present in the small images and skewed the resulting ellipses. Figure 49 shows representative images of FM and IFM and the resultant thresholded FFT fields using the Max_Entropy method[232], which was the most reliable in that it had the fewest fields that it failed to threshold. Despite this, even with the Max_Entropy method a number of the sub-images could not be properly thresholded. This can be seen in Figure 49 where some individual sub-images are black or contain multiple discrete spots.

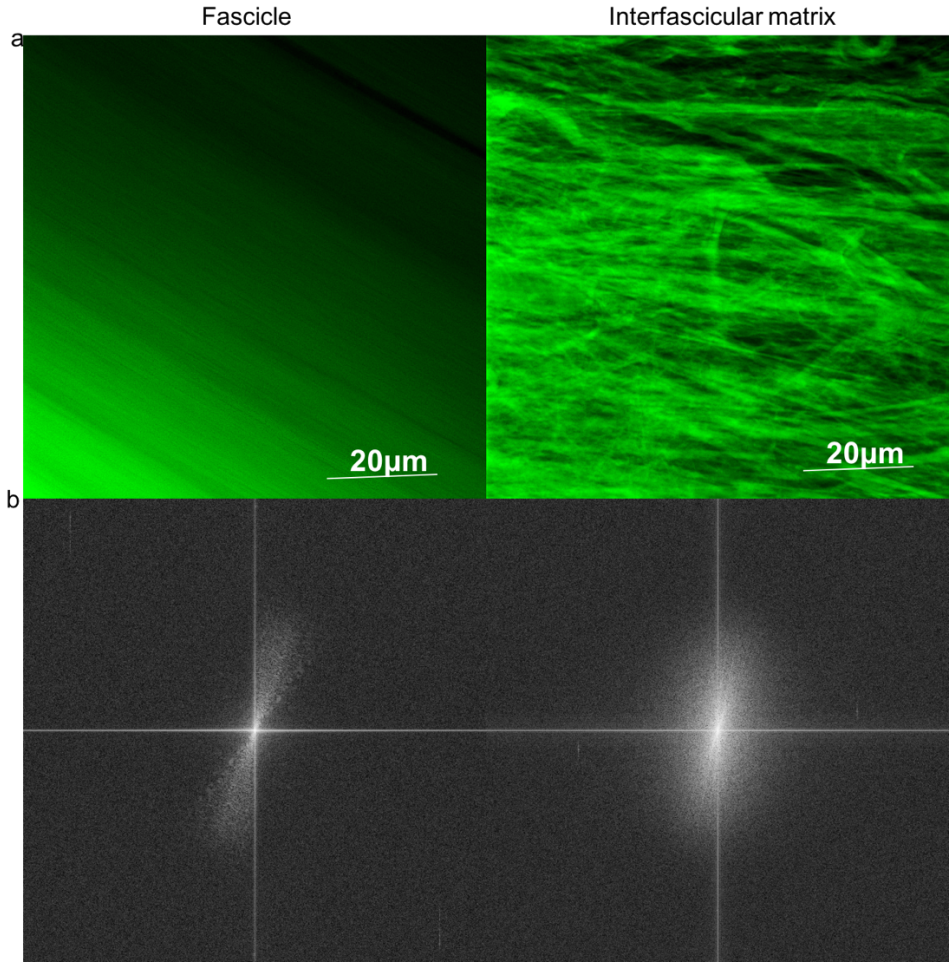

Figure 48: Figure showing (a) confocal images of fascicle collagen and IFM collagen labelled with DTAF and (b) respective Fast Fourier Transforms.

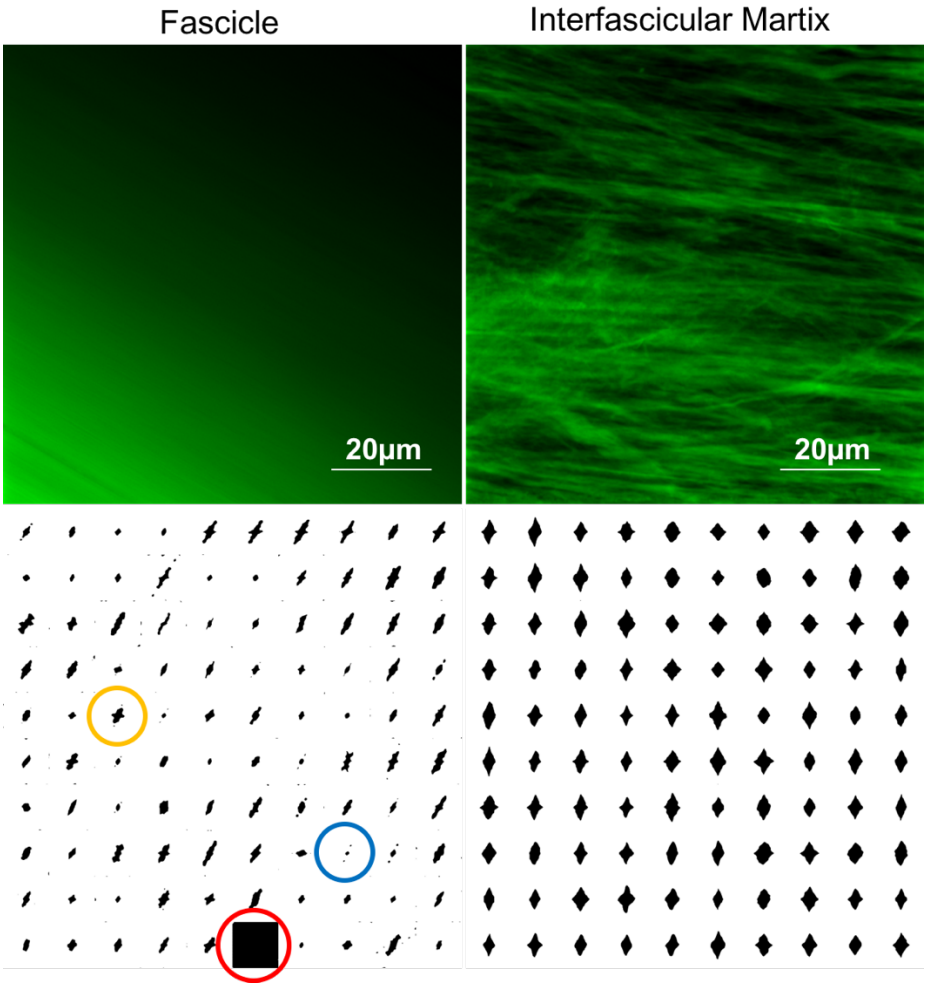

Figure 49:Representative images showing DTAF images of collagen above tiled thresholded FFT sub images. *The yellow circle shows a thresholded sub image where the horizontal edge artefacts are distorting the thresholded shape. The blue circle shows a sub image where there are multiple discrete thresholded objects. The red circle shows a sub image where the thresholding has failed.*

Due to the difficulty of developing a custom method for analysing collagen images with an FFT, the directionality plugin for ImageJ was used. This plugin uses an FFT to calculate the proportion of fibres in an image that lie in each direction. This essentially achieves what was attempted above but using a pre built algorithm[233]. The algorithm utilises a similar method to that attempted above. It splits the image into smaller images and performs a Fourier power analysis using spatial filters[233]. The algorithm produces a radial frequency distribution for the alignment of the image. From this frequency

distribution the dispersion (circular standard deviation) of the alignment can be calculated. An example with the same images used previously is shown in Figure 50.

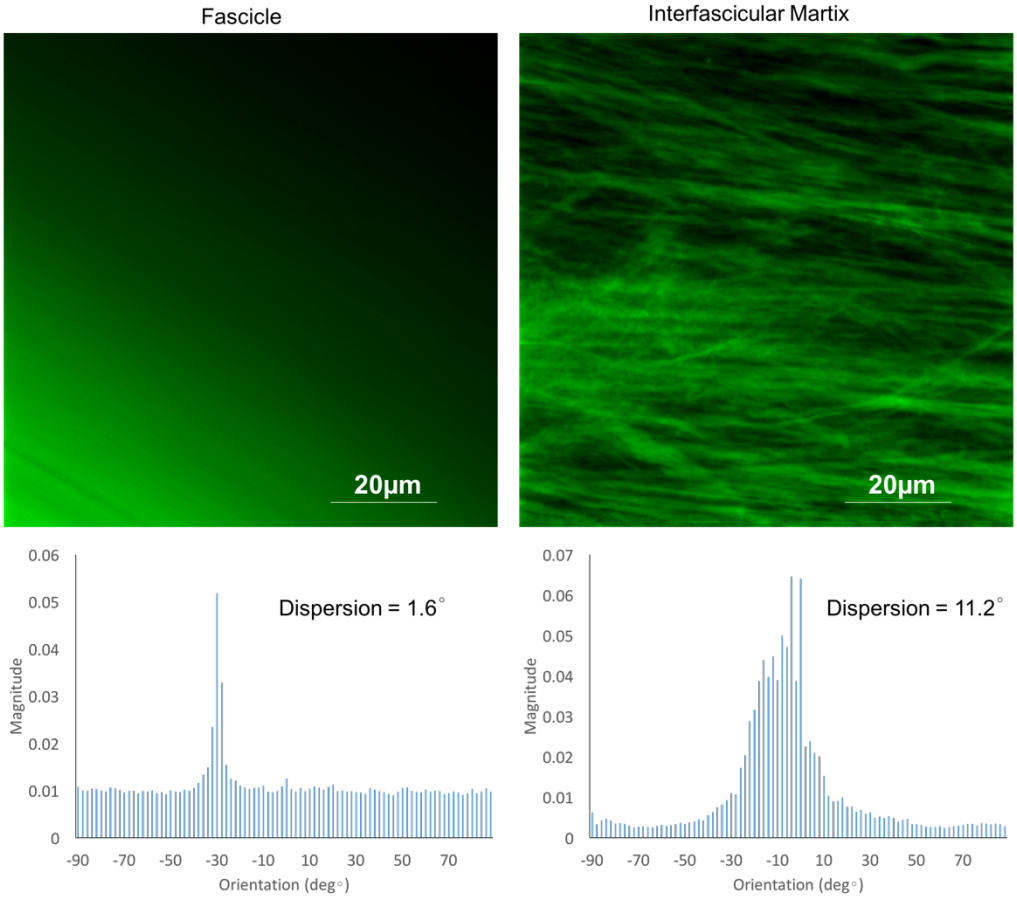

Figure 50: A DTAF image of the FM (left) and the IFM (right) above circular frequency distribution plots of directionality. *Calculated using the directionality plugin for ImageJ. The dispersion values are calculated as the circular standard deviations of these frequency distributions.*

6.2.3 Box Fitting Method (Fractal Dimension)

To calculate the fractal dimension of the images the box fitting method was used. For the collagen images the box fitting method was performed by first thresholding the image using the median auto local threshold plugin in ImageJ, then using the ImageJ box fitting plugin boxes of size 64^2, 32^2, 16^2, 12^2, 8^2, 6^2, 4^2, 3^2 and 2^2 were used.

An example of a thresholded image and the way results are calculated as a fractal dimension is shown in Figure 51 using a confocal image of the IFM.

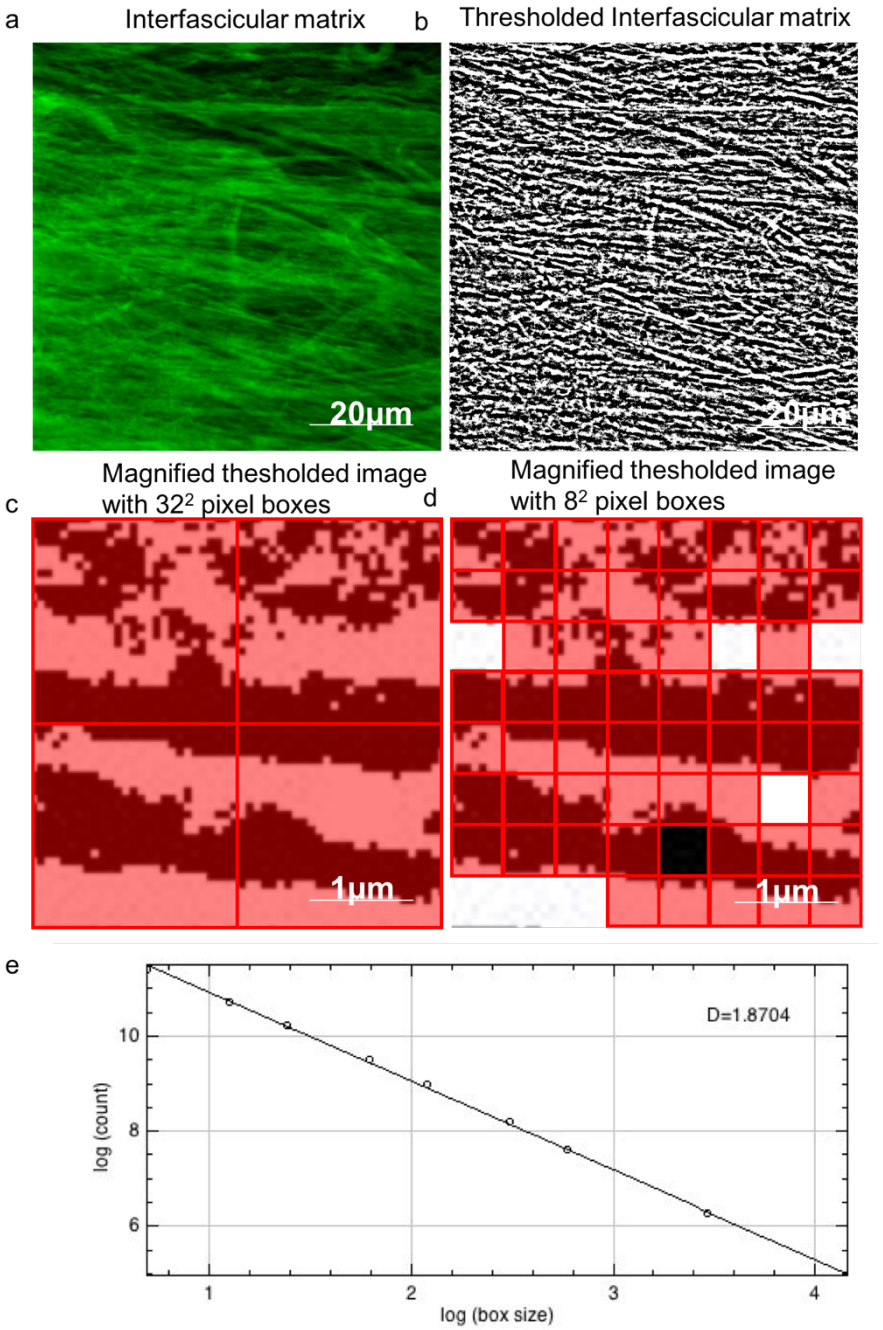

Figure 51: Shows an example of using the box fitting method to calculate fractal dimension. *(a) Shows a confocal image of the IFM. (b) The IMF image has been thresholded using the median local threshold method in ImageJ. (c) Shows a magnified region of the thresholded image with 32x32 pixel boxes fitted to it. (d) Shows the same magnified region with 8x8 pixel boxes fitted to it. (e) Shows a log-log scatter plot of box size against number of boxes required to cover the image and the calculated trend line which gives the dimensionality, D=1.8704.*

6.2.4 Testing Fourier Transform and Dimensionality Methods

2 potential methods, the FFT directionality plugin (dispersion) method and the box fitting (fractal dimension) method were tested using the 6 strained and 6 unstrained fascicles. Firstly, the image stacks for a cyclically strained and unstrained fascicle used during method development were tested using both methods on each image in the stack. Secondly, each of the 12 fascicles was imaged at a depth of 4μm (IFM) and 20μm (FM) and both methods tested on the resultant images.

6.3 Results

Both methods were tested on image stacks through a strained and unstrained fascicle (Figure 52). For the dispersion method the tissue at the exterior IFM region had a high dispersion which decreased as the images transition from IFM to FM which can be seen to occur between 5-10μm into the tissue (Figure 52b). This is as expected since higher dispersion indicates more disorganised fibres. For the fractal dimension method a similar transition can be seen, going from low dimensionality in the IFM to higher dimensionality in the fascicle (Figure 52c). This is somewhat counterintuitive since higher dimension usually implies higher complexity. However, in this case it may be due to the fact that the fascicular matrix is very close to being a plane with tightly packed collagen fibres. Neither method showed a clear apparent difference between unstrained and strained samples. However, this is not conclusive due to there only being one sample.

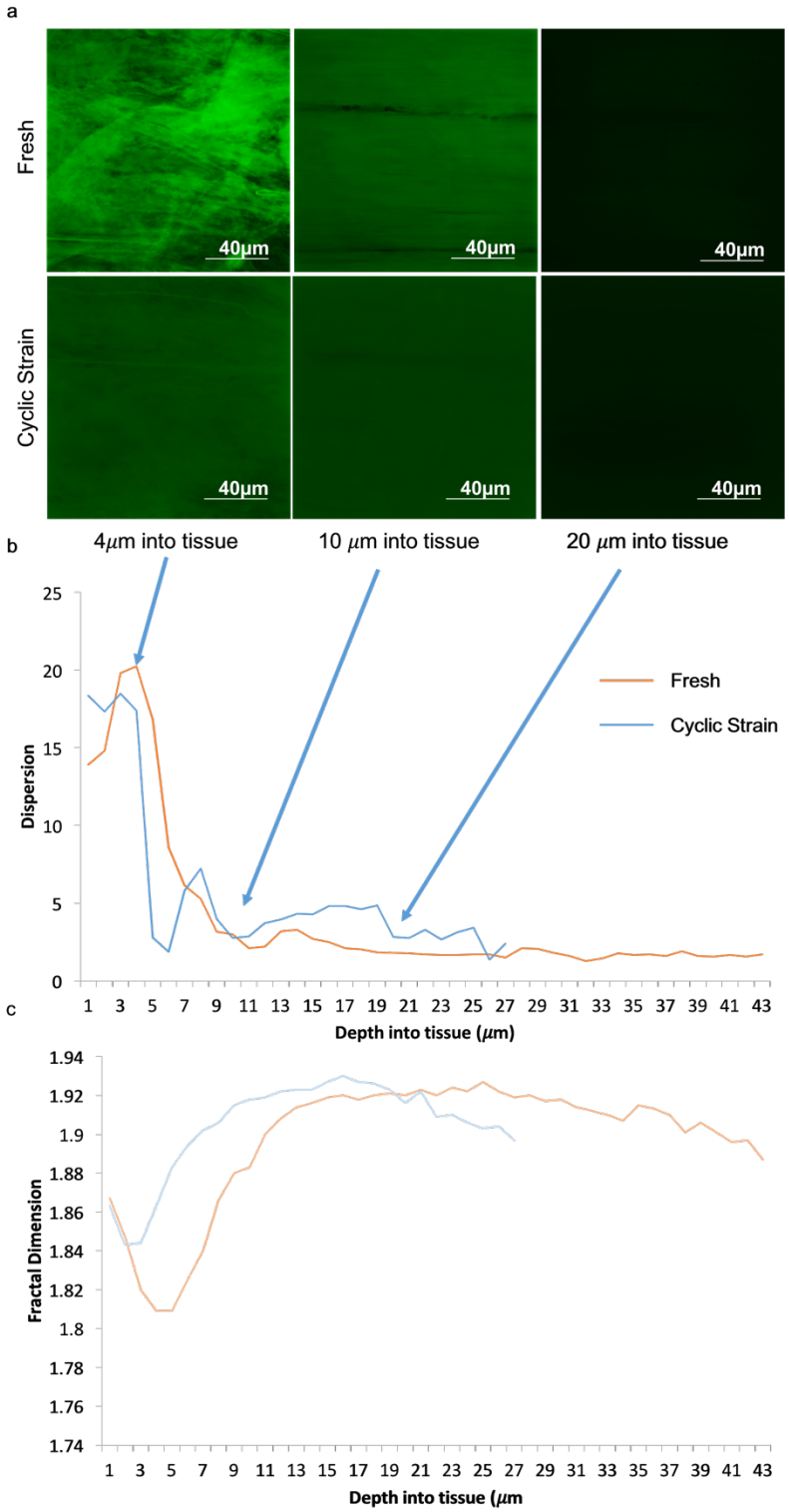

Figure 52: Example showing both the FFT directionality plugin (dispersion) method and the box fitting (fractal dimension) method applied to a strained and unstrained fascicle image stack. (a) Shows representative images 3µm, 10µm and 25µm into fresh and cyclically strained tissue. (b) Shows a graph of fibre orientation dispersion for both fresh and cyclically strained tissue from the surface going into the tissue at 1µm increments. (c) Shows a graph of fractal dimension for both fresh and cyclically strained tissue from the surface going into the tissue at 1µm increments.

Both the FFT directionality plugin (dispersion) method and the box fitting method (fractal dimension) were used to assess collagen organisation in the FM and IFM of 6 loaded and 6 unloaded fascicles. Both methods show significant differences in collagen organisation between the FM and IFM in both fresh and cyclically strained tissue (Figure 53). However, while the box-fitting method showed significant differences between collagen organisation in the fresh and cyclic FM, the FFT directionality plugin method did not. Further, neither method showed significant differences between the IFM of the fresh and cyclically strained samples. With both methods it was observed that there was more variation in results for the IFM than for the FM. There was also more variation for the FFT directionality plugin method, across all conditions, than for the box fitting method.

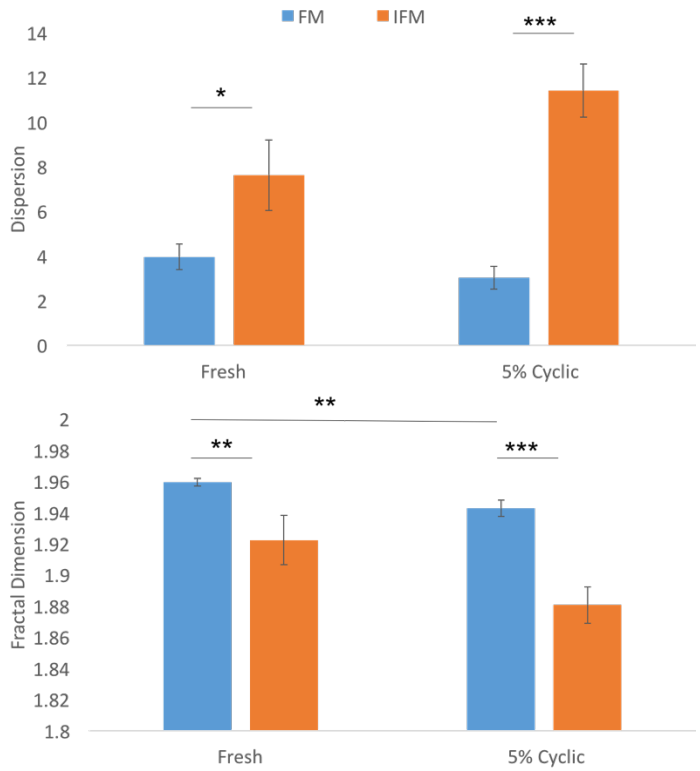

Figure 53: Mean dispersion (top) and fractal dimension (bottom) values for unstrained and cyclically loaded tendon fascicles in both the IFM and the FM. *IFM images were taken at a depth of 4µm into the tissue and FM images were taken at a depth of 20µm. 1 images taken per fascicle, per condition, N=6 fascicles. *=p<0.05, **=p<0.01, ***=p<0.001. Error bars show SEM.*

6.4 Discussion

The box fitting method (fractal dimension), was found to show a small but significant difference between collagen organisation in FM and IFM as well as between loaded and unloaded samples. Since this level of loading has been shown to cause damage in previous papers, it seems likely that the fractal dimension method is effective at determining differences in collagen fibre organisation.

Developing a method to interpret Fourier Transforms of entire images proved problematic, mainly due to edge artefacts. The method of separating an image into small sections, performing FFT, thresholding the results and fitting ellipses seemed promising. However, the challenge of finding a method of thresholding that worked across the

range of FFT outputs proved impractical in the given period. Furthermore, the edge effects gave extra prominence to the vertical and horizontal direction. A way to offset this might be to apply a radial filter (like a vignette) around each image which stops edge effects from occurring because there is no longer a discontinuity when tiling. While it would introduce its own artefacts, these may be easier to process.

An alternative method, the FFT directionality plugin (dispersion) method, was then applied. This method gave results which allowed for differentiation between FM and IFM. However, it was not able to differentiate between loaded and unloaded samples. The reason for this may be that the difference between the images was not great enough. The box fitting method found differences between these images and this suggests that the FFT directionality plugin (dispersion) method is not as sensitive to small differences in collagen organisation as the box fitting (fractal dimension) method. It may be the case that larger strain amounts are needed to simulate the levels of collagen damage which have previously been assessed using FFT derived methods in diseased tissue[231]. However, it seems more likely, due to the differences visible to the eye in the FFT images, that a better method of getting values out of FFT data is what is required to make FFT based methods work.

An alternative method that could be used is blind scoring where humans are used to score the damage on a scale without being told which groups the images belong to. This method has some issues with reliability and consistency between scorers but does make use of impressive human pattern recognition skills and their ability to differentiate between small differences in images.

Another approach, which may become commonplace in the future, could be to develop an iterative machine learning algorithm to assess collagen damage.

A method for quantifying collagen organisation in tendon tissue was developed using the box fitting (fractal dimension) method. Cyclic loading was previously shown in this thesis to lead to cilia disassembly, in both tissue and isolated cells, with increasing loading duration resulting in more disassembly. This is seen as a reduction in both length and prevalence which increases with loading duration. The purpose of this disassembly is not known. However, it is important in the future to do further work comparing cilia length and tissue damage to see whether there is any correlation as was seen when testing stress deprived samples. The work in chapter 3 suggested a link between tissue damage and cilia length. It seems likely, based on the work in both chapter 3 and chapter 4, that this is not direct but is due to factors associated with load and damage, namely TGFβ. Investigating the relationship between TGFβ and tissue damage is important further work that should be investigated.

Assessing collagen damage is an important area and this study has touched on it. The subject merits further research expanding on some of techniques, mentioned above, that have been successfully implemented by other groups researching in the field. With the box fitting (fractal dimension) method it is now possible to relate primary cilia to quantifiable tendon damage.

7 Discussion

7.1 Loading Regimes and Model Systems

7.1.1 Rat Tail Model

The rat tail tendon model was used throughout much of this thesis. The two primary advantages of this model are that tissue is easy to acquire and that fascicles are distinct and easily dissected, facilitating comparative tests between fascicles. Furthermore, rat tail tendon fascicles, usually dissected at between 5-8cm in length and approximately 300μm in diameter, are an ideal size for mechanical testing and intervention.

A further crucial determining factor for using rat tail tendon was, as discussed in chapter 2.5, the ability to image cilia within rat tail tissue since this proved not to be possible with bovine tissue.

However, there are a number of limitations to the use of rat tails. One disadvantage is that the rat tail has a unique structure, with each fascicle operating almost like a distinct tendon and consequently the IFM is particularly weak, allowing for large amounts of fascicle sliding. This is distinct from most human tendons where the IFM more tightly binds the fascicles, such that fascicle sliding is, while potentially implicated in determining gross tendon mechanics, somewhat contentious[16,17].

Another disadvantage is that some molecular pathways, proteins and protein expression is different in rat tenocytes compared with humans. For example, in rat MMP13 may play a similar role in collagen breakdown to that played by MMP1 in human tendon[193].

A third disadvantage of the rat tail model is that rat tail tendons are positional rather than energy storing tendons, and it is the energy storing tendons which usually experience higher strains and are more prone to injury.

Overall, however, the number of testable fascicles that can be obtained from rat tail makes it a valid model to use and the advantages outweigh the limitations. It is probably for these reasons that the model is so widely used in tendon biomechanics and mechanobiology research[9,51,55,82,234].

7.1.2 Isolated human cell model

In addition to the intact rat tail fascicle model described above, this thesis also used an isolated human tenocyte model. The main advantage of the isolated human cell model is that the cells are human and therefore directly applicable to human physiology and medicine. Furthermore, isolated cells can be reliably used in a wide variety of biological techniques and investigations. Cells used in this project were obtained from young (18-21) healthy human hamstring tendons by digestion. The digestion method obtains cells from both the fascicle matrix and interfascicular matrix and therefore likely includes a mixed population of tenocytes, including small numbers of non-tenocyte cells found in tendon such as synovial cells[235,236]. Cells in these studies were used at passage 2, which is considered a low passage number for tenocytes, and is below what is considered the maximum for tenocytes to avoid substantial phenotypic drift[79]. This is particularly important in the context of this work since in cilia in chondrocytes have been shown to reduce in both prevalence and length with increasing passage[187]. Cell lines often provide a consistent and reliable alternative to using primary cells. However, there are no commercially available tenocyte cell lines available at this time.

A key part of this project was the ability to reliably measure the primary cilia in isolated cells. Isolated cells also allow for the use of the flex cell system in which cells are strained consistently. This is much harder to do in tissue due to the relaxation effects and to the fact that local strain in tissue is not equal to gross strain[215]. However, the strain experienced by cells *in vivo*, while predominantly longitudinal tensile strain, also involves complex tensile, compressive and shear strain: this is hard to simulate in isolated cells. The flex cell system only provides tensile strain via the focal adhesions by which the cell attaches to the silicone membrane. The 3D nature of tendon means that cells experience strain from all directions, both from external matrix forces as well as bindings between cells and matrix and cells and cells. A further issue is that while in tendon cells are orientated predominantly in parallel with the long axis of the tendon, when grown on membranes they are randomly orientated and thus experience tensile stress differently depending upon the orientation. A further difference between a 2D flex cell system and the 3D nature of tendon is the way that cell signalling operates. The TGFβ pathway which is a key focus of this thesis is a paracrine pathway which operates by the diffusion of cytokines into the ECM surrounding the cell. In the 2D flex cell system the media surrounding the cells is an agitated liquid, unlike the dense collagen matrix of tendon, this means that cytokines can travel much further and faster in the 2D system than they can in tendon tissue, with all cells on the membrane signalling to all other cells on the membrane. In tissue, due to a slower diffusion rate and the absence of mixing, paracrine signalling is much more localised to the area and cells close to the signalling cell.

The flex cell system, while predominantly providing longitudinal strain does cause media agitation which adds fluid shear stress. The system is also not perfectly homogenous in strain particularly close to the edges of the membrane and for this reason cells close to the membrane edges were removed before imaging or lysis. Despite these limitations,

due to the difficulty of quantifying and consistently repeating tests in tissue, isolated cells and the flex cell system, can be very useful for the ability to apply reliable and consistent strain.

There are numerous techniques available to try and make isolated cell models more similar to tissue while still retaining the advantages of control and repeatability. These include seeding cells into 3D constructs, usually containing one or more different hydrogels, or by applying both strain and fluid shear to 2D isolated cell models[80,237]. In these studies, isolated cells were used and imaged in 2D, which simplified imaging and the application of strain, at the expense of not having a more realistic 3D construct.

A related disadvantage of using isolated cells is that they are no longer in their native physical environment, which is especially problematic given so much of this work relates to the effects of changes in mechanics. One specific example of differences between isolated cells and cells in tendon tissue is the difference observed between cilia length in isolated cells (quite long) compared with in tissue (generally short). Again, this has been abrogated in some studies by the use of 3D hydrogel constructs[166].

7.1.3 Loading Regimes in Isolated cells

Many loading regimes have been used to investigate the response of tenocytes to mechanical strain, in tissue and isolated cells in both 2D and 3D constructs. Loading regimes need to be physiologically relevant. Achieving this can be challenging because in vivo strains vary widely between species and tendon type. For example, human Achilles tendon is reported to stretch up to 11.4% during hopping, whereas many positional tendons, including the rat tail, experience substantially lower strains during normal activity and fail at strains regularly experience by other tendons[14,19]. Studies have investigated the strain experienced by tenocytes *in vivo* and found that they experience

mostly tensile strain in the direction of the long axis of the tendon. In addition, they experience lateral tension and compression, fluid shear and shear from fibre and fascicle sliding. Further, the strains experienced by the tenocytes are substantially lower than the gross strain applied to the tendon with local cell strains being around 40% of gross strain at low gross strains (1-2%) and only around 20% at higher gross strains (6-8%)[215]. Local shear strains, while consistently lower than gross longitudinal strain (approx. 50%), increase roughly linearly with gross strain[215].

As discussed above, the complex strains experienced *in vivo* make determining an appropriate strain regime for isolated cells challenging. Further complicating the matter is the need to use a strain regime that is consistent with regimes used in other studies to provide comparability and consistency. Studies in isolated cells have used a number of different strain magnitudes, frequencies, and durations (Table 3). In looking at gene expression data, differences can be seen between different loading regimes, suggesting that loading regime is important. The most common loading frequency is 1Hz. This is likely because it is of the same order of magnitude as many human actions, including running. However, numerous other strain frequencies have been used, including 10Hz, 2Hz, 0.5Hz and 0.15Hz[113,80]. In terms of strain magnitude, isolated cell model experiments mostly range from 3-5%, with some studies going higher or lower. This is likely to be at the higher end of physiological strains for energy storing tendons[215]. In terms of duration most studies seem to be either short term 1, 2 or 4 hours or longer term 24 or 48 hours. Some studies have used intermittent loading to simulate human activity (Table 3)[189].

Taking these factors into account, the following measures were used for all isolated cell experiments in this thesis. Strains of 3% at 1Hz were applied, with durations of up to 24 hours. 3%, 1Hz strain seems to be most similar to other studies whilst intermittent

loading was not used due to the difficulty of comparing results. For many of the studies in this thesis a 2-hour strain free recovery period was added. Longer recovery periods were considered but, as discussed in chapter 4, complete cilia recovery had occurred within 2 hours and so longer time periods were abandoned.

7.2 Heterogeneity of cilia expression in tenocytes

7.2.1 Cilia Length

The cells in the FM and IFM exhibit a number of differences, including cell shape and gene expression[15]. It seems likely that different cell populations exist in FM and IFM with specialised functions within the tendon. It may be the case that these differences are due to the different mechanical environments within the two regions[15,74]. There are two aspects to this, the mechanical properties of the surrounding matrix, which is much softer in the IFM than the FM[17], as well as the differing local strains experienced in these regions, with the IFM cells likely experiencing more shear due to fascicle sliding than those in the FM[17,215].

Cilia in tendon tissue are typically shorter than those in many other tissues, averaging between 1-2μm in all but one study of rat tail tendons (Table 5)[9,173,174,209]. One possible reason for the reported difference in tendon cilia length is a difference in length measuring methodology. A custom image processing system that measures cilia in 3D from image stacks was used in the study that found longer cilia[173], while all other studies measured cilia by hand from maximal projections and reconstructed the full 3D length, similar to the method described in section 2.6.1.[9,174,238].

The work in this thesis was the first to distinguish between cilia from cells in the IFM and those of the FM (section 3.3). While no significant difference in cilia length was

found (both with a mean value of 1.2μm), differences in orientation were found. In the FM cilia were orientated parallel to the long axis of the fascicle but in the IFM there was no predominant orientation. Previous studies had not looked at this distinction and had come to contradictory conclusions about cilia orientation in tissue with some studies finding cilia alignment with the long axis of the fascicle and some finding no alignment at all[173,174]. This difference in the findings of previous studies may be due to differences in the regions of the tissue analysed and the local collagen environment.

Looking at this distinction it was found that while cilia in the FM did align with the long axis of the fascicle, those within the IFM did not, potentially explaining the previous contradictory results[173,174,209].

7.2.2 Cilia Orientation

The differences in orientation between the cilia of the FM and IFM are likely to be due to three possible reasons. The first reason is that the cell populations themselves are different. The second reason is the different strain profiles of the two regions, the cells of the fascicle experience predominantly cyclic tensile strain, whereas the cells of the IFM experience more complex tensile, compressive and shear strains[17,215]. The third reason is due to the constraints of the matrix they are within, which is highly orientated collagen fibres in the FM but more disorganised in the IFM. With regard to the latter, previous studies have reported stem cell cilia orientation associated with topographical cues in the form of parallel micro-grooves[197]. Experiments with isolated tenocytes found that mechanical loading had no effect on cilia orientation (section 4.3.2), suggesting that local collagen organisation may be the cause of cilia alignment in the FM.

The human hamstring tenocytes used in the experiments described in chapter 4 were obtained by the digestion of tendon explants. This means that the population likely

consists of both FM and IFM cells. From observing the population of isolated cells there is no clear bimodal distribution of cilia orientation or length, indicating that the cell isolation does not obtain two distinct populations. Further, the lack of any bimodal distribution of cilia orientation with respect to nucleus direction suggests that cilia orientation in tissue is not due to differences in cell population. Studies performed with cells isolated from the FM and IFM separately would help to confirm this hypothesis but this is not yet possible.

A further difference was observed between the regions when tissue is stress deprived. As discussed in chapter 3, it is seen that the cilia of IFM cells increase in length more than those of the FM. It is not clear whether this reflects different sensitivity in the two populations or differences in the internal mechanical response to stress deprivation in FM and IFM regions.

Interestingly, cilia length in isolated human tenocytes was much greater than that in intact rat tail tendon fascicles, with a mean length between 3-3.5μm in each study in this thesis, compared with cilia in fresh tissue which had a mean length between 1-1.5μm in every study in this thesis. Although species differences cannot be ruled out it is likely due to the lack of strain experienced by the cells rather than any constraints as will be discussed below.

7.3 Mechanically Induced Cilia Length Changes

7.3.1 Mechanism of Cilia Disassembly by Mechanical Load

There are a number of mechanisms by which cilia disassembly can occur, including mechanical removal via Katanin, tubulin deacetylation via HDAC6, a reduction in available tubulin potentially caused by increased actin tension or impaired IFT[135,168].

However, this work has shown that load induced cilia disassembly is caused by TGFβ activation, which in turn activates HDAC6. In tendon TGFβ is activated by cyclic strain and leads to changes in the expression of key matrix genes including Col1A1, ADAMTS5 and various MMPs[80]. It has been shown in osteoblasts and stem cells that direct application of TGFβ leads to cilia disassembly. Further, the primary cilium was recently shown to be involved in TGFβ signalling[154]. TGFβ receptors predominantly localise to the ciliary base with some also localising to the ciliary tip[164]. TGFβ$_1$ induced SMAD nuclear translocation was significantly reduced in ORPK mutant mice, a mouse mutant with a dysfunctional IFT88 gene leading to stunted or missing cilia[164]. Similarly, TGFβ transcription in response to increased intraocular pressure was abrogated in cells with mutated OCRL (a cilia localised protein involved in trafficking)[7]. Further, studies have shown that Clatherin Dependent Endocytosis, a method by which TGFβ receptors are protected from breakdown, requires a functioning cilium and is regulated by IFT[164]. The work of this thesis provides the link from cyclic strain through to cilia disassembly.

With regards to the elongation of cilia under stress deprivation it may be that the reverse of the above process is being observed. The slow rate of the elongation of cilia in response to stress deprivation suggests that elongation is not due to direct cilia mechanosensitivity and is likely to be a secondary effect with another cause. One possible cause is a decrease in activated HDAC6. As discussed above, cyclic strain likely leads to HDAC6 activation via TGFβ. It seems plausible that, with the complete absence of strain, active TGFβ slowly declines, leading to a slow decline in activated HDAC6 and thus causing cilia to increase in length. It is possible that the differences observed between the FM and IFM here are due to internal strain in the fascicle maintaining higher levels of activated TGFβ than in the IFM.

7.3.2 Modulation of TGFβ signalling

Cyclic strain has been previously shown to lead to small reductions in cilia length in isolated chondrocytes[198]. In the work of this thesis, cyclic strain was found to shorten and eventually fully disassemble primary cilia with increasing duration. As discussed in chapter 4, this appears to be caused by the cyclic load induced activation of TGFβ, which in turn activated HDAC6, which leads to tubulin deacetylation and the disassembly of the primary cilia.

An important consideration is that primary cilia is required for TGFβ signalling in retinal cells[164]. As discussed in chapter 4, this implies that the effects of TGFβ induced cilia disassembly may be a self-limiting, negative feedback loop, (Figure 41) thus causing TGFβ increases to be transient. In tissue, this is likely to work as a regulatory mechanism, maintaining both cilia length and levels of activated TGFβ within distinct ranges, influenced by the complex cyclic strains that tendons encounter during everyday life. This prospective mechanism is also likely to be protective, stopping TGFβ levels from getting too high, as well as potentially stopping other strain activated processes from being over activated. The fact that cilia returned to their original length quickly after strain was stopped suggests that levels of activated HDAC6 quickly decrease after loading is ceased. An important further study would be to look at activated TGFβ and HDAC6 levels over a 24 hour period of cyclic loading as well as in the 2 hours after loading is ceased.

Another factor that may influence TGFβ bioavailability in tendon are SLRPs. SLRPs including decorin have been shown in bone and cartilage to bind to TGFβ[239–241]. Further, it has been shown that TGFβ binding to decorin reduces the binding of TGFβ to type

I receptors while type II receptor binding is unchanged[240]. Decorin is the most abundant proteoglycan in tendon and is found between fibrils as well as in the IFM and work from Thorpe et al has suggested that there are no significant differences between decorin concentrations between tendon region and type[15]. It may therefore be the case that in tendon decorin serves a secondary purpose beyond fibrillogenesis, of sequestering TGFβ, but not in a regionally dependent way. This sequestration may potentially result in a time lag between TGFβ activation by strain and its binding to receptors, smoothing out the response to load over time, with some of the initial influx of TGFβ being sequestered and slowly released. This is an effect that would not be present in isolated cells due to the lack of ECM. Interestingly SLRP TGFβ interaction also goes the other way with TGFβ signalling leading to increased production of SLRPs[241].

As discussed in chapter 5, PCR was performed on cyclic load with and without Tubacin and TGFβ inhibitor in order to try and confirm whether the presence or absence of cilia has an effect on gene expression. However, a limited range of genes were investigated and the results were inconclusive.

The fact that cilia length seems to be controlled by downstream proteins, particularly HDAC6, rather than directly by strain, suggests that the long cilia seen in isolated cells is due to low levels of TGFβ and to a lack of mechanical stimulation. Differences between the levels of TGFβ between isolated cells, fresh tissue and stress deprived tissue have not been investigated and this would be an important follow up experiment.

This linking of TGFβ and cilia mechanotransduction in tendon could have implications for mechanotransduction in other tissue types, which may have similar mechanisms.

7.4 Other Pathways Which may be Regulated by Cilia Disassembly

7.4.1 Downstream effects of length changes

As discussed in chapter 1 primary cilia are important centres for signalling in many different cell types, although not yet demonstrated in tendon, many of these signalling functions are likely to be similar to those in other cell types. However, those that may be different, or perhaps particularly interesting in tendon, are those that relate to the cilia and its involvement with the cellular mechanical environment.

While cilia length changes and disassembly in tendon appear to be controlled by TGFβ, there are many downstream effects of cilia length changes that have not been explored in tendon. Firstly, there is the hypothesis detailed above that cilia length negatively influences TGFβ signalling, potentially as some kind of protective mechanism. Beyond this, there are many other signalling pathways that are controlled by tendon such as Ca^{2+}, Wnt and Hh. These pathways require cilia to function and it seems likely that cilia length and prevalence influence signalling rate. With specific regard to Hh signalling, Thompson et al found in chondrocytes that primary cilia are required for mechanosensitive Hh signalling. Further it was shown that increasing the strain magnitude led to cilia shortening and reduction of mechanosensitive Hh signalling. Treating cells with Tubacin to inhibit HDAC6 restored both cilia length and mechanosensitive Hh signalling. This is similar to the TGFβ negative feedback hypothesis detailed above. The exact relationship between the various cilia mediated signalling pathways, cyclic strain and cilia length merits further investigation, to confirm whether cilia length affects signalling rate in other pathways.

Cilia length also affects IFT, in longer cilia it takes longer for IFT proteins to reach the tip of the cilium[217,242]. Therefore, because as the cilium lengthens it takes longer for IFT proteins to reach the tip, the assembly rate decreases with increasing cilia length. This means that any proteins that need to reach the tip will take longer to do so. This implies that signalling will be faster in cells with shorter cilia. It is therefore interesting that shorter cilia appear to inhibit signalling and that longer cilia appear to enhance mechanosensitive signalling[157]. It may be that reduced signalling is more a function of prevalence rather than length. It may also be the case that the difference in IFT rate is not a limiting factor of cilia localised signalling pathways. Finally, it may be the case that shorter cilia do signal faster but other factors such as reduced receptor numbers offset the difference.

It seems likely that these mechanisms also operate within tendon, with the additional factor that differences between cilia length response to strain in the FM and IFM cells may be important for differentially regulating signalling within those regions. A further investigation into TGFβ activation within the FM and IFM in response to strain would help to confirm the differential signalling hypothesis.

7.4.2 Tendinopathy

The relationship between tendinopathy and primary cilia is not at all clear. One study found that mildly tendinopathic tissue contained cilia that were longer than those in healthy tissue[243]. However, what this might mean is unclear. It is possible that this indicates lower levels of TGFβ in the tissue, potentially suggesting a breakdown in the response of the tissue to cyclic strain. This could, however, be an artefact of those with tendinopathy not straining their tendons due to pain. It is also very possible that other mechanisms apart from TGFβ are at play here. There are numerous other mechanisms

that have been found to influence cilia length, and ascribing everything to TGFβ would be presumptuous. A theory for this was proposed by Lavagnino, who suggests that this may be due to collagen damage leading to areas of local stress deprivation which cause both tendinopathy as well as the increased number of long cilia[9].

7.5 Further Work

Firstly, the gene expression work from Chapter 5, should be repeated and expanded to investigate more potentially mechanosensitive genes and how cyclic strain affects them in the presence of tubacin and TGFβ receptor inhibitor.

As described in chapter 5, IFT88 knockdown with SiRNA was attempted to allow for the investigation of the effects of cyclic strain in the absence of cilia. However, the IFT88 knockdown did not result in any significant changes in cilia length, although the size of the study was small (section 5.2.3). Whether this was due to the transfection not working is unknown. A western blot was attempted, but found inconclusive. However, positive control with SiGlow did suggest that the transfection was working. It is possible that the transfection did work but while IFT88 was knocked down this did not affect cilia length in agreement with anecdotal reports in other cell types.

Alternative methods are also possible for knocking out cilia, including chloral hydrate, CRISPR and mutant models. However, each of these has their own challenges. That said, if IFT88 is found not to lead to cilia knockdown in tenocytes then these methods should be tested to find the most appropriate one to use for these experiments. In addition there is increasing evidence that IFT may have a role in cell signalling independent of cilia expression. Thus further experiments should be conducted following successful SiRNA treatment to examine the role of IFT in tenocyte function.

Given a reliable cilia knockdown model there are a number of avenues that could be investigated. The first test of a knockout model would be to investigate the hypothesis that cilia are necessary in tenocytes for TGFβ signalling. This would allow the negative feedback model described above and in Figure 41, to be evaluated. Further, it would allow for even greater expansion of the gene expression experiment from Chapter 5 by investigating the effects of cyclic loading on gene expression in the presence or absence of cilia. This would confirm which, if any, matrix genes require cilia.

While this thesis hypothesises that the relationship between stress deprivation, primary cilia length and tendon region may involve TGFβ, further work needs to be done to confirm this. One potential method would be to measure levels of active TGFβ in the IFM and FM of stress deprived tissue. This ties into related work to confirm that TGFβ activation increases occur within tissue and are the reason for the shortening of cilia within tissue. This could also be confirmed by using tubacin and TGFβ receptor inhibitor on cyclically strained tissue as an expansion of the work in Chapter 4.

As discussed in Chapter 7.4, there are a number of other signalling pathways which may be affected by changes in cilia length including wingless and hedgehog, investigating how these pathways interact with cyclic strain, cilia length and TGFβ is important to build up a more complete understanding of signalling in tendon. The development of a knockdown model would help with this. However, there are still experiments that could be performed without a knockdown model, such as investigating the expression of pathway genes and the trafficking of ligands into the cilium before and after cyclic strain

The work in Chapter 6 on developing methods by which collagen damage can be assessed needs to be refined and thoroughly tested before it can be reliably used.

However, once refined, the techniques could be used to quantify damage caused by certain loading regimes and compare these with clinically degenerated tissue to help develop better loading regimes for tendon testing. Further, they could be used to compare the fibre structure of different tendon types, regions and ages.

7.6 Conclusion

The work in this thesis has made a number of novel contributions to the understanding of the primary cilia in tendon as well as tendon mechanobiology as a whole. This work has shown zonal differences in the response of primary cilia to changes in mechanical loading. Further, this work suggests that cilia orientation in tendon is a function of matrix constraints as opposed to the strain environment. Cyclic strain was found to lead to progressive disassembly of isolated tenocytes and crucially, the mechanism for strain induced disassembly was identified to be the activation of HDAC6 via TGFβ activation. Based on this discovery, a hypothesis was developed linking TGFβ to a negative feedback mechanism, although further work needs to be done to confirm this. Additionally, a method was developed to determine collagen disorganisation in DTAF images of tendon tissue.

This work is important since understanding tenocyte mechanobiology is crucial for understanding how healthy tissue operates and tendinopathy might work. This is particularly important in tendon since it is a highly mechanoresponsive tissue and the most effective clinical treatments for tendinopathy have involved the supplication of strain. Gaining a further understanding of stress deprivation is important due to its potential relationship with tendinopathy. Furthermore, understanding the TGFβ pathway and its involvement with cilia, mechanotransduction and potentially

tendinopathy both furthers the understanding of a key signalling pathway in many tissues but also opens up the potential for therapeutic applications.

References

1. Gray, H. in *Anatomy of the Human Body* 376–378 (John William Parker, 1858).
2. Maffulli, N., Sharma, P. & Luscombe, K. L. Achilles tendinopathy: aetiology and management. *J. R. Soc. Med.* **97,** 472–6 (2004).
3. Riley, G. The pathogenesis of tendinopathy. A molecular perspective. *Rheumatology (Oxford).* **43,** 131–42 (2004).
4. Cook, J. L. & Purdam, C. R. Is tendon pathology a continuum? A pathology model to explain the clinical presentation of load-induced tendinopathy. *Br. J. Sports Med.* **43,** 409–16 (2009).
5. Nauli, S. M. *et al.* Polycystins 1 and 2 mediate mechanosensation in the primary cilium of kidney cells. *Nat. Genet.* **33,** 129–37 (2003).
6. Wann, A. K. T. *et al.* Primary cilia mediate mechanotransduction through control of ATP-induced Ca2+ signaling in compressed chondrocytes. *FASEB J.* **26,** 1663–71 (2012).
7. Luo, N. *et al.* Primary cilia signaling mediates intraocular pressure sensation. *Proc. Natl. Acad. Sci. U. S. A.* **111,** 12871–6 (2014).
8. Spasic, M. & Jacobs, C. Primary Cilia Length is Critical to Cellular Mechanotransduction. *Biophys. J.* **108,** 561a (2015).
9. Gardner, K., Arnoczky, S. P. & Lavagnino, M. Effect of in vitro stress-deprivation and cyclic loading on the length of tendon cell cilia in situ. *J. Orthop. Res.* **29,** 582–7 (2011).
10. Wiltse, L. L. & Pait, T. G. Herophilus of Alexandria (325-255 B. C.). The father of anatomy. *Spine (Phila. Pa. 1976).* **23,** 1904–14 (1998).
11. Heringa, G. C. & Lohr, H. A. On collagenous fibrils; their origin, structure and arrangement. in (1924).
12. Elliott, D. H. The Growth of Tendon Structure. *Bull Br Assoc Sport Med* **3,** 46–51 (1968).
13. Kastelic, J., Galeski, A. & Baer, E. The Muilticomposite Structure of Tendon. *Connect. Tissue Res.* **6,** 11–23 (1978).

14. Lichtwark, G. a & Wilson, a M. In vivo mechanical properties of the human Achilles tendon during one-legged hopping. *J. Exp. Biol.* **208,** 4715–25 (2005).

15. Thorpe, C. T. *et al.* Distribution of proteins within different compartments of tendon varies according to tendon type. *J. Anat.* **229,** 450–458 (2016).

16. Thorpe, C. T., Udeze, C. P., Birch, H. L., Clegg, P. D. & Screen, H. R. C. Specialization of tendon mechanical properties results from interfascicular differences. *J. R. Soc. Interface* **9,** 3108–17 (2012).

17. Thorpe, C. T. *et al.* The interfascicular matrix enables fascicle sliding and recovery in tendon, and behaves more elastically in energy storing tendons. *J. Mech. Behav. Biomed. Mater.* 1–10 (2015). doi:10.1016/j.jmbbm.2015.04.009

18. Abrahams, M. Mechanical behaviour of tendon. *Med. Biol. Eng.* **5,** 433–443 (1967).

19. Rigby, B. J., Hirai, N., Spikes, J. D. & Eyring, H. The Mechanical Properties of Rat Tail Tendon. *J. Gen. Physiol.* **43,** 265–83 (1959).

20. Hooley, C. J., McCrum, N. G. & Cohen, R. E. The viscoelastic deformation of tendon. *J. Biomech.* **13,** 521–8 (1980).

21. Yamamoto, E., Hayashi, K. & Yamamoto, N. Mechanical properties of collagen fascicles from the rabbit patellar tendon. *J. Biomech. Eng.* **121,** 124–31 (1999).

22. Kannus, P. Structure of the tendon connective tissue. *Scand. J. Med. Sci. Sports* **10,** 312–20 (2000).

23. Spadaro, J. A., Becker, R. O. & Bachman, C. H. The distribution of trace metal ions in bone and tendon. *Calcif. Tissue Res.* **6,** 49–54 (1970).

24. Lehninger, A. *Biochemistry: Molecular Basis of Cell Structure and Function*. (Worth Inc, 1975).

25. Gelse, K. Collagens - structure, function, and biosynthesis. *Adv. Drug Deliv. Rev.* **55,** 1531–1546 (2003).

26. Bozec, L. & Horton, M. Topography and mechanical properties of single molecules of type I collagen using atomic force microscopy. *Biophys. J.* **88,** 4223–31 (2005).

27. Sasaki, N. & Odajima, S. Elongation mechanism of collagen fibrils and force-

strain relations of tendon at each level of structural hierarchy. *J. Biomech.* **29,** 1131–1136 (1996).

28. Cusack, S. & Miller, A. Determination of the elastic constants of collagen by Brillouin light scattering. *J. Mol. Biol.* **135,** 39–51 (1979).

29. Buehler, M. J. Nature designs tough collagen: explaining the nanostructure of collagen fibrils. *Proc. Natl. Acad. Sci. U. S. A.* **103,** 12285–12290 (2006).

30. Lorenzo, A. C. & Caffarena, E. R. Elastic properties, Young's modulus determination and structural stability of the tropocollagen molecule: a computational study by steered molecular dynamics. *J. Biomech.* **38,** 1527–33 (2005).

31. Yoon, J. H. & Halper, J. Tendon proteoglycans: Biochemistry and function. *J. Musculoskelet. Neuronal Interact.* **5,** 22–34 (2005).

32. Watanabe, T. *et al.* Concerted and adaptive alignment of decorin dermatan sulfate filaments in the graded organization of collagen fibrils in the equine superficial digital flexor tendon. *J. Anat.* **220,** 156–63 (2012).

33. Vogel, K. G. & Meyers, A. B. Proteins in the tensile region of adult bovine deep flexor tendon. *Clin. Orthop. Relat. Res.* S344–S355 (1999).

34. Vogel, K. G., Sandy, J. D., Pogány, G. & Robbins, J. R. Aggrecan in bovine tendon. *Matrix Biol.* **14,** 171–9 (1994).

35. Vertel, B. & Ratcliffe, A. in *Proteoglycans* (CRC Press, 2000). doi:10.1201/9780203909720.ch14

36. Özkaya, N., Nordin, M., Goldsheyder, D. & Leger, D. in *Fundamentals of Biomechanics* 221–236 (Springer New York, 2012). doi:10.1007/978-1-4614-1150-5_15

37. Screen, H. R. C. Hierarchical Approaches to Understanding Tendon Mechanics. *J. Biomech. Sci. Eng.* **4,** 481–499 (2009).

38. BEAR, R. S. The structure of collagen fibrils. *Adv. Protein Chem.* **7,** 69–160 (1952).

39. Birk, D. E. & Zycband, E. Assembly of the tendon extracellular matrix during development. *J. Anat.* **184 (Pt 3,** 457–63 (1994).

40. Eppell, S. J., Smith, B. N., Kahn, H. & Ballarini, R. Nano measurements with

micro-devices: mechanical properties of hydrated collagen fibrils. *J. R. Soc. Interface* **3,** 117–21 (2006).

41. Buehler, M. J. Nanomechanics of collagen fibrils under varying cross-link densities: atomistic and continuum studies. *J. Mech. Behav. Biomed. Mater.* **1,** 59–67 (2008).

42. Franchi, M., Ottani, V., Stagni, R. & Ruggeri, A. Tendon and ligament fibrillar crimps give rise to left-handed helices of collagen fibrils in both planar and helical crimps. *J. Anat.* **216,** 301–9 (2010).

43. Lujan, T. J., Underwood, C. J., Henninger, H. B., Thompson, B. M. & Weiss, J. A. Effect of dermatan sulfate glycosaminoglycans on the quasi-static material properties of the human medial collateral ligament. *J. Orthop. Res.* **25,** 894–903 (2007).

44. Liu, X., Yeh, M.-L., Lewis, J. L. & Luo, Z.-P. Direct measurement of the rupture force of single pair of decorin interactions. *Biochem. Biophys. Res. Commun.* **338,** 1342–5 (2005).

45. Wenstrup, R. J. *et al.* Type V Collagen Controls the Initiation of Collagen Fibril Assembly. *J. Biol. Chem.* **279,** 53331–53337 (2004).

46. Parry, D. A. D. & Craig, A. S. in *Ultrastructure of the Connective Tissue Matrix* 34–64 (Springer US, 1984). doi:10.1007/978-1-4613-2831-5_2

47. Provenzano, P. P. & Vanderby, R. Collagen fibril morphology and organization: implications for force transmission in ligament and tendon. *Matrix Biol.* **25,** 71–84 (2006).

48. Miyazaki, H. & Hayashi, K. Tensile Tests of Collagen Fibers Obtained from the Rabbit Patellar Tendon. *Biomed. Microdevices* **2,** 151–157 (1999).

49. Diamant, J., Keller, A., Baer, E., Litt, M. & Arridge, R. G. Collagen; ultrastructure and its relation to mechanical properties as a function of ageing. *Proc. R. Soc. London. Ser. B, Biol. Sci.* **180,** 293–315 (1972).

50. Lavagnino, M., Brooks, A. E., Oslapas, A. N., Gardner, K. L. & Arnoczky, S. P. Crimp length decreases in lax tendons due to cytoskeletal tension, but is restored with tensional homeostasis. *J. Orthop. Res.* **35,** 573–579 (2017).

51. Franchi, M. *et al.* Crimp morphology in relaxed and stretched rat Achilles tendon. *J. Anat.* **210,** 1–7 (2007).

52. Wang, J. H.-C. Mechanobiology of tendon. *J. Biomech.* **39,** 1563–82 (2006).

53. Cohen, R. E., Hooley, C. J. & McCrum, N. G. Viscoelastic creep of collagenous tissue. *J. Biomech.* **9,** 175–84 (1976).

54. Yamamoto, E., Hayashi, K. & Yamamoto, N. Mechanical Properties of Collagen Fascicles From the Rabbit Patellar Tendon. *J. Biomech. Eng.* **121,** 124 (1999).

55. Haraldsson, B. T., Aagaard, P., Crafoord-Larsen, D., Kjaer, M. & Magnusson, S. P. Corticosteroid administration alters the mechanical properties of isolated collagen fascicles in rat-tail tendon. *Scand. J. Med. Sci. Sports* **19,** 621–6 (2009).

56. Thorpe, C. T., Birch, H. L., Clegg, P. D. & Screen, H. R. C. The role of the non-collagenous matrix in tendon function. *Int. J. Exp. Pathol.* **94,** 248–59 (2013).

57. James, R., Kesturu, G., Balian, G. & Chhabra, a B. Tendon: biology, biomechanics, repair, growth factors, and evolving treatment options. *J. Hand Surg. Am.* **33,** 102–12 (2008).

58. Fung, Y. C., Perrone, L. & Anliker, M. Stress-strain history relations of soft tissues in simple elongation, in Biomechanics: Its Foundations and Objectives. *Am. J. Physiol.* (1971).

59. Duenwald, S. E., Vanderby, R. & Lakes, R. S. Constitutive equations for ligament and other soft tissue: evaluation by experiment. *Acta Mech.* **205,** 23–33 (2009).

60. Duenwald, S. E., Vanderby, R. & Lakes, R. S. Stress relaxation and recovery in tendon and ligament: experiment and modeling. *Biorheology* **47,** 1–14 (2010).

61. Provenzano, P. P., Lakes, R. S., Corr, D. T. & Vanderby, R. Application of nonlinear viscoelastic models to describe ligament behavior. *Biomech. Model. Mechanobiol.* **1,** 45–57 (2002).

62. Kahn, C. J. F., Wang, X. & Rahouadj, R. Nonlinear Model for Viscoelastic Behavior of Achilles Tendon. *J. Biomech. Eng.* **132,** 111002 (2010).

63. Dussault, I. *et al.* A Structural Model of the Constitutive Androstane Receptor Defines Novel Interactions That Mediate Ligand-Independent Activity. *Mol. Cell. Biol.* **22,** 5270–5280 (2002).

64. Fang, F. & Lake, S. P. Modelling approaches for evaluating multiscale tendon mechanics. *Interface Focus* **6,** 20150044 (2016).

65. Ault, H. K. & Hoffman, A. H. A Composite Micromechanical Model for Connective Tissues: Part I—Theory. *J. Biomech. Eng.* **114,** 137 (1992).

66. Ault, H. K. A Composite Micromechanical Model for Connective Tissues: Part II—Application to Rat Tail Tendon and Joint Capsule. *J. Biomech. Eng.* **114,** 142 (1992).

67. Pensalfini, M., Duenwald-Kuehl, S., Kondratko-Mittnacht, J., Lakes, R. & Vanderby, R. Evaluation of Global Load Sharing and Shear-Lag Models to Describe Mechanical Behavior in Partially Lacerated Tendons. *J. Biomech. Eng.* **136,** 091006 (2014).

68. Hwang, E., Carpenter, J. E., Hughes, R. E. & Palmer, M. L. Shoulder labral pathomechanics with rotator cuff tears. *J. Biomech.* **47,** 1733–1738 (2014).

69. Goh, K. L., Meakin, J. R., Aspden, R. M. & Hukins, D. W. L. Stress transfer in collagen fibrils reinforcing connective tissues: Effects of collagen fibril slenderness and relative stiffness. *J. Theor. Biol.* **245,** 305–311 (2007).

70. Reese, S. P., Maas, S. A. & Weiss, J. A. Micromechanical models of helical superstructures in ligament and tendon fibers predict large Poisson's ratios. *J. Biomech.* **43,** 1394–1400 (2010).

71. Riley, G. Chronic tendon pathology: molecular basis and therapeutic implications. *Expert Rev. Mol. Med.* **7,** 1–25 (2005).

72. Kannus, P. & Kannus, P. Structure of the tendon connective tissue. *Scand J Med Sci Sport. Copyr. C MUNKSGAARD* **10,** 312–320 (2000).

73. Thorpe, C. T. *et al.* Tendon overload results in alterations in cell shape and increased markers of inflammation and matrix degradation. *Scand. J. Med. Sci. Sports* **25,** e381–e391 (2015).

74. Spiesz, E. M. *et al.* Tendon extracellular matrix damage, degradation and inflammation in response to in-vitro overload exercise. *J. Orthop. Res.* n/a-n/a (2015). doi:10.1002/jor.22879

75. Mcneilly, C. M., Banes, A. J., Benjamin, M. & Ralphs, J. R. Tendon cells in vivo

form a three processes linked by gap junctions dimensional network of cell. 593–600 (1996).

76. Maeda, E. *et al.* Gap junction permeability between tenocytes within tendon fascicles is suppressed by tensile loading. *Biomech. Model. Mechanobiol.* **11,** 439–47 (2012).

77. Stanley, R. L., Goodship, a E., Edwards, B., Firth, E. C. & Patterson-Kane, J. C. Effects of exercise on tenocyte cellularity and tenocyte nuclear morphology in immature and mature equine digital tendons. *Equine Vet. J.* **40,** 141–6 (2008).

78. Taylor, S. E. *et al.* Gene expression markers of tendon fibroblasts in normal and diseased tissue compared to monolayer and three dimensional culture systems. *BMC Musculoskelet. Disord.* **10,** 27 (2009).

79. Yao, L., Bestwick, C. S., Bestwick, L. a, Maffulli, N. & Aspden, R. M. Phenotypic drift in human tenocyte culture. *Tissue Eng.* **12,** 1843–9 (2006).

80. Jones, E. R., Jones, G. C., Legerlotz, K. & Riley, G. P. Cyclical strain modulates metalloprotease and matrix gene expression in human tenocytes via activation of TGFβ. *Biochim. Biophys. Acta - Mol. Cell Res.* **1833,** 2596–2607 (2013).

81. Smith, R. K. W. in *Diagnosis and Management of Lameness in the Horse* 694–706 (Elsevier, 2011). doi:10.1016/B978-1-4160-6069-7.00068-7

82. Rigby, B. J., Hirai, N., Spikes, J. D. & Eyring, H. The Mechanical Properties of Rat Tail Tendon. *J. Gen. Physiol.* **43,** 265–83 (1959).

83. ALi, O., Comerford, E., Canty-Laird, E. & Clegg, P. THREE-DIMENSIONAL ANATOMY OF EQUINE SUPERFICIAL DIGITAL FLEXOR TENDON (SDFT). *Orthop. Proc.* **97–B,** 17 (2015).

84. Maganaris, C. N. & Paul, J. P. In vivo human tendon mechanical properties. *J. Physiol.* **521 Pt 1,** 307–13 (1999).

85. de Jonge, S. *et al.* Incidence of midportion Achilles tendinopathy in the general population. *Br. J. Sports Med.* **45,** 1026–8 (2011).

86. Choo, H. J. *et al.* Delaminated Tears of the Rotator Cuff: Prevalence, Characteristics, and Diagnostic Accuracy Using Indirect MR Arthrography. *AJR. Am. J. Roentgenol.* **204,** 360–6 (2015).

87. Angermann, P. & Lohmann, M. Injuries to the hand and wrist. A study of 50,272 injuries. *J. Hand Surg. Br.* **18,** 642–644 (1993).

88. Schöffl, V. Tendon injuries of the hand. *World J. Orthop.* **3,** 62 (2012).

89. Lewis, J. S. Rotator cuff tendinopathy: a model for the continuum of pathology and related management. *Br. J. Sports Med.* **44,** 918–923 (2010).

90. Arya, S. & Kulig, K. Tendinopathy alters mechanical and material properties of the Achilles tendon. *J. Appl. Physiol.* 670–675 (2010). doi:10.1152/japplphysiol.00259.2009.

91. Aronow, M. S. Posterior heel pain (retrocalcaneal bursitis, insertional and noninsertional Achilles tendinopathy). *Clin. Podiatr. Med. Surg.* **22,** 19–43 (2005).

92. Järvinen, M. Epidemiology of tendon injuries in sports. *Clin. Sports Med.* **11,** 493–504 (1992).

93. Kujala, U. M., Sarna, S. & Kaprio, J. Cumulative incidence of achilles tendon rupture and tendinopathy in male former elite athletes. *Clin. J. Sport Med.* **15,** 133–5 (2005).

94. Nirschl, R. P. & Ashman, E. S. Tennis elbow tendinosis (epicondylitis). *Instr. Course Lect.* **53,** 587–98 (2004).

95. Stovitz, S. D. & Johnson, R. J. 'Underuse' as a cause for musculoskeletal injuries: is it time that we started reframing our message? *Br. J. Sports Med.* **40,** 738–9 (2006).

96. Cho, N. S., Hwang, J. H., Lee, Y. T. & Chae, S. W. Tendinosis-like histologic and molecular changes of the Achilles tendon to repetitive stress: a pilot study in rats. *Clin. Orthop. Relat. Res.* **469,** 3172–80 (2011).

97. Majima, T. *et al.* Biomechanical effects of stress shielding of the rabbit patellar tendon depend on the degree of stress reduction. *J. Orthop. Res.* **14,** 377–83 (1996).

98. Wang, W., Tang, X., Zhang, J., Yan, X. & Ma, Y. Complete stress shielding of the Achilles tendon: ultrastructure and level of interleukin-1 and TGF-β. *Orthopedics* **33,** 810 (2010).

99. Wang, T. *et al.* Programmable mechanical stimulation influences tendon homeostasis in a bioreactor system. *Biotechnol. Bioeng.* **110,** 1495–507 (2013).

100. Lavagnino, M., Arnoczky, S. P., Egerbacher, M., Gardner, K. L. & Burns, M. E. Isolated fibrillar damage in tendons stimulates local collagenase mRNA expression and protein synthesis. *J. Biomech.* **39,** 2355–2362 (2006).

101. Scott, A. *et al.* Tenocyte responses to mechanical loading in vivo: a role for local insulin-like growth factor 1 signaling in early tendinosis in rats. *Arthritis Rheum.* **56,** 871–81 (2007).

102. Andarawis-Puri, N., Sereysky, J. B., Sun, H. B., Jepsen, K. J. & Flatow, E. L. Molecular response of the patellar tendon to fatigue loading explained in the context of the initial induced damage and number of fatigue loading cycles. *J. Orthop. Res.* **30,** 1327–1334 (2012).

103. Hannafin, J. A., Arnoczky, S. P., Hoonjan, A. & Torzilli, P. A. Effect of stress deprivation and cyclic tensile loading on the material and morphologic properties of canine flexor digitorum profundus tendon: Anin vitro study. *J. Orthop. Res.* **13,** 907–914 (1995).

104. Hayashi, K. Biomechanical studies of the remodeling of knee joint tendons and ligaments. *Journal of Biomechanics* **29,** 707–716 (1996).

105. Yamamoto, N. *et al.* Effects of Stress Shielding on the Mechanical Properties of Rabbit Patellar Tendon. *J. Biomech. Eng.* **115,** 23 (1993).

106. Yamamoto, E., Hayashi, K. & Yamamoto, N. Mechanical properties of collagen fascicles from stress-shielded patellar tendons in the rabbit. *Clin. Biomech. (Bristol, Avon)* **14,** 418–25 (1999).

107. Yamamoto, E., Hayashi, K. & Yamamoto, N. Effects of stress shielding on the transverse mechanical properties of rabbit patellar tendons. *J. Biomech. Eng.* **122,** 608–14 (2000).

108. Shepherd, J. H. & Screen, H. R. C. Fatigue loading of tendon. *Int. J. Exp. Pathol.* **94,** 260–70 (2013).

109. Heinemeier, K. M. *et al.* Expression of collagen and related growth factors in rat tendon and skeletal muscle in response to specific contraction types. *J. Physiol.* **582,** 1303–1316 (2007).

110. Sun, Y.-L. *et al.* Temporal response of canine flexor tendon to limb suspension. *J. Appl. Physiol.* **109,** 1762–1768 (2010).

111. Verma, R. P. & Hansch, C. Matrix metalloproteinases (MMPs): Chemical–biological functions and (Q)SARs. *Bioorg. Med. Chem.* **15,** 2223–2268 (2007).

112. Legerlotz, K., Jones, G. C., Screen, H. R. C. & Riley, G. P. Cyclic loading of tendon fascicles using a novel fatigue loading system increases interleukin-6 expression by tenocytes. *Scand. J. Med. Sci. Sport.* **23,** 31–37 (2013).

113. Yang, G., Im, H.-J. & Wang, J. H.-C. Repetitive mechanical stretching modulates IL-1β induced COX-2, MMP-1 expression, and PGE2 production in human patellar tendon fibroblasts. *Gene* **363,** 166–172 (2005).

114. Archambault, J. M., Elfervig-Wall, M. K., Tsuzaki, M., Herzog, W. & Banes, A. J. Rabbit tendon cells produce MMP-3 in response to fluid flow without significant calcium transients. *J. Biomech.* **35,** 303–9 (2002).

115. Maeda, E. *et al.* Functional analysis of tenocytes gene expression in tendon fascicles subjected to cyclic tensile strain. *Connect. Tissue Res.* **51,** 434–444 (2010).

116. Klein, M. B., Yalamanchi, N., Pham, H., Longaker, M. T. & Chan, J. Flexor tendon healing in vitro: Effects of TGF-β on tendon cell collagen production. *J. Hand Surg. Am.* **27,** 615–620 (2002).

117. Ohno, K., Yasuda, K., Yamamoto, N., Kaneda, K. & Hayashi, K. Effects of complete stress-shielding on the mechanical properties and histology of in situ frozen patellar tendon. *J. Orthop. Res.* **11,** 592–602 (1993).

118. Uchida, H. *et al.* Stress deprivation simultaneously induces over-expression of interleukin-1beta, tumor necrosis factor-alpha, and transforming growth factor-beta in fibroblasts and mechanical deterioration of the tissue in the patellar tendon. *J. Biomech.* **38,** 791–8 (2005).

119. Arnoczky, S. P., Tian, T., Lavagnino, M. & Gardner, K. Ex vivo static tensile loading inhibits MMP-1 expression in rat tail tendon cells through a cytoskeletally based mechanotransduction mechanism. *J. Orthop. Res.* **22,** 328–33 (2004).

120. Miyatake, S. *et al.* Local administration of interleukin-1 receptor antagonist inhibits deterioration of mechanical properties of the stress-shielded patellar tendon. *J. Biomech.* **41,** 884–9 (2008).

121. Schwartz, M. A. Integrins and Extracellular Matrix in Mechanotransduction. *Cold Spring Harb. Perspect. Biol.* **2,** a005066–a005066 (2010).

122. Beales, P. & Jackson, P. K. Cilia - the prodigal organelle. *Cilia* **1,** 1 (2012).

123. Otho Fridericus Müller. *Animalcula infusoria fluviatilia et marina, quæ detexit, systematice descripsit et ad vivum delineari curavit. Hauniae, Typis N. Mölleri* (Typis NICOLAl MOLLERI, HAUNAE, 1786). at <http://medcontent.metapress.com/index/A65RM03P4874243N.pdf>

124. Bloodgood, R. a. Sensory reception is an attribute of both primary cilia and motile cilia. *J. Cell Sci.* **123,** 505–9 (2010).

125. Sorokin, S. P. Reconstructions of centriole formation and ciliogenesis in mammalian lungs. *J. Cell Sci.* **3,** 207–30 (1968).

126. Nauli, S. M. *et al.* Loss of polycystin-1 in human cyst-lining epithelia leads to ciliary dysfunction. *J. Am. Soc. Nephrol.* **17,** 1015–25 (2006).

127. Hernandez-Hernandez, V. *et al.* Bardet-biedl syndrome proteins control the cilia length through regulation of actin polymerization. *Hum. Mol. Genet.* **22,** 3858–3868 (2013).

128. Walczak-Sztulpa, J. *et al.* Cranioectodermal Dysplasia, Sensenbrenner Syndrome, Is a Ciliopathy Caused by Mutations in the IFT122 Gene. *Am. J. Hum. Genet.* **86,** 949–956 (2010).

129. Tuz, K. *et al.* Mutations in CSPP1 cause primary cilia abnormalities and joubert syndrome with or without Jeune asphyxiating thoracic dystrophy. *Am. J. Hum. Genet.* **94,** 62–72 (2014).

130. Lodish H, Berk A, Zipursky SL, et al. in *Molecular Cell Biology.* (W.H. Freeman, 2000).

131. Janke, C. & Chloë Bulinski, J. Post-translational regulation of the microtubule cytoskeleton: mechanisms and functions. *Nat. Rev. Mol. Cell Biol.* **12,** 773–786 (2011).

132. Al-Bassam, J. & Corbett, K. D. α-Tubulin acetylation from the inside out. *Proc. Natl. Acad. Sci. U. S. A.* **109,** 19515–6 (2012).

133. Splettstoesser, T. Tubulin Microtubule. *scistyle* at <https://commons.wikimedia.org/wiki/File:Microtubule_structure.png>

134. SOROKIN, S. Centrioles and the formation of rudimentary cilia by fibroblasts

and smooth muscle cells. *J. Cell Biol.* **15,** 363–77 (1962).

135. Ishikawa, H. & Marshall, W. F. Ciliogenesis: building the cell's antenna. *Nat. Rev. Mol. Cell Biol.* **12,** 222–34 (2011).

136. Kobayashi, T. & Dynlacht, B. D. Regulating the transition from centriole to basal body. *J. Cell Biol.* **193,** 435–44 (2011).

137. Currie, a. R. & Wheatley, D. N. Cilia of a Distinctive Structure (9 + 0) in Endocrine and other Tissues. *Postgrad. Med. J.* **42,** 403–408 (1966).

138. Lidow, M. S. & Menco, B. P. Observations on axonemes and membranes of olfactory and respiratory cilia in frogs and rats using tannic acid-supplemented fixation and photographic rotation. *J. Ultrastruct. Res.* **86,** 18–30 (1984).

139. Kozminski, K. G., Johnson, K. a, Forscher, P. & Rosenbaum, J. L. A motility in the eukaryotic flagellum unrelated to flagellar beating. *Proc. Natl. Acad. Sci. U. S. A.* **90,** 5519–5523 (1993).

140. McMurray, R. J., Wann, A. K. T., Thompson, C. L., Connelly, J. T. & Knight, M. M. Surface topography regulates wnt signaling through control of primary cilia structure in mesenchymal stem cells. *Sci. Rep.* **3,** 3545 (2013).

141. Hirokawa, N. Kinesin and Dynein Superfamily Proteins and the Mechanism of Organelle Transport. *Science (80-.).* **279,** 519–526 (1998).

142. Hirokawa, N. Kinesin and Dynein Superfamily Proteins and the Mechanism of Organelle Transport. *Science (80-.).* **279,** 519–526 (1998).

143. Nussey, S. & Whitehead, S. *Endocrinology: An Integrated Approach.* (BIOS SChientific Publishers, 2001).

144. May-Simera, H. L. & Kelley, M. W. Cilia, Wnt signaling, and the cytoskeleton. *Cilia* **1,** 7 (2012).

145. Schneider, L. *et al.* PDGFRαα signaling is regulated through the primary cilium in fibroblasts. *Curr. Biol.* **15,** 1861–1866 (2005).

146. Christensen, S. *et al.* Transforming growth factor beta (TGF b) signaling is regulated at the pocket region of primary cilia. **1,** 2012 (2012).

147. Nüsslein-Volhard, C. & Wieschaus, E. Mutations affecting segment number and polarity in Drosophila. *Nature* **287,** 795–801 (1980).

148. Rohatgi, R., Milenkovic, L. & Scott, M. P. Patched1 regulates hedgehog signaling at the primary cilium. *Science* **317,** 372–6 (2007).

149. Dorn, K. V, Hughes, C. E. & Rohatgi, R. A Smoothened-Evc2 complex transduces the Hedgehog signal at primary cilia. *Dev. Cell* **23,** 823–35 (2012).

150. Gupta, S., Takebe, N. & Lorusso, P. Review: Targeting the Hedgehog pathway in cancer. *Ther. Adv. Med. Oncol.* **2,** 237–250 (2010).

151. Inoki, K. *et al.* TSC2 Integrates Wnt and Energy Signals via a Coordinated Phosphorylation by AMPK and GSK3 to Regulate Cell Growth. *Cell* **126,** 955–968 (2006).

152. Ma, R. *et al.* PKD2 Functions as an Epidermal Growth Factor-Activated Plasma Membrane Channel PKD2 Functions as an Epidermal Growth Factor-Activated Plasma Membrane Channel. *Mol. Cell. Biol.* **25,** 8285–8298 (2005).

153. Schneider, L. *et al.* PDGFRalphaalpha signaling is regulated through the primary cilium in fibroblasts. *Curr. Biol.* **15,** 1861–6 (2005).

154. Ehnert, S. *et al.* TGF-β1 impairs mechanosensation of human osteoblasts via HDAC6-mediated shortening and distortion of primary cilia. *J. Mol. Med.* (2017). doi:10.1007/s00109-017-1526-4

155. DeCaen, P. G., Delling, M., Vien, T. N. & Clapham, D. E. Direct recording and molecular identification of the calcium channel of primary cilia. *Nature* **504,** 315–8 (2013).

156. Wheatley, D. N. Landmarks in the first hundred years of primary (9+0) cilium research. *Cell Biol. Int.* **29,** 333–9 (2005).

157. Spasic, M. & Jacobs, C. R. Lengthening primary cilia enhances cellular mechanosensitivity. *Eur. Cells Mater.* **33,** 158–168 (2017).

158. Delling, M. *et al.* Primary cilia are not calcium-responsive mechanosensors. *Nature* **531,** 656–660 (2016).

159. Massagué, J. TGFβ signalling in context. *Nat. Rev. Mol. Cell Biol.* **13,** 616–30 (2012).

160. Horiguchi, M., Ota, M. & Rifkin, D. B. Matrix control of transforming growth factor-β function. *J. Biochem.* **152,** 321–329 (2012).

161. Massagué, J. TGFβ signalling in context. *Nat. Rev. Mol. Cell Biol.* **13,** 616–30 (2012).

162. Guo, X. & Wang, X.-F. Signaling cross-talk between TGF-b/BMP and other pathways. *Cell Res.* **19,** 71–88 (2009).

163. Huang, F. & Chen, Y. Regulation of TGF- b receptor activity. *Cell Biosci.* **2,** 9 (2012).

164. Clement, C. A. *et al.* TGF-β signaling is associated with endocytosis at the pocket region of the primary cilium. *Cell Rep.* **3,** 1806–14 (2013).

165. McGlashan, S. R. *et al.* Mechanical loading modulates chondrocyte primary cilia incidence and length. *Cell Biol. Int.* **34,** 441–6 (2010).

166. McGlashan, S. R. *et al.* Mechanical loading modulates chondrocyte primary cilia incidence and length. *Cell Biol. Int.* **34,** 441–6 (2010).

167. Thompson, C. L., Chapple, J. P. & Knight, M. M. Primary cilia disassembly down-regulates mechanosensitive hedgehog signalling: A feedback mechanism controlling ADAMTS-5 expression in chondrocytes. *Osteoarthr. Cartil.* **22,** 490–498 (2014).

168. Liang, Y. *et al.* Mechanism of ciliary disassembly. *Cell. Mol. Life Sci.* **73,** 1787–1802 (2016).

169. Pugacheva, E. N., Jablonski, S. A., Hartman, T. R., Henske, E. P. & Golemis, E. A. HEF1-dependent Aurora A activation induces disassembly of the primary cilium. *Cell* **129,** 1351–1363 (2008).

170. Pitaval, A., Tseng, Q., Bornens, M. & Théry, M. Cell shape and contractility regulate ciliogenesis in cell cycle-arrested cells. *J. Cell Biol.* **191,** 303–312 (2010).

171. Miyoshi, K., Kasahara, K., Miyazaki, I. & Asanuma, M. Factors that influence primary cilium length. *Acta Med. Okayama* **65,** 279–85 (2011).

172. Ehnert, S. *et al.* TGF-β1 impairs mechanosensation of human osteoblasts via HDAC6-mediated shortening and distortion of primary cilia. *J. Mol. Med.* (2017). doi:10.1007/s00109-017-1526-4

173. Donnelly, E., Ascenzi, M.-G. & Farnum, C. Primary cilia are highly oriented with respect to collagen direction and long axis of extensor tendon. *J. Orthop. Res.* **28,**

77–82 (2010).

174. Lavagnino, M., Arnoczky, S. P. & Gardner, K. In situ deflection of tendon cell-cilia in response to tensile loading: an in vitro study. *J. Orthop. Res.* **29,** 925–30 (2011).

175. Lavagnino, M. & Arnoczky, S. P. Tendon cell ciliary length as a biomarker of in situ cytoskeletal tensional homeostasis. **3,** 118–121 (2013).

176. Saggese, T., Young, A. a, Huang, C., Braeckmans, K. & McGlashan, S. R. Development of a method for the measurement of primary cilia length in 3D. *Cilia* **1,** 11 (2012).

177. Helander, K. G. Formaldehyde prepared from paraformaldehyde is stable. *Biotech. Histochem.* **75,** 19–22 (2000).

178. Stradleigh, T. W. & Ishida, A. T. Fixation strategies for retinal immunohistochemistry. *Prog. Retin. Eye Res.* **48,** 181–202 (2015).

179. Hopwood, D. Cell and tissue fixation. *Histochem. J.* **17,** 389–442 (1985).

180. Hobro, A. J. & Smith, N. I. An evaluation of fixation methods: Spatial and compositional cellular changes observed by Raman imaging. *Vib. Spectrosc.* **91,** 31–45 (2017).

181. Hua, K. & Ferland, R. J. Fixation methods can differentially affect ciliary protein immunolabeling. *Cilia* **6,** 5 (2017).

182. sigmaaldrich. Monoclonal Anti-Acetylated Tubulin antibody produced in mouse. *www.sigmaaldrich.com* (2017). at <https://www.sigmaaldrich.com/catalog/product/sigma/t7451?lang=en&region=GB>

183. abcam. Anti-ARL13B antibody (ab83879). *www.abcam.com*

184. abcam. Anti-Ki67 antibody (ab15580). (2007). at <http://www.abcam.com/ki67-antibody-ab15580.html>

185. thermofisher. Alexa Fluor™ 555 Phalloidin. (2017). at <https://www.thermofisher.com/order/catalog/product/A34055>

186. Donnelly, E., Williams, R. & Farnum, C. The primary cilium of connective tissue cells: imaging by multiphoton microscopy. *Anat. Rec. (Hoboken).* **291,** 1062–73

(2008).

187. Thompson, C. L. *et al.* Chondrocyte expansion is associated with loss of primary cilia and disrupted hedgehog signalling. *Eur. Cells Mater.* **34,** 128–141 (2017).

188. Ridler, T. & Calvard, S. Picture Thresholding Using an Iterative Selection Method. *IEEE Trans. Syst. Man. Cybern.* **8,** 630–632 (1978).

189. Thornton, G. M. *et al.* Changes in mechanical loading lead to tendonspecific alterations in MMP and TIMP expression: influence of stress deprivation and intermittent cyclic hydrostatic compression on rat supraspinatus and Achilles tendons. *Br. J. Sports Med.* **44,** 698–703 (2010).

190. Kathem, S. H., Mohieldin, A. M. & Nauli, S. M. The Roles of Primary cilia in Polycystic Kidney Disease. **1,** 27–46 (2013).

191. Wann, A. K. T. & Knight, M. M. Primary cilia elongation in response to interleukin-1 mediates the inflammatory response. *Cell. Mol. Life Sci.* **69,** 2967–77 (2012).

192. Dean, B. J. F., Dakin, S. G., Millar, N. L. & Carr, A. J. Review: Emerging concepts in the pathogenesis of tendinopathy. *Surgeon* **15,** 349–354 (2017).

193. Sun, H. B. *et al.* Coordinate regulation of IL-1beta and MMP-13 in rat tendons following subrupture fatigue damage. *Clin. Orthop. Relat. Res.* **466,** 1555–61 (2008).

194. Asundi, K. R. & Rempel, D. M. MMP-1, IL-1??, and COX-2 mRNA expression is modulated by static load in rabbit flexor tendons. *Ann. Biomed. Eng.* **36,** 237–243 (2008).

195. Birch, H. L. *et al.* Matrix metabolism rate differs in functionally distinct tendons. *Matrix Biol.* **27,** 182–9 (2008).

196. Lui, P. P. Y. & Chan, K. M. Tendon-derived stem cells (TDSCs): from basic science to potential roles in tendon pathology and tissue engineering applications. *Stem Cell Rev.* **7,** 883–97 (2011).

197. Mcmurray, R. & Knight, M. M. Topographical regulation of primary cilia orientation and length in mesenchymal stem cells. *Cilia* **1,** P34 (2012).

198. Thompson, C. L., Chapple, J. P. & Knight, M. M. Primary cilia disassembly down-regulates mechanosensitive hedgehog signalling: a feedback mechanism

controlling ADAMTS-5 expression in chondrocytes. *Osteoarthritis Cartilage* **22,** 490–8 (2014).

199. Prodromou, N. V. *et al.* Heat shock induces rapid resorption of primary cilia. *J. Cell Sci.* **125,** 4297–4305 (2012).

200. Besschetnova, T. Y. *et al.* Identification of signaling pathways regulating primary cilium length and flow-mediated adaptation. *Curr. Biol.* **20,** 182–7 (2010).

201. Bruneau, A., Champagne, N., Cousineau-Pelletier, P., Parent, G. & Langelier, E. Preparation of rat tail tendons for biomechanical and mechanobiological studies. *J. Vis. Exp.* 3–7 (2010). doi:10.3791/2176

202. Screen, H. R. C., Seto, J., Krauss, S., Boesecke, P. & Gupta, H. S. Extrafibrillar diffusion and intrafibrillar swelling at the nanoscale are associated with stress relaxation in the soft collagenous matrix tissue of tendons. *Soft Matter* **7,** 11243–11251 (2011).

203. Abreu, E. L., Leigh, D. & Derwin, K. a. Effect of altered mechanical load conditions on the structure and function of cultured tendon fascicles. *J. Orthop. Res.* **26,** 364–373 (2008).

204. Thompson, C. L., Wiles, A., Poole, C. A. & Knight, M. M. Lithium chloride modulates chondrocyte primary cilia and inhibits Hedgehog signaling. *FASEB J.* (2015). doi:10.1096/fj.15-274944

205. McMurray, R. J., Wann, a. K. T., Thompson, C. L., Connelly, J. T. & Knight, M. M. Surface topography regulates wnt signaling through control of primary cilia structure in mesenchymal stem cells. *Sci. Rep.* **3,** 25–28 (2013).

206. Wann, A., Thompson, C., Chapple, J. & Knight, M. Interleukin-1β sequesters hypoxia inducible factor 2α to the primary cilium. *Cilia* 1–14 (2013). at <http://www.biomedcentral.com/content/pdf/2046-2530-2-17.pdf>

207. Yamamoto, E., Iwanaga, W., Miyazaki, H. & Hayashi, K. Effects of Static Stress on the Mechanical Properties of Cultured Collagen Fascicles From the Rabbit Patellar Tendon. *J. Biomech. Eng.* **124,** 85 (2002).

208. Buchanan, C. I. & Marsh, R. L. Effects of exercise on the biomechanical, biochemical and structural properties of tendons. *Comp. Biochem. Physiol. - A Mol. Integr. Physiol.* **133,** 1101–1107 (2002).

209. Rowson, D., Knight, M. M. & Screen, H. R. C. Zonal variation in primary cilia elongation correlates with localized biomechanical degradation in stress deprived tendon. *J. Orthop. Res.* **34,** 2146–2153 (2016).

210. Chen, B., Co, C. & Ho, C.-C. Cell Shape Dependent Regulation of Nuclear Morphology Bo. *Biomaterials* **67,** 129–136 (2015).

211. Greiner, A. M., Chen, H., Spatz, J. P. & Kemkemer, R. Cyclic Tensile Strain Controls Cell Shape and Directs Actin Stress Fiber Formation and Focal Adhesion Alignment in Spreading Cells. *PLoS One* **8,** (2013).

212. McGlashan, S. R., Haycraft, C. J., Jensen, C. G., Yoder, B. K. & Poole, C. a. Articular cartilage and growth plate defects are associated with chondrocyte cytoskeletal abnormalities in Tg737orpk mice lacking the primary cilia protein polaris. *Matrix Biol.* **26,** 234–46 (2007).

213. Livne, A., Bouchbinder, E. & Geiger, B. Cell reorientation under cyclic stretching. *Nat. Commun.* **5,** 1–8 (2014).

214. Screen, H. R., Lee, D. A., Bader, D. L. & Shelton, J. C. Development of a technique to determine strains in tendons using the cell nuclei. *Biorheology* **40,** 361–368 (2003).

215. Screen, H. R. C., Bader, D. L., Lee, D. a. & Shelton, J. C. Local Strain Measurement within Tendon. *Strain* **40,** 157–163 (2004).

216. Zhang, J. *et al.* Topography of calcium phosphate ceramics regulates primary cilia length and TGF receptor recruitment associated with osteogenesis. *Acta Biomater.* **57,** 487–497 (2017).

217. Marshall, W. F. Flagellar Length Control System: Testing a Simple Model Based on Intraflagellar Transport and Turnover. *Mol. Biol. Cell* **16,** 270–278 (2004).

218. Screen, H. R. C., Shelton, J. C., Bader, D. L. & Lee, D. A. Cyclic tensile strain upregulates collagen synthesis in isolated tendon fascicles. *Biochem. Biophys. Res. Commun.* **336,** 424–429 (2005).

219. Waxman, A. S., Kornreich, B. G., Gould, R. A., Sydney Moïse, N. & Butcher, J. T. Interactions between TGFβ1 and cyclic strain in modulation of myofibroblastic differentiation of canine mitral valve interstitial cells in 3D culture. *J. Vet. Cardiol.* **14,** 211–221 (2012).

220. Ireland, D. *et al.* Multiple changes in gene expression in chronic human Achilles tendinopathy. *Matrix Biol.* **20,** 159–169 (2001).

221. PORTER, S., CLARK, I. M., KEVORKIAN, L. & EDWARDS, D. R. The ADAMTS metalloproteinases. *Biochem. J.* **386,** 15–27 (2005).

222. Nelson, D. L. Preparation of cilia and subciliary fractions from Paramecium. *Methods Cell Biol.* **47,** 17–24 (1995).

223. Labour, M.-N., Riffault, M., Christensen, S. T. & Hoey, D. A. TGFβ1 – induced recruitment of human bone mesenchymal stem cells is mediated by the primary cilium in a SMAD3-dependent manner. *Sci. Rep.* **6,** 35542 (2016).

224. Berbari, N. F. *et al.* Microtubule modifications and stability are altered by cilia perturbation and in cystic kidney disease. *Cytoskeleton* **70,** 24–31 (2013).

225. Zhu, D., Shi, S., Wang, H. & Liao, K. Growth arrest induces primary-cilium formation and sensitizes IGF-1-receptor signaling during differentiation induction of 3T3-L1 preadipocytes. *J. Cell Sci.* **122,** 2760–8 (2009).

226. Delaval, B., Bright, A., Lawson, N. D. & Doxsey, S. The cilia protein IFT88 is required for spindle orientation in mitosis. *Nat. Cell Biol.* **13,** 461–468 (2011).

227. Sereysky, J. B., Andarawis-Puri, N., Ros, S. J., Jepsen, K. J. & Flatow, E. L. Automated image analysis method for quantifying damage accumulation in tendon. *J. Biomech.* **43,** 2641–2644 (2010).

228. 'University of New Mexico'. INTRODUCTION TO FOURIER TRANSFORMS FOR IMAGE PROCESSING. *University of New Mexico* (2017). at <https://www.cs.unm.edu/~brayer/vision/fourier.html>

229. Harte, D. in *Multifractals* 3–4 (Chapman and Hall, 2001).

230. Prokofiev. Estimating the box-counting dimension of the coast of Great Britain. *Wikipedia* (2010). at <https://en.wikipedia.org/wiki/Minkowski–Bouligand_dimension#/media/File:Great_Britain_Box.svg>

231. Frisch, K. E. *et al.* Quantification of collagen organization using fractal dimensions and Fourier transforms. *Acta Histochem.* **114,** 140–144 (2012).

232. Sacha, J. Maximum Entropy Threshold. *imageJ.net* (2004). at <http://imagej.net/Maximum_Entropy_Threshold>

233. Tinevez, J.-Y. No Title. *imageJ.net* (2017). at <https://imagej.net/Directionality>

234. Calve, S. *et al.* Engineering of functional tendon. *Tissue Eng.* **10,** 755–61 (2004).

235. Banes, A. J. *et al.* Cell populations of tendon: A simplified method for isolation of synovial cells and internal fibroblasts: Confirmation of origin and biologic properties. *J. Orthop. Res.* **6,** 83–94 (1988).

236. Benjamin, M., Kaiser, E. & Milz, S. Structure-function relationships in tendons: a review. *J. Anat.* **212,** 211–28 (2008).

237. Patel, D., Sharma, S., Bryant, S. J. & Screen, H. R. C. Recapitulating the Micromechanical Behavior of Tension and Shear in a Biomimetic Hydrogel for Controlling Tenocyte Response. *Adv. Healthc. Mater.* **6,** 1–7 (2017).

238. Dvm, S. P. A. *et al.* Loss of Homeostatic Strain Alters Mechanostat "' Set Point "' of Tendon Cells In Vitro. 1583–1591 (2008). doi:10.1007/s11999-008-0264-x

239. Järvinen, T. A. H. & Prince, S. Decorin: A Growth Factor Antagonist for Tumor Growth Inhibition. *Biomed Res. Int.* **2015,** 1–11 (2015).

240. Ferdous, Z., Wei, V. M., Iozzo, R., Höök, M. & Grande-Allen, K. J. Decorin-transforming Growth Factor-β Interaction Regulates Matrix Organization and Mechanical Characteristics of Three-dimensional Collagen Matrices. *J. Biol. Chem.* **282,** 35887–35898 (2007).

241. Burton-Wurster, N. *et al.* TGF beta 1 and biglycan, decorin, and fibromodulin metabolism in canine cartilage. *Osteoarthr. Cartil.* **11,** 167–176 (2003).

242. Wren, K. N. *et al.* A differential cargo-loading model of ciliary length regulation by IFT. *Curr. Biol.* **23,** 2463–71 (2013).

243. Gardner, K., Arnoczky, S. P. & Dicarlo, E. F. Elongated Primary Cilia as a Biomarker for the Loss of Cellular Tensional Homeostasis in Tendinopathy. *ORS 2014 Annu. Meet.* 4–6 (2014).